GRI-91/0033

QUANTIFICATION OF FLOW UNIT AND BOUNDING ELEMENT PROPERTIES AND GEOMETRIES, FERRON SANDSTONE, UTAH: IMPLICATIONS FOR HETEROGENEITY IN GULF COAST TERTIARY DELTAIC RESERVOIRS

ANNUAL REPORT

(January 1990 - December 1990)

Prepared by

Noel Tyler, R. S. Fisher, and M. D. Barton
Bureau of Economic Geology
W. L. Fisher, Director

and

M. A. Miller, Jon Holder, and K. E. Gray
Center for Petroleum and Geosystems Engineering
The University of Texas at Austin
Austin, Texas 78713

For

GAS RESEARCH INSTITUTE
Contract No. 5089-260-1902
Anthony W. Gorody, Project Manager

April 1991

DISCLAIMER

LEGAL NOTICE This report was prepared by the Bureau of Economic Geology as an account of work sponsored by the Gas Research Institute (GRI). Neither GRI, members of GRI, nor any person acting on behalf of either:

a. Makes any warranty or representation, expressed or implied, with respect to the accuracy, completeness, or usefulness of the information contained in this report, or that the use of any apparatus, method, or process disclosed in this report may not infringe privately owned rights; or

b. Assumes any liability with respect to the use of, or for damages resulting from the use of, any information, apparatus, method, or process disclosed in this report.

50272-101

REPORT DOCUMENTATION PAGE	1. REPORT NO. GRI-91/0033	2.	3. Recipient's Accession No.

4. Title and Subtitle
Quantification of Flow Unit and Bounding Element Properties and Geometries, Ferron Sandstone, Utah: Implications for Heterogeneity in Gulf Coast Tertiary Deltaic Reservoirs

5. Report Date
April 1991

6.

7. Author(s) Noel Tyler, R. S. Fisher, M. D. Barton, M. A. Miller, Jon Holder, K. E. Gray

8. Performing Organization Rept. No.

9. Performing Organization Name and Address
Bureau of Economic Geology
The University of Texas at Austin
University Station, Box X
Austin, TX 78713-7508

10. Project/Task/Work Unit No.

11. Contract(C) or Grant(G) No.
(C) 5089-260-1902
(G)

12. Sponsoring Organization Name and Address
Gas Research Institute
8600 West Bryn Mawr Avenue
Chicago, IL 60631

Project Manager:
Anthony W. Gorody

13. Type of Report & Period Covered
Annual Report
Jan. 1, 1990 - Dec. 31, 1990

14.

15. Supplementary Notes

16. Abstract (Limit: 200 words)

Outcrop exposures are being studied to quantify the internal permeability distribution of fluvial-deltaic sandstones, which results in reservoir compartments bounded by baffles or barriers to gas flow. This information will be used to develop reservoir models that can guide infill drilling to optimize incremental gas reserve growth from sandstone reservoirs. The objectives are being accomplished through integration of (1) outcrop characterization, (2) petrophysical measurements, and (3) pore-level modeling.

Projected long-term benefits of the study are two-fold. First, increased understanding of internal architecture and improved methods for quantification of heterogeneity will facilitate development of strategies to minimize risk in the extended development of fluvial-dominated deltaic gas reservoirs. Second, targeting of incremental gas resources in mature reservoirs will lead to extended recovery of a low-cost, low-risk resource.

Results of the first year of studies show that the architecture, geometry, and internal permeability distribution of fluvial-deltaic sandstones are generally predictable and that a four-order hierarchy of bounding surfaces exists. Initial tests have been completed, and reliable measurements of petrophysical properties of flow units, flow baffles, and flow barriers are being performed on outcrop samples. Development of a pore-level simulator has been essentially completed. Results in general indicate that the field approach is sound and that information gained on outcrop can be used to produce realistic reservoir models.

17. Document Analysis a. Descriptors
Texas, Utah, Ferron Sandstone, Wilcox sandstones, depositional systems, gas reserves, reservoir heterogeneity, permeability distributions, petrophysical properties, pore-level simulator

b. Identifiers/Open-Ended Terms

c. COSATI Field/Group

18. Availability Statement	19. Security Class (This Report)	21. No. of Pages
Release Unlimited	Unclassified	
	20. Security Class (This Page) Unclassified	22. Price

RESEARCH SUMMARY

Title	QUANTIFICATION OF FLOW UNIT AND BOUNDING ELEMENT PROPERTIES AND GEOMETRIES, FERRON SANDSTONE, UTAH: IMPLICATIONS FOR HETEROGENEITY IN GULF COAST TERTIARY DELTAIC RESERVOIRS
Contractors	Bureau of Economic Geology and Center for Petroleum and Geosystems Engineering, The University of Texas at Austin.
	GRI Contract No. 5089-260-1902
Principal Investigators	Noel Tyler, M. A. Miller, K. E. Gray
Report Period	January 1990 - December 1990

Objectives

Outcrop exposures of the Ferron Sandstone are being studied to test two fundamental hypotheses regarding sandstone architecture and resulting controls on natural gas reservoir properties: (1) that depositional and diagenetic processes produce a predictable internal permeability distribution in fluvial-deltaic sandstones, which results in reservoir compartments separated from each other by baffles or barriers to gas flow, and (2) that realistic three-dimensional reservoir models can be developed from knowledge gained at the outcrop and in the laboratory and can be used to guide infill drilling to optimize incremental gas reserve growth from sandstone reservoirs. Establishing efficient methods for conducting such outcrop studies and translating the results to a reservoir model constitute the second major goal of this 3-year project. Among the final products of this research will be a complete data set suitable for construction and production testing of a gas reservoir in a fluvial-deltaic sandstone.

The objectives of this project are to investigate the geologic and petrophysical factors that produce reservoir compartments (flow units), bounding elements, and baffles in sandstone reservoirs through combined field and laboratory investigations, and to predict the distribution of these units in the subsurface. These objectives are being accomplished through integration of three related studies: (1) outcrop characterization, including field mapping, field permeability

measurements, petrographic analyses, and construction of three-dimensional reservoir models, (2) petrophysical measurements of flow units, baffles, and barriers, and (3) pore-level modeling. The resulting reservoir model, developed from outcrop studies, will be tested against the known sandstone architecture and production performance of the Lake Creek field (Eocene Wilcox sandstones, Montgomery County, Texas).

Technical Perspectives

The predictability of reservoir and seal properties composes the crux of the proposed research, which is directed at solving the causes and predictability of heterogeneity in a reservoir class that accounts for 64 percent of total production from Texas Gulf Coast reservoirs. Ferron outcrop studies will provide a predictive tool for definition of geometric characteristics of reservoir properties that will be of direct application in the Secondary Gas Recovery (SGR) project. In that project volumes and recoverability of unrecovered gas form the research and development objective. Analogous reservoirs in Lake Creek field (Montgomery County, Texas) are being studied as part of the SGR project, providing an opportunity to field-test data and hypotheses developed on the outcrop.

The projected long-term benefits of the study are two-fold. First, increased understanding of internal architecture and improved methods for quantification of heterogeneity will facilitate development of strategies to mitigate, or at least minimize, risk in the extended development of fluvial-dominated deltaic gas reservoirs. Second, targeting of incremental gas resources in mature reservoirs will lead to extended recovery of a low-cost, low-risk resource.

This report summarizes the conceptual approach, methods, and initial results obtained during the first year of the 3-year project and outlines plans for work during years 2 and 3 of the study.

Results

Outcrop Characterization

The first year of study produced the following preliminary conclusions. First, sandstone architecture in the fluvial-deltaic system is generally predictable; principal features of the external and internal geometry of the major sand bodies either remain the same or change predictably as a function of position in the facies tract. This information is critical for defining the internal geometric architecture of sandstone reservoir models. A four-order hierarchy of bounding surfaces has been recognized, and general relations between bounding surfaces and sandstone geometry can be

reasonably predicted. Second, early results of petrographic studies suggest a relation exists between depositional facies, type of cement, and importance of secondary porosity. Third, important, systematic permeability trends are identified on the outcrop; these trends can be used to define petrophysical properties within sandstone reservoir models. Mean permeability varies significantly between the three major stratification types, although there is considerable overlap of actual measurements. These trends are readily attributed to differences in composition and texture of the sandstones. Regular permeability trends exist within the major stratal types, and these permeability profiles can generally be traced for hundreds of feet along the outcrop. Highest permeability values occur in the center of channels; values near channel margins are systematically lower. Variogram analysis of permeability distributions within the two established sample grids shows that the resultant permeability structure is dependent on lithofacies and sampling scale. Permeability profiles can be correlated for hundreds of feet along outcrop, and results of the variogram analysis on data from sample grids suggest correlation ranges of 18 to 2 ft, depending on how closely measurements are taken.

Petrophysical Measurements

A suite of survey measurements were carried out on specimens of material from five blocks of Ferron material selected as being representative of flow and bounding unit material. The petrophysical properties were measured under various test conditions to evaluate the range in anticipated behavior and to determine appropriate test procedures. The principal observations from these measurements are

1. The measured permeabilities and especially the formation factors were sensitive to the salinity of the pore fluid, reflecting a nontrivial clay content;

2. The absolute brine permeabilities range from microdarcys to hundreds of millidarcys in the outcrop material, for which porosity variations are only a few percent;

3. The measured permeabilities are relatively insensitive to the measurement stress conditions;

4. The measured mechanical properties are sensitive to the measurement stress conditions but follow an effective stress dependence; and

5. The measured brine permeabilities are smaller but on the same order as, and follow the same trends as, air minipermeameter measurements carried out on the same blocks from which the laboratory test specimens were taken.

Pore-Level Modeling

Based on previous research at The University of Texas at Austin, a suitable pore-level simulator has been essentially completely developed. Currently, equations for the following are implemented in the model: flow of an incompressible fluid in a pore, flow of an ideal gas in a pore, capillary pressure between two phases, electrical current flow in a pore, and volume of pores. With these equations the following properties are modeled: porosity, saturation, capillary pressure, absolute permeability, relative permeability, and the ratio of core resistivity to brine resistivity. At present, there is some difficulty with the nonwetting phase relative permeability calculations, but the other calculations appear to agree well with previous studies done at The University of Texas at Austin and elsewhere.

We also began a study to investigate the sensitivity of various petrophysical properties to pore structure parameters (such as pore throat size distributions). We have been careful to construct the model in a dimensionless form that will provide insight into the key relationships between model results and pore structure parameters. This work will provide the basis for later "history-matching" studies of the model to actual laboratory measurements.

Technical Approach

Outcrop Characterization

Most outcrop characterization efforts were dedicated to mapping the size, continuity, and distribution of facies exposed in three canyons, and measuring permeability at closely spaced intervals using a field minipermeameter to assess the reservoir characteristics within and between various facies. Fifty-eight vertical transects along outcrop exposures were described and measured, producing a total of nearly 3,100 permeability values. In addition, a 40 × 40 ft grid with an embedded 6 × 6 ft grid was established on the outcrop face, and nearly 850 permeability values were measured on these detailed grids at 2-ft and 4-inch spacings, respectively. These data are currently being examined for permeability trends and correlations with geologic features, and for predictable relations between permeability distributions and sandstone facies. Related activities included sampling for petrologic examination and petrophysical measurements and initiating petrologic and petrophysical investigations. More than 200 core plugs were collected from outcrop for

petrographic examination, and 29 sandstone blocks were selected from representative facies for petrophysical measurements and petrologic analyses.

Petrophysical Measurements

The program of laboratory measurements is designed to generate a data base of carefully measured petrophysical properties that is central to development of the pore-level network models. The first activity during this year of the project has been the development, calibration, and performance evaluation of the experimental capabilities necessary for the simultaneous measurements, under simulated reservoir conditions, of petrophysical properties that are coupled to related internal rock features. Specifically, simultaneous laboratory measurements of porosity, permeability, electrical resistivity (formation factor), and static and dynamic moduli are being carried out under triaxial test conditions. Most of the measurements are being carried out in one system within the Earth Sciences and Engineering Laboratory (ESEL), which has capabilities for the simultaneous measurements during steady-state flow of a liquid (water) through the specimen. Several ancillary apparatuses, such as bench-top permeameters and other ESEL simultaneous property measurement systems, have been used in the evaluation of system performance. The performance evaluation and system calibrations were carried out using specimens from one block of the Ferron outcrop and from a block of in-house quarry sandstone whose properties have been thoroughly documented in previous ESEL studies.

A second major activity during the first project year has been the development and calibration of facilities for the incorporation of air flow into the system used for the simultaneous petrophysical property measurements. These capabilities are necessary to provide measurements of properties sensitive to the effects of capillarity. The two-phase flow measurements will permit the determination of relative air/brine permeabilities, saturation exponents, and variations in dynamic moduli with saturation. Shakedown measurements in the modified system have been carried out for one of the original Ferron specimens, and a preliminary set of complete measurements has been carried out on 1 of the 29 blocks of Ferron material collected recently.

Pore-Level Modeling

The objective of this project is to develop a methodology for relating gas reservoir petrophysical property variability patterns to geologic heterogeneity structure in fluvial-deltaic reservoirs. Although descriptive geologic studies and minipermeameter measurements in outcrops provide means to study reservoir heterogeneity both qualitatively and

quantitatively, an important element that is missing from these techniques is a methodology for determining the variability and continuity of important petrophysical properties other than permeability. These properties, including porosity, cementation factor, saturation exponent, capillary pressure, and relative permeability, play important roles in the performance of gas reservoirs. Understanding their variability could provide important insight into reservoir modeling and into the development of operational strategies for optimizing gas reservoir performance.

The premise of this work is that geologic setting can be related to a variety of key petrophysical properties through the use of pore-level network models. These models, which simulate transport and storage properties of porous media, provide a theoretical link between pore structure and petrophysical measurements. By utilizing such a simulator to replicate a large number of simultaneous petrophysical property measurements, it can then be used to provide a link between geologic outcrop studies and quantitative petrophysical property measurements made in the laboratory. The first stage of this project has been to develop a suitable pore-level network simulator that can be used to match the simultaneous laboratory petrophysical measurements being conducted for this project. This model needed to have several key features: (a) capability of modeling three-dimensional pore networks, (b) capability of modeling all of the petrophysical properties of interest, and (c) ability to be utilized in a stochastic sense, that is, to be amenable to intensive computer usage.

Project Implications

This first year's work has been focused on developing and calibrating field sampling and laboratory testing methods. The stage is now set to test the contractor's unique premise: that heterogeneity of natural gas clastic reservoirs can be characterized simply and effectively using a three-part characterization system: flow units, flow barriers, and flow baffles. Using a well-exposed outcrop and calibrating outcrop permeability measurements with relative permeability laboratory data, the contractor will now begin to develop methods to construct reservoir engineering models of heterogeneous, fluvial-deltaic reservoirs. The greatest challenges in this endeavor will be twofold: (1) assign a range of distinct petrophysical properties to each of the three flow types and (2) devise methods to interactively map and adjust the continuity of each flow type in a geologically realistic three-dimensional computer model. The progress described in this annual report suggests that such challenges can be adequately addressed in the work planned for the next year.

CONTENTS

FIGURES

TABLES

INTRODUCTION

This research integrates outcrop and petrologic characterization of fluvial-deltaic sandstones with measurements of petrophysical properties and computer simulations of pore-level networks to better understand the distribution of flow units, flow baffles, and flow barriers in sandstone gas reservoirs. The ultimate goal of this work is to learn how to transport information from outcrop studies to realistic reservoir models that can be used to optimize recovery of natural gas from sandstone reservoirs.

Most efforts during the first year of this three-year study were devoted to testing and refining methods in each of the related programs. The major lithofacies were identified and mapped on the selected reservoir analog, the Ferron Sandstone in east-central Utah, and permeability was measured along vertical transects and within two grids to establish the geologic and reservoir framework of Ferron Sandstone unit 5. On the basis of this outcrop characterization, samples of flow units, barriers, and baffles were collected for petrophysical investigations. Initial efforts in this program were devoted to determining optimal experimental conditions for the various measurements. This work has largely been completed, and samples can now be routinely analyzed. First-year activities in the pore-level simulation program involved development, testing, and sensitivity analysis of the model. This too is essentially complete, and the simulator is ready to be run using data from the laboratory measurements as input.

This first annual report summarizes activities in each of these research areas, discusses directions for continued work in the second and third years of the study, and describes plans for final integration of results to meet project goals.

OUTCROP CHARACTERIZATION OF ARCHITECTURE AND PERMEABILITY STRUCTURE

R. Stephen Fisher, Noel Tyler, and Mark D. Barton
Bureau of Economic Geology

INTRODUCTION

Purpose

Reservoir architecture, the internal fabric or structure of reservoirs, governs paths of fluid migration during oil and gas production. Reservoir architecture is, in turn, the product of the depositional and diagenetic processes that cause the reservoir to form. Therefore, if an understanding of the origin of the reservoir is developed, reservoir architecture, and hence, the paths of fluid migration, become predictable. Thus, with greater understanding of the fabric of the reservoir and its inherent control on the paths of fluid flow, we can more efficiently target remaining, conventionally recoverable hydrocarbons that are prevented from migrating to the well bore by intrareservoir seals or bounding surfaces. Furthermore, advanced recovery strategies that account for the internal compartmentalization of the reservoir can be designed and implemented.

Production attributes of gas reservoirs are controlled by the depositional and diagenetic character (that is, the petrophysical character) of the reservoir rock. Petrophysical character in turn defines the efficiency with which hydrocarbons in a given reservoir compartment migrate to the well bore. Of potentially greater importance, and the fundamental focus of this project, are lithologies bounding individual compartments. Bounding surfaces may provide efficient intrareservoir stratigraphic traps causing substantial volumes of recoverable gas to be left unaddressed in abandoned reservoirs.

The research under way is attempting to determine the controls of sedimentary architecture on permeability structure in a superbly exposed and cored delta/distributary channel complex, and how this permeability structure would affect gas mobility in a sandstone reservoir. The project aims to (1) document and quantify the geometric and petrophysical attributes and production behavior of flow units and their associated flow baffles on the outcrop, (2) quantify directional attributes and properties of flow barriers bounding flow units on the outcrop, (3) transport outcrop architecture and petrophysical relations to a three-dimensional reservoir model, and (4) use the reservoir model to determine predictability of locations and volumes of unrecovered gas potentially remaining in analogous reservoirs following drilling to conventional well spacings. The approach is to establish the depositional framework and diagenetic modification of fluvial-deltaic sandstones, and then to determine how these factors affect the spatial distribution of permeability. The steps involved in this characterization of heterogeneity are the determination of facies architecture, delineation of the position, continuity, and causes of both permeable zones and barriers to gas flow, and the establishment of predictable permeability trends common to fluvial-deltaic sandstones. Ultimately, the goal is to translate this understanding of outcrop architecture to a reservoir model that can be used to test hypotheses concerning the most efficient methods for recovery of incremental gas reserves in a heterogeneous, compartmented sandstone.

Applicability of Outcrop Studies to the Subsurface: Data Portability

Reservoir characterization from outcrop studies allows the continuous sampling necessary for a more detailed reservoir description than is available from subsurface data alone. An obvious limitation of surface studies is the transfer (that is, portability) of outcrop permeability values to the subsurface. Several studies have demonstrated the portability of outcrop observations to the

subsurface (Stalkup and Ebanks, 1986; Goggin, 1988; Kittridge, 1988; Chandler and others, 1989). In general, it has been found that the mean of the permeability measurements is not portable. However, distribution type, coefficient of variation, and correlation measures are portable between outcrop and subsurface. In particular, Stalkup and Ebanks (1986) investigated permeability of sandstones in the Ferron study area. They compared outcrop to subsurface rocks of the same stratigraphic interval in a nearby well and found that permeability contrast among lithofacies is greater in the subsurface than in the outcrops. They attributed this to the effects of surface weathering. However, they also found that the vertical arrangement of statistically different permeabilities is preserved in the two situations, indicating the portability of outcrop data to core.

Several recent studies have shown that sedimentary facies exert an important control on permeability distribution in clastic rocks (Weber, 1982; Stalkup and Ebanks, 1986; Jones and others, 1987; Dreyer and others, 1990). The most influential variables influencing permeability are grain size, grain sorting, mineralogy, fabric, and degree of cementation (Dreyer and others, 1990). Thus based on the results of these earlier studies the approach we follow is to relate permeability measurements at the outcrop to quantification of these same variables. Permeability variation on the outcrop can then be compared with rock-property variation to establish discrete permeability groups for specific depositional systems and settings. This information provides the basis for assigning values and distributions of petrophysical properties to reservoir models of sandstones from similar depositional systems and settings.

Study Area

Extensive discussions of the geology of the Ferron Sandstone are presented by Ryer (1981) and summarized by Gardner in the appended briefing document (Appendix A). This well-documented geological framework allowed us to focus rapidly on a single pulse of the Ferron deltaic system (unit 5) that appeared representative of

the styles and scales of heterogeneity that exemplify Gulf Coast deltaic gas reservoirs. The rationale for the selection of the Ferron and a comparison of Ferron sandstones of Utah and Wilcox sandstones of the Texas Gulf Coast are outlined by Fisher in Appendix A.

Three-dimensional exposures of the Ferron Sandstone exist where small canyons dissect the western limb of the San Rafael Swell, east-central Utah. Sparse vegetation and the absence of structural complexity allow continuous examination and sampling of outcrops both parallel and perpendicular to the direction of sediment transport. Outcrops of Ferron deltaic unit 5 expose a wide range of depositional facies that include fluvial through coastal plain and marine strata. In the area of study, the upper Ferron includes facies that were deposited in several closely associated deltaic environments including fluvial point bar, meandering distributary channel, distributary mouth bar, delta-front, and transgressive sandstones.

METHODS

Architectural Analysis of Retrogradational Deltaic Sandstones

Three outcrops along the canyon walls that are oriented approximately parallel to depositional dip and two that are oriented approximately perpendicular to depositional dip are being studied. During 1990 we concentrated on outcrop windows of three channel complexes in Muddy Creek Canyon, which is more proximal in the distributary system, and Picture Flats Canyon, which is more distal (Fig. 1). Delta-front and distributary channel complexes along these canyons were selected for detailed study on the basis of their exposure, accessibility, and permeability characteristics. Three windows for detailed examination in Muddy Creek were selected to examine heterogeneity in the proximal area of the delta, where distributary channels are dominant (Fig. 1). These sandstones will be compared and contrasted with those deposited farther seaward,

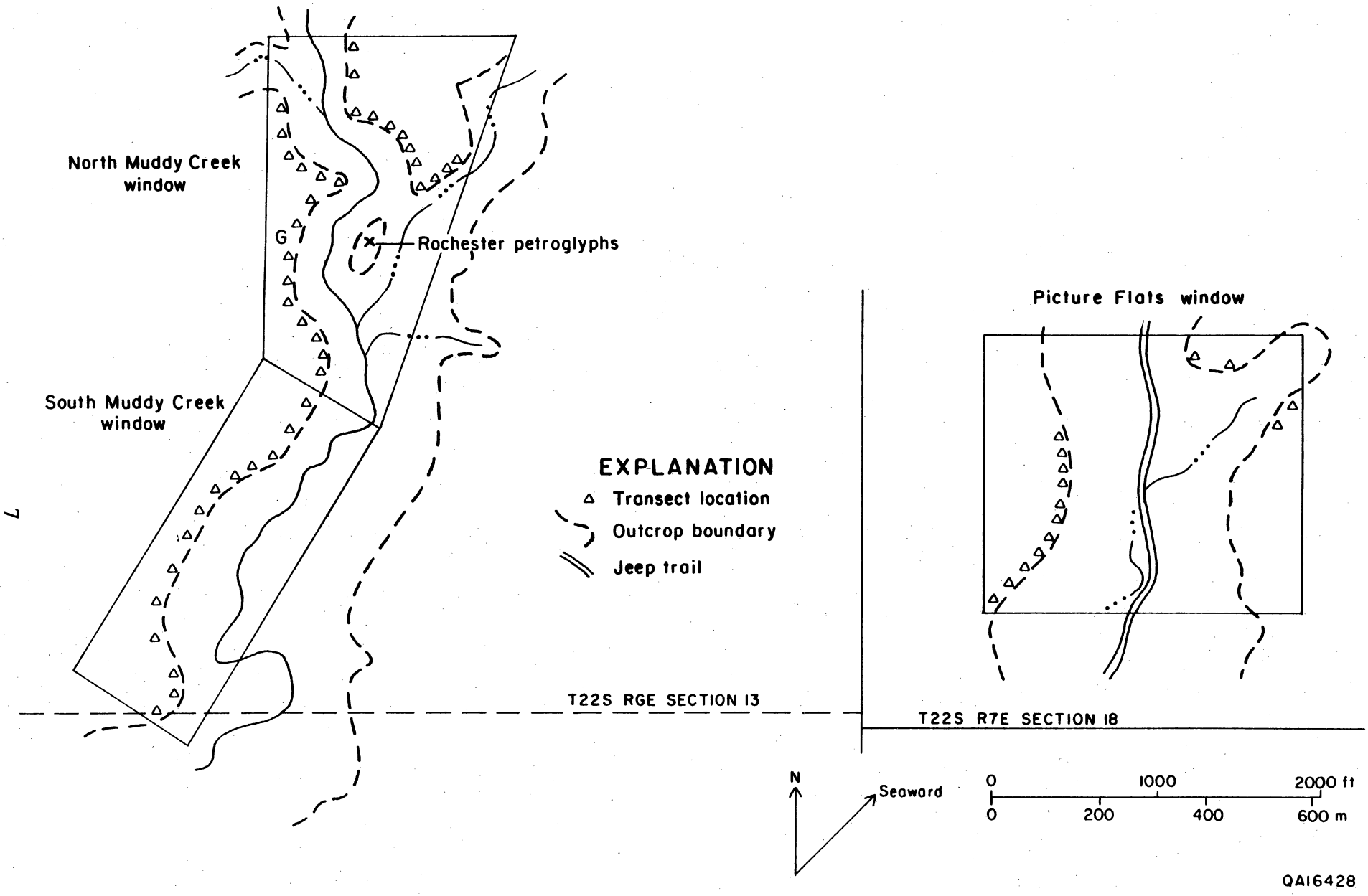

Figure 1. Location map of measured sections in Muddy Creek and Picture Flats canyons. Study area is approximately 3 mi east and 1 mi south of Emery, Utah. Location of grids for detailed permeability measurements is indicated by "G" in the North Muddy Creek window. Measured sections of the South Muddy Creek window provide data for the cross-section panel (Fig. 5).

where the increased influence of marine processes is manifested, and where marine reworking of the delta platform results in markedly different sand-body geometries from those in Muddy Creek. This report discusses the architecture of the more landward parts of unit 5. The seaward extremities of this unit will be examined during the 1991 field season and will be discussed in the 1991 annual report.

Fifty-eight detailed vertical sections, spaced 100 to 200 ft apart (Fig. 1), were established, marked, and measured; grain size, rock type, lithologic discontinuities, and sedimentary structures were recorded. The orientation of directional features was taken from paleocurrent measurements of various stratification types. In addition to detailed logging of these vertical sections, color photomosaics of the outcrop were assembled and used to map the distribution and interrelations of component architectural elements between measured vertical sections and in areas beyond outcrop windows. Geometric elements recognized on the photographs were identified and confirmed during measured sectioning on the outcrop face.

Permeability Measurements

A portable minipermeameter was used to make permeability measurements at 1-ft intervals along each of the 58 measured vertical sections using. The minipermeameter is a gas-flow measuring system that is ideal for quickly making a large number of permeability determinations on the outcrop with minimal sample preparation. Effects of outcrop weathering are reduced by choosing relatively fresh surfaces and then chipping away the weathered surface of the rock. Numerous studies have demonstrated the accuracy of the minipermeameter measurements in comparison with conventional measures of permeability (Weber, 1982; Goggin, 1988; Kittridge, 1988). In general, good correspondence between minipermeameter and conventional measurements is reported over the range of approximately one to several thousand millidarcys. The minipermeameter used in this investigation has a detection range of about 0.1 to 3,000 md. Permeabilities below about 10 md tend to be

slightly overestimated; however, application of a tip sealant such as petroleum jelly eliminates instrument bias. Comparison of measured and accepted permeability values for 60 specimens over the range of 5 to 1,000 md showed agreement to be within ± 5 percent. Repeated permeability measurements collected from a single sample point show that precision is better than 5 percent over the range of one to several hundred millidarcys.

In addition to permeability measurements along vertical sections, sample grids were constructed to examine the detailed spatial variability of permeability within and between lithofacies. This task was designed to provide information regarding how far permeability data could be extrapolated for inclusion in reservoir models. Two sampling grids were constructed: a 40 × 40 ft grid wherein permeabilities were measured at 2-ft intervals and an embedded 6 × 6 ft grid wherein permeabilities were measured at 4-inch intervals. The sampling grids were located on a vertical exposure to minimize the effects of surface weathering and to ensure that profiles were truly vertical. Figure 2 illustrates the technique used to prepare sampling grids. In total, nearly 4,000 permeability measurements were taken on the outcrop during the 1990 field season.

Sampling for Petrographic and Petrophysical Analyses

To meet the needs of all the researchers and to optimize the amount of information derived from Ferron sandstones by both the Bureau of Economic Geology (BEG), the Earth Sciences and Engineering Laboratory (ESEL), and the University of Texas Center for Petroleum and Geosystems Engineering (CPGE), a three-tier, hierarchical sampling plan was designed (Fig. 3). The first level of investigation comprises field mapping of lithologic facies and genetic associations within depositional systems, measuring and describing vertical outcrop sections at multiple locations along the fluvial-deltaic facies tract, and measuring permeability at 1-ft intervals on each vertical section. As noted above, approximately 4,000 such determinations were performed during the past year; we expect that

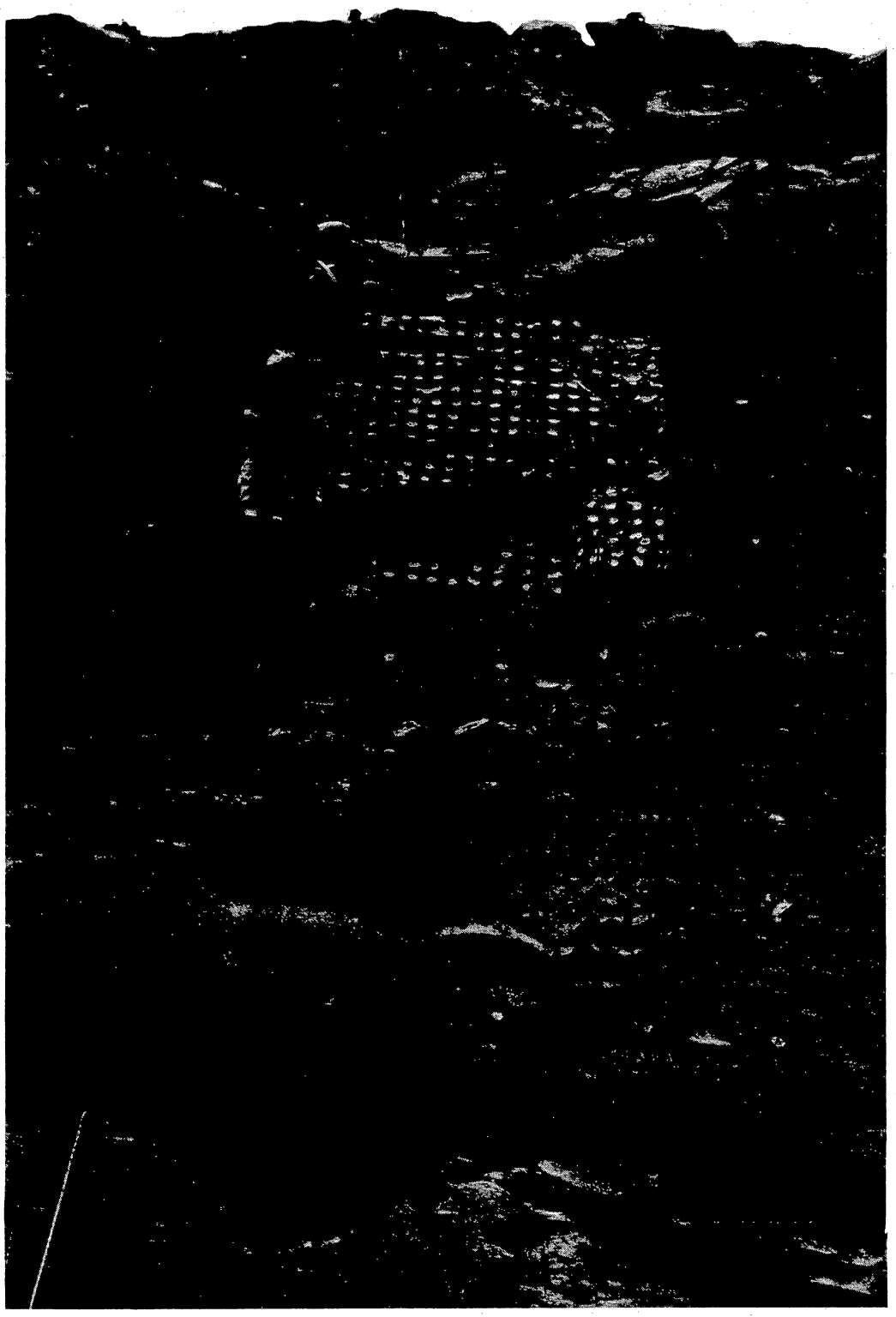

Figure 2. Photograph showing outcrop preparation of sampling grids. A large net was constructed and suspended from the top of the cliff; the outcrop surface was prepared, and minipermeameter measurements were made from the net.

FERRON SAMPLING PLAN

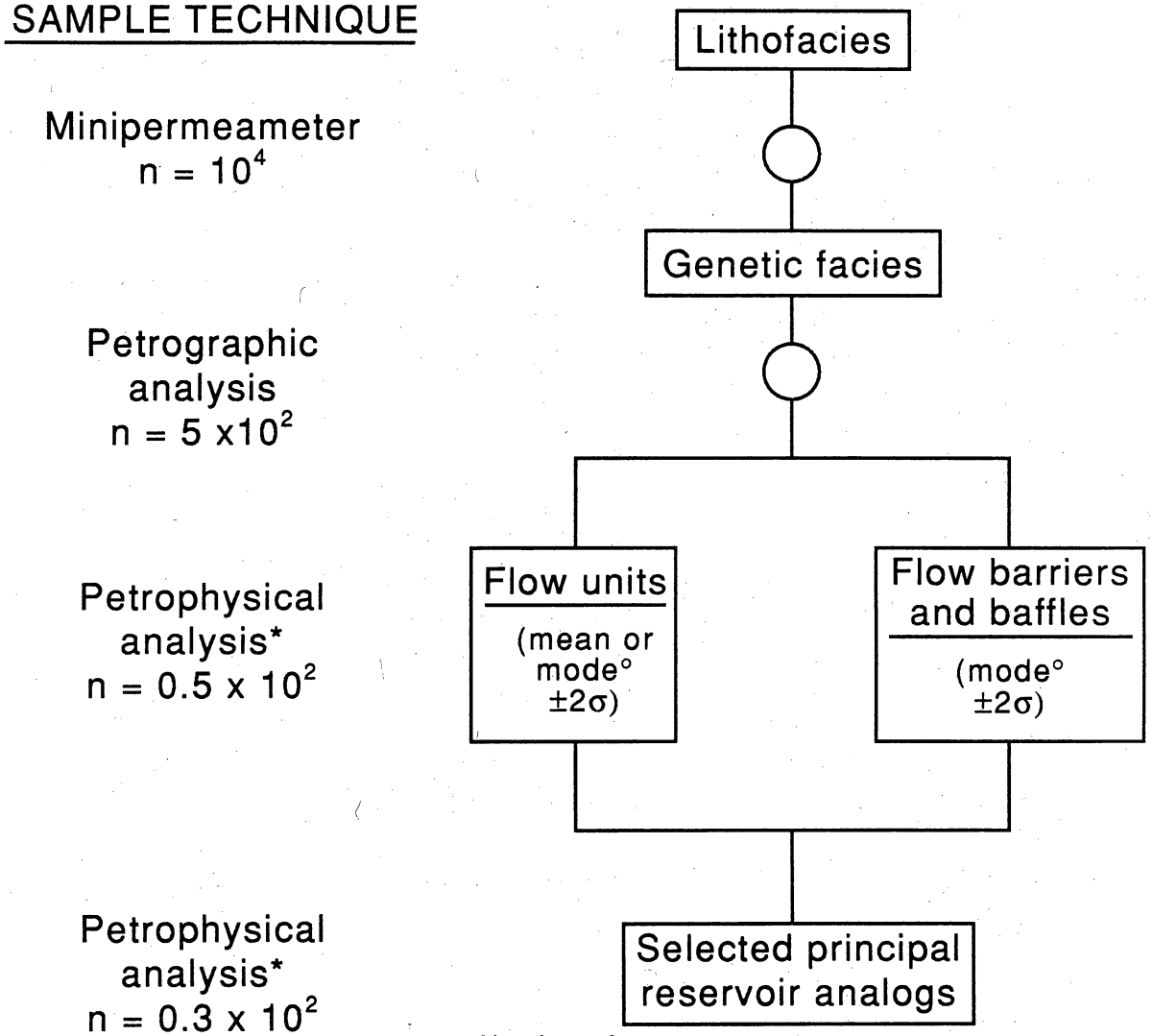

n = Number of measurements

* Sample selection based on minipermeameter information

° "Representative" samples will be collected based on average values (mean, median, mode) determined from permeability distribution

QA15162c

Figure 3. Hierarchical sampling plan to provide material for petrographic and petrophysical analyses.

10,000 to 15,000 field permeability measurements will be made during the investigation. Information derived from the outcrop characterization and field minipermeameter measurements guide sample selection for levels two and three of the study.

The second level of investigation comprises petrographic analyses of sandstone flow units, baffles, and barriers. This activity is described below in the section on petrologic investigations. It is designed to answer such basic questions as (1) How are porous and permeable zones distributed within primary depositional units? and (2) To what extent are the distribution and petrophysical properties of flow barriers and baffles controlled by zones of preferential cementation? Samples for petrographic examination are selected largely on the basis of facies relations and measured permeability values. Approximately 200 samples have been collected for petrographic analysis during the first year of the study; we expect that a total of 300 to 500 samples will be collected during the course of this project.

The third level is composed of samples selected for measurement of petrophysical properties at ESEL and modeling of pore-level network properties at CPGE. These activities are discussed later in this report. On the basis of outcrop characterization, we plan to select samples for petrophysical analysis that will provide three specimens for each principal flow unit, barrier, and baffle: one having representative permeability, one having permeability approximately two standard deviations greater than the typical value, and one having permeability about two standard deviations less than the typical value. We expect this suite of samples to provide the most useful information regarding relations between sandstone architecture, petrophysical properties, reservoir characteristics, and gas mobility. Twenty-nine samples were collected during the past year; we anticipate that a total of 50 to 75 samples will be analyzed during the course of the project.

Petrologic Investigations

Petrologic investigations are being conducted to determine what mineralogic and textural parameters characterize flow units, barriers, and baffles, and to relate these features to depositional processes and burial history to develop criteria for predicting reservoir heterogeneity and compartmentalization in fluvial-deltaic reservoir sandstones. The principal goals of this work are

1. To determine what relations among depositional processes, detrital and authigenic mineralogy, primary and secondary porosity, and permeability affect reservoir properties of flow units,
2. To determine the type, distribution, and origin of detrital and authigenic minerals that characterize bounding surfaces, flow barriers, and baffles within and between flow units,
3. To deduce the diagenetic history of the Ferron Sandstone so that similarities and differences between the Ferron Sandstone of Utah and Wilcox sandstone gas reservoirs of the Texas Gulf Coast can be evaluated, and
4. To provide data to constrain and refine pore-network models.

Samples collected from outcrop during the past year as well as thin sections and core on loan to the Bureau of Economic Geology are being examined. Core plugs and sandstone blocks collected from Ferron outcrops in Muddy Creek Canyon, Picture Flats Canyon, Cedar Ridge Canyons (northeast of Picture Flats) and along the I-70 road cut through the Ferron (south of Muddy Creek) form the primary sample set. Approximately 200 1-inch-diameter, 3- to 6-inch-long cylinders have been collected using a portable drill equipped with a coring bit. Sample sites were chosen on the basis of facies relations and results of field minipermeameter measurements; samples are given identification numbers that allow them to be related to vertical section descriptions and minipermeameter values. Twenty-nine larger (approximately 0.5-ft^3) sandstone blocks collected from representative reservoir facies for laboratory measurement of

petrophysical properties are also being studied. In addition to the outcrop samples, 7 cores and approximately 400 thin sections on loan from ARCO Oil and Gas Company are being examined. These cores cannot be sampled for mineralogical or textural analyses; however, this material greatly increases the sample data base and can be used to augment and guide outcrop sampling.

Petrologic investigations are following the hierarchical strategy outlined in the discussion of our sampling plan. Outcrop samples collected for petrophysical analysis receive the most complete examination, including

1. Thin section point-counting to quantify the amount and type of detrital grains, authigenic cements, and primary and secondary porosity. Grain-to-grain, grain-to-cement, and grain-to-pore textural relations are also examined.
2. Scanning electron microscope (SEM) examination of thin sections using backscattered electron (BSE) detection to accurately measure pore-body and pore-throat geometries.
3. SEM examination of rock chips to determine the nature of grain surfaces and the dimensions of pores and pore throats.
4. X-ray diffraction analysis to determine the mineralogic content of sandstones, particularly the clay minerals.
5. Grain-size analysis to quantify size, sorting, and percent clay.
6. Preparation and SEM examination of epoxy pore casts to provide a three-dimensional view of pore throats and pore bodies.

Samples collected for routine petrologic analysis receive the same attention described above with the exceptions that SEM/BSE examination of pore dimensions and preparation of pore casts will not be routinely performed and grain-size distributions will be estimated from thin-section examination. Other analyses, including geochemical analyses needed to reconstruct burial diagenetic history, will be performed as needed.

Thin sections have been made of all outcrop samples, and the sections have been stained to assist in distinguishing between potassium and plagioclase feldspar, and between calcite, iron-calcite,

ankerite, and dolomite. All thin sections will be examined using standard light microscope methods, and representative sections from all facies and bounding elements will be point-counted to quantify detrital and authigenic minerals and porosity types. Textural information such as grain size, shape, and sorting is obtained by microscopic examination of outcrop core plugs.

We are experimenting to find the best way to prepare pore casts and to obtain images of pore structures from which accurate dimensions of pore bodies and pore throats can be obtained. Work to date has been directed toward optimizing ways to remove carbonate, silicate, oxide, and sulfide minerals from epoxy-impregnated sandstone chips without destroying delicate pore-throat features. We are also experimenting to determine optimal conditions for imaging pore dimensions on the basis of density differences between sandstone grains or cements and epoxy-filled pore space.

Initial efforts to interpret the burial history of the Ferron Sandstone are directed toward collecting published data on the total thickness of sediments that overlie the Ferron and the thermal history of central Utah. We are also collecting analyses of Ferron coals, particularly carbon content, moisture content, and reflectance data, in order to estimate the maximum burial temperature of the sandstones from the coal composition.

RESULTS

Architectural Analysis of Retrogradational Deltaic Sandstones

In the Picture Flats and Muddy Creek windows located in the updip parts of the delta platform, Ferron deltaic unit 5 consists of basal delta-front sandstones that are erosionally overlain by distributary channel and associated sandstones. Most field efforts during the first year of this study were devoted to mapping and measuring the geometries of these strata and the bounding units surrounding them, so that gas reservoir models can later be

constructed with accurate dimensions and geometries of flow units and bounding elements.

Delta-Front Sandstones

Because some delta-front sandstones have been eroded by overlying strata, thickness and geometries of the delta-front sandstones have been influenced by both depositional and erosional processes. Thicknesses of the delta-front sands range from 0 (where erosionally removed) to 35 ft.

The delta-front sandstone interval is a composite of at least four subintervals (Fig. 4). Grain size in each of the subintervals is very fine and does not appreciably increase vertically. The basal subinterval contains relict, locally preserved, hummocky crossstratification; however, intense bioturbation is the dominant characteristic of this sandstone. M. H. Gardner (personal communication, 1990) has interpreted this zone as the maximum flooding surface that marks the base of Ferron deltaic unit 5.

Overlying the bioturbated zone are three discrete subintervals. Bedding in the subintervals is largely hummocky cross-stratified and to a lesser extent planar, trough, and ripple cross-stratified. Lateral facies variation in the subintervals is subtle, and no well-defined facies boundaries have been detected.

Vertical variation, in contrast, is pronounced. The lower bounding surface of each delta-front subinterval is erosional; upper bounding surfaces are composed of laterally continuous interbedded siltstone and mudstone layers. The uppermost of the subintervals is the thickest. Its basal surface is strongly erosional into the underlying subinterval.

The external geometry of the fluvially dominated, wave-modified delta-front sandstones is lobate. Internally, however, individual sandstone subunits display a tabular geometry. Each of the tabular subintervals extends downdip for at least 1 mi. Thus, the dominant style of heterogeneity in the delta-front sandstones is vertical stratification with subintervals ranging between 3 and >10 ft thick. Lateral heterogeneity resulting from depositional processes in

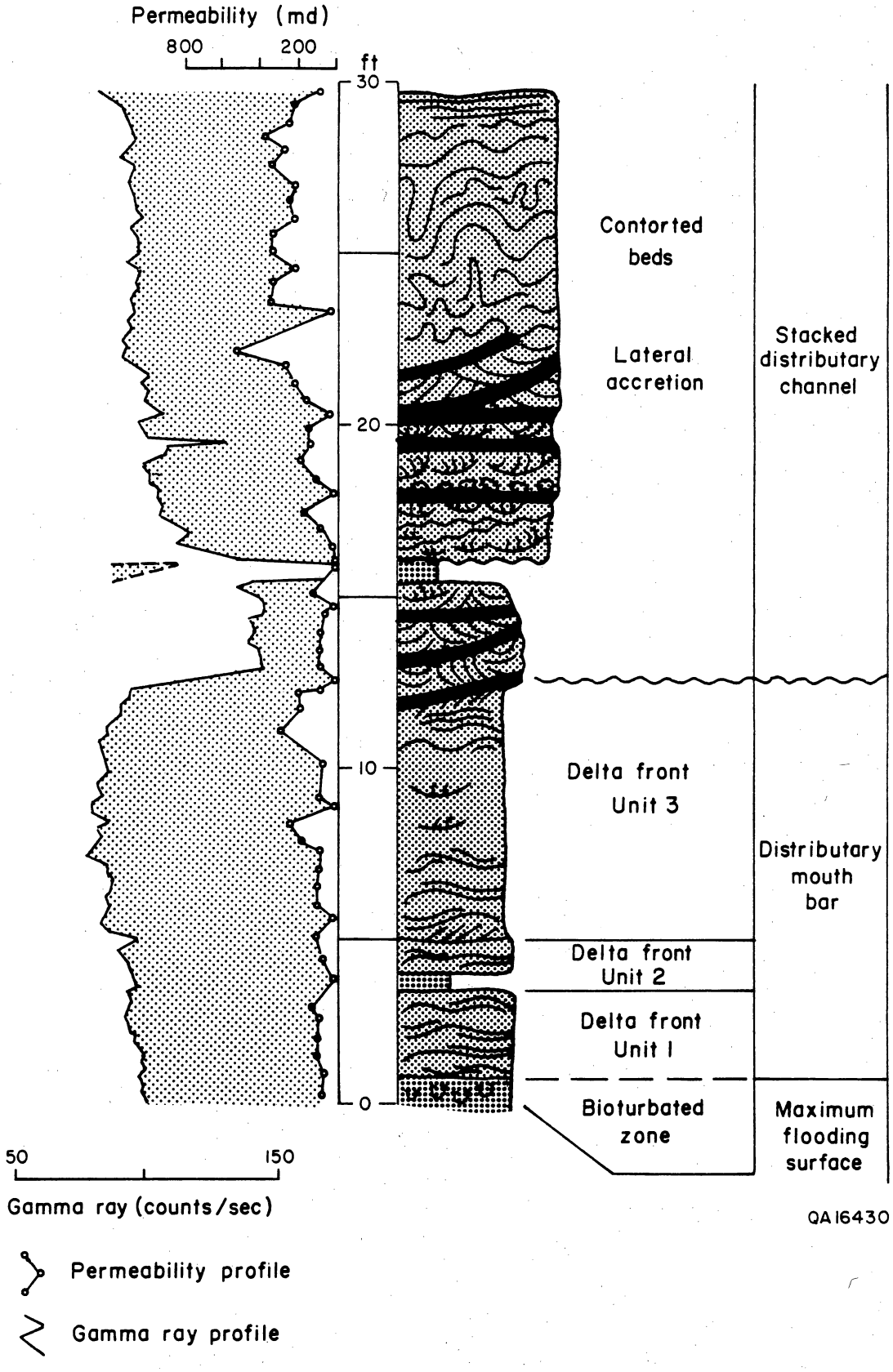

Figure 4. Vertical profile through typical delta-front and distributary channel sandstones, showing vertical changes in depositional environment, lithofacies, permeability, and gamma-ray response.

the subintervals is minimal; lateral variability of the delta-front sandstones is more a product of the erosive processes associated with the deposition of the superposed distributary sandstones. Pinch and swell associated with erosive truncation of the delta-front sandstones is well demonstrated on the north wall of Muddy Creek Canyon.

Distributary Channel and Associated Sandstones

Sandstones deposited in the distributary system are characterized by a high degree of both lateral and vertical heterogeneity. Three stages of channel formation are recognized in the distributary system: early, tidally influenced channels, followed by a second stage of channel sedimentation that was dominated by lateral accretion, and then the final stage of channel sedimentation characterized by deep, relatively narrow channels. Each stage of channel sedimentation is characterized by distinctive internal and external geometries.

Tidally influenced channels.—At the base of the distributary complex and erosive into the underlying, tabular delta-front sandstones are a series of relatively narrow and laterally isolated channel sandstones. The channels are mostly small features that are characterized by remarkably consistent width-to-thickness ratios (average of 9.5; Table 1). One of the channels is considerably larger than the other three, with an apparent width of 200 ft and a maximum thickness of 25 ft; the other channels have apparent widths of several tens of feet and thickness of less than 10 ft (Table 1). Bedding in the tidally influenced channels is varied. Large avalanche foresets are locally present in the main axis of the channel. Herringbone crossbedding may be present on the shallower flanks of the channels. Paleocurrent directions are bimodal.

Early Meandering Distributary Channels.—Early stage meandering distributary channel sandstones are much more laterally extensive than the subjacent tidally modified channel sandstones. The two distributary channel complexes exposed in Muddy Creek are 1,200 and 1,320 ft wide, respectively. The channels are strongly erosional into the underlying channels and into the delta-front sands

Table 1. Apparent dimensions of point-bar sandstones in amalgamated Ferron unit 5 distributary channel sand bodies.

Laterally Migrating Channels—Muddy Creek Canyon: Sand-Body Dimensions

Sand body	Thickness	Width	W/T
1	9.5	430	45.3
2	6	447	74.5
3	11	640	58.5
4	5	227	45.4
5	7.5	418	55.7
6	2.5	100	40
7	7	119	17
8	6.5	83	12.8
9	7.5	74	9.9
10	9.3	204	21.9
11	6.5	563	86.6
12	6.8	629	92.5
13	17	681	40.1
14	6.5	510	78.5
15	8.5	589	69.3
16	9	332	36.9
17	4.5	140	31.1
Average	7.7	363.9	48.0

Laterally Migrating Channels—Picture Flats: Sand-Body Dimensions

Sand body	Thickness	Width	W/T
1	15.5	192	12.6
2	27	353	13.1
3	16.5	610	37
4	19	636	33.5
5	15.5	262	16.9
6	20.5	430	21
7	16	278	17.4
8	12.5	308	24.6
9	12.5	250	20
10	16.5	195	11.8
11	10.5	200	19
12	11	71	6.5
13	4	83	20.5
14	13	612.6	47.1
15	10.5	133	12.7
Average	14.7	307.6	20.9

Tidally Influenced Channels—Muddy Creek Canyon: Sand-Body Dimensions

Sand Body	Thickness	Width	W/T
1	7	120	17.1
2	7.5	152	20.3
3	3.5	82	23.4
4	25	200	8
Average	10.8	138.5	17.2

Late-Stage Distributaries—Muddy Creek Canyon: Sand-Body Dimensions

Sand Body	Thickness	Width	W/T
1	57	580	10.2
2	35	400	11.4
Average	46.0	490.0	10.8

and locally erode completely through the delta-front sandstones. The channel complexes shale out laterally into overbank muds and silts or are truncated by superjacent distributary channel sandstones.

A typical vertical sequence contains three stratal types beginning with a basal zone of clay-clast-bearing trough crossbeds that overlie a sharp erosional base. These mud clasts typically deform into pseudomatrix during compaction. As will be shown in a later section of this report these mud-clast-rich zones display substantially lower permeabilities than the mid-to-upper distributary sediments and may provide effective baffles to fluid flow. Scale of trough crossbeds decreases upward from 1 to 2.5 ft to 0.5 to 1 ft. Grain size decreases upward, ranging from very coarse to medium-fine. Planar crossbeds with minor amounts of horizontal stratification abruptly overlie trough crossbeds and also display an upward-decreasing trend in stratification and grain size, from medium to small scale and medium to fine grained, respectively. The sequence is capped by fine to very fine grained, moderately to highly contorted strata or less commonly by very fine grained ripple-laminated sandstones.

The dominant characteristic of this lithofacies is well-defined lateral accretion surfaces (Fig. 5) that dip gently toward the channel thalweg. Angles of dip of the accretion surfaces are between 4 and 8 degrees. There is considerable variability in the dimensions of the point-bar packages bounded by the accretion surfaces (Table 1). Updip in the distributary system (in Muddy Creek) widths of the sigmoid-shaped point-bar bodies average 360 ft but range from 75 to almost 700 ft. Individual lenses are 3 to 15 ft thick (average 7.7 ft; Table 1) and erosionally overlap to form multilateral sand bodies with cumulative thicknesses of 15 to 40 ft. Individual sand lenses are 100 to 400 ft wide; belt width is up to 1,200 ft. There are also substantial differences between the lateral-accretion-bounded point-bar sandstones in Muddy Creek and those farther seaward in Picture Flats canyon, where the sigmoidal bodies have narrowed slightly (average of 308 ft) but are twice as thick as the equivalent units in Muddy Creek. These assemblages compose two distinct populations

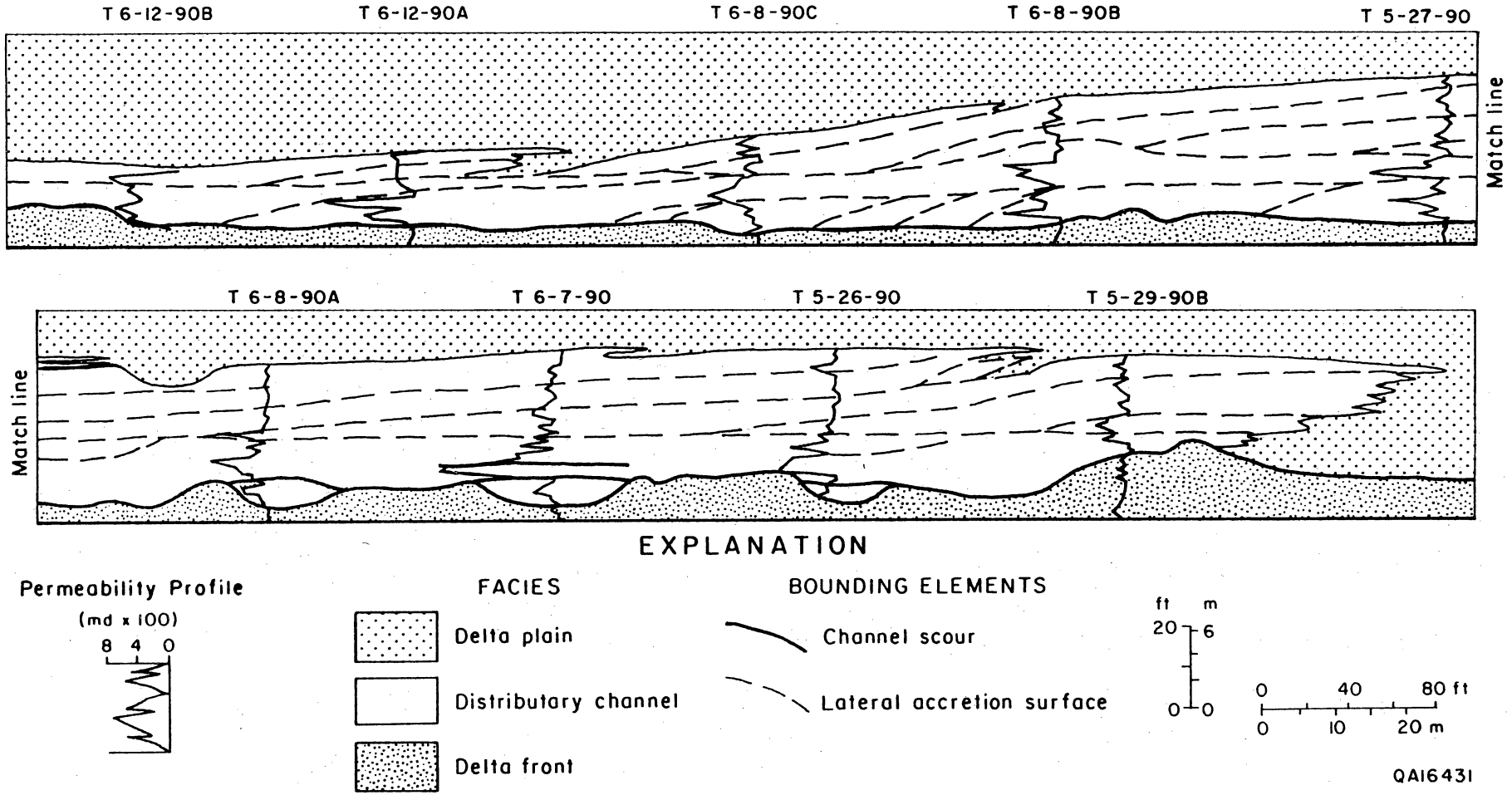

Figure 5. Cross section of outcrop profile, South Muddy Creek window, showing geometry of major facies and bounding elements, and permeability profiles at each measured section.

(Fig. 6). Width-to-thickness ratios decrease seaward from 481 in Muddy Creek to 211 in Picture Flats canyon (Table 1).

Laterally across the complex in the direction of accretion, the three main stratal types (as discussed above) are not continuous but pinch out over the underlying stratal type. The lower trough crossbedded facies is 5 to 18 ft (averaging about 15 ft) thick and has the greatest lateral dimensions, extending 1,000 to 1,200 ft across the sandbelt. The planar crossbedded facies is 5 to 15 ft thick and extends approximately 750 to 800 ft. The upper contorted facies is about 5 ft thick and has a width of approximately 500 ft.

Bounding elements are subhorizontal to inclined discontinuities that divide stratal types into subsets as well as separate genetic facies. Bounding elements considered in this investigation include contacts between different stratal types, channel scours, and lateral accretion surfaces. In the lower part of the complex, bounding elements separating individual sand bodies consist dominantly of a scoured surface overlain by poorly sorted, mud-clast-rich sandstone. In the middle to upper part of the complex the bounding elements consist of scoured sand-on-sand contacts and lateral accretion surfaces. Clay drapes are not a common feature in this channel type.

Late-Stage Distributary Channels.—Channel deposits formed during the final stage of distributary channel sedimentation are narrower than those in the underlying, highly meandering distributary complex but are considerably thicker (Table 1). Typically, these late-stage point bars are perched above and erode deeply into the subjacent sandstones. The basal point-bar contacts are typically rich in intraformational mud clasts.

Because lateral accretion surfaces in the late-stage distributaries are not accentuated by abundant mudchips, they are less well defined than those of the early meandering distributaries. In the Teardrop Hill window remnant accretion surfaces are mainly preserved at the base of the channel sandstones, the upper part of the point bar being characterized by intense contortion of the fine-grained sandstones.

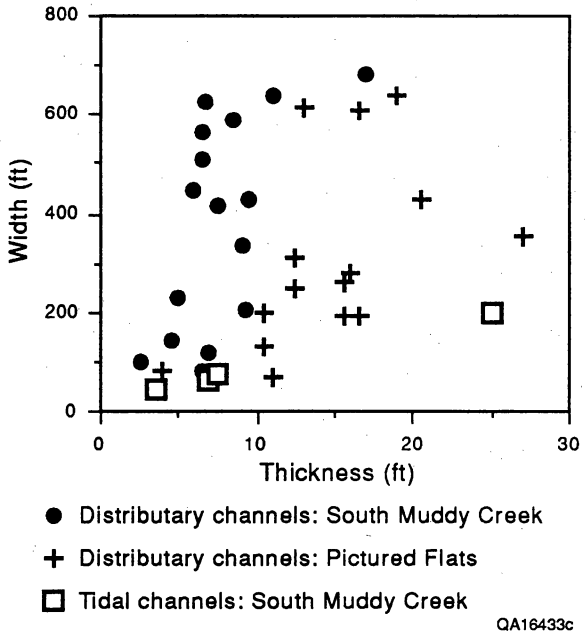

Figure 6. Plot of apparent width and thickness dimensions of distributary channel and tidal channel sandstones.

Nature of Bounding Surfaces

A hierarchy of bounding elements and surfaces present in retrogradational deltaic sandstones has been delineated from analysis of the updip delta-front distributary complex (Table 2). As the study proceeds this hierarchy will be modified and expanded. Bounding elements range from first to fourth orders. First-order bounding elements relate to system changes such as pinch-out of distributary sandstone into interdistributary bay mudstone. Second-order bounding elements are defined largely by depositional or diagenetic facies changes. Third-order elements separate similar facies such as channel-on-channel contacts, and fourth-order elements define bounding surfaces internal to a given facies (Table 2).

Petrography and Diagenetic Overprint

Initial studies have focused on the major sandstone units exposed at the Teardrop Hill window in Muddy Creek, specifically on those units that were sampled for laboratory determination of petrophysical properties at CPGE. The major units studied, from bottom to top, are bioturbated delta front, delta front, lower distributary channel, and upper distributary channel.

All sandstones are subangular to angular, poorly sorted subarkoses to sublitharenites. Framework compositions are 70 to 90 percent quartz, 5 to 15 percent feldspar, and 5 to 15 percent rock fragments. Potassium feldspar is slightly more abundant than plagioclase. Sedimentary rock fragments, particularly chert and shale clasts, are the most common lithic component. Quartz, kaolinite, calcite, and iron-rich calcite are the typical cements; pseudomatrix (shale and clay clasts deformed around harder detrital grains during compaction) and true matrix are present in some samples. Kaolinite is the only clay mineral present in volumetrically significant amounts. Porosity ranges from 10 to 20 percent, secondary porosity

Table 2. Hierarchy of bounding elements and surfaces
Ferron fluvial-deltaic sandstone, unit 5.

Order	Type	Examples	Character
First	System changes	Incised, mud-filled valley	10°–$<10^{1}$
		Distributary to Interdistributary bay	$10^{2} - 10^{3} \rightarrow <10^{1}$
Second	Facies changes (depositional)	Abandoned channel fill	$<10^{\circ}$
		Channel→levee	$>10^{2} \rightarrow 10^{1}$
		Channel→floodplain	$>10^{2} \rightarrow <10^{\circ}$
		Delta-front sandstones to mudstones	$\leq 10^{2} \rightarrow 10^{\circ}$
	Facies changes (diagenetic)	Delta front→distributary	$10^{1} \rightarrow 10^{2}$
Third	Interfacies	Channel base/margin	$\leq 10^{1}$ (variable)
Fourth	Intrafacies	Lateral accretion surfaces	$\leq 10^{1}$–$.5 \times 10^{2}$
		Changes in stratification types	------
		Diagenetic fronts/paleosols	$\pm 10^{3}$–$<10^{\circ}$

as partially to fully leached grains accounting for 5 to 40 percent of total porosity.

Quartz:feldspar:rock fragment ratios are not significantly different among the facies. However, type of predominant cement, percent secondary porosity, and grain size do vary, as outlined below.

Bioturbated delta-front sandstones are very fine grained. Quartz overgrowths and pseudomatrix are approximately equally abundant cementing agents; minor amounts of calcite and ferroan calcite are present. Secondary porosity occurs as partially leached feldspar grains and shale fragments.

Delta-front sandstones are very fine grained. Quartz overgrowths are the only volumetrically significant cement. Most porosity is primary intergranular space. Carbonate grain-replacement and cement are present in minor amounts.

Sandstones from the base of meandering distributary channel are coarser grained than the delta-front sandstones (very fine to medium sand size). Kaolinite fills primary and secondary pores; minor amounts of quartz overgrowths are common.

Sandstones from the top of meandering distributary channel are very fine to medium sand size and ripple laminated. Within laminations, pseudomatrix is abundant, and no other cements are volumetrically important. Between laminae, kaolinite fills primary and secondary pore space. Quartz overgrowths are nearly as abundant as kaolinite cement. Secondary porosity as totally leached grains is common.

Late-stage distributary channel sandstones are very fine grained. These samples have approximately equal amounts of pseudomatrix and kaolinite cement; carbonate grain replacement is common but not volumetrically significant. Metamorphic quartz, metamorphic rock fragments, muscovite, and biotite are much more common than in the underlying meandering distributary sandstones, suggesting a possible change in source area. Most porosity is primary intergranular pore space.

On the basis of the samples examined thus far, several trends appear. First, sand grains are larger in the meandering distributary

channel than in sands above or below. Second, carbonate cement is commonly observed in delta-front sandstones but is rare in distributary channel sands. Third, kaolinite is most abundant in the distributary channel sands and is rarely found in delta-front sandstones. Fourth, changes in the detrital mineral suite between upper distributary channel sands and distributary channel or delta-front sands below suggest a change in source area to a region in which metamorphic rocks were more abundant. Work in progress will test these interpretations and explore relations between detrital mineralogy, grain size, type and amount of cement, and permeability.

Permeability Characteristics of Ferron Retrogradation Sandstones

The permeability of each volumetrically important sandstone lithofacies and associated bounding elements was measured so that permeability structure, as well as facies geometry, could be input to gas reservoir models and pore-level network models. The numbers of permeability measurements taken and their distribution are presented in Table 3. No one distribution type (normal, log normal, and so forth) best fits all permeability measurements. In the following preliminary discussions, the various sample populations were first examined to determine how the measured permeability values were distributed. Statistical parameters and comparisons were computed on transformed data if populations were not normally distributed.

Permeability Groups

Permeability characteristics of the three dominant stratification types (contorted bedding, planar crossbedded, and trough cross-bedded) and associated bounding surfaces were investigated because these are the volumetrically most important components of the sandstone architecture. A comparison of permeability values and stratification types shows a close correspondence (Fig. 7; and Table 4). Contorted strata have low permeabilities, ranging from 19 to 406

Table 3. Permeability sampling locations and numbers of measurements.

Section	Transects	Measurements	Grid size	Spacing	Measurements
North Muddy Creek	29	1,474	40 × 40 ft	2 ft	441
			6 × 6 ft	4 inch	400
South Muddy Creek	14	705			
Picture Flats Canyon	15	916			

Table 4. South Muddy Creek outcrop permeability statistics.

Facies	No.	Mean permeability (md)	C_V	Range (md)
Distributary channel	226	249	106	0.12 – 1,638
Contorted bedding	28	115	77	19 – 406
Planar crossbedded	52	197	76	18 – 674
Trough crossbedded	92	409	77	31 – 1,638
Bounding elements	51	84	134	0.12 – 814

Grain size (phi)	No.	Mean permeability (md)	C_V	Range (md)
–1.0 (very coarse)	11	316	85	8 814
0.0 (coarse)	41	341	94	20 – 1,638
0.5 (med.–coarse)	72	376	65	24 – 2,194
1.0 (med.)	90	392	108	10 – 1,603
1.5 (fine–med.)	30	278	86	2 – 928
2.0 (fine)	76	165	79	0.12 – 558
2.5 (v. fine–fine)	18	114	70	6 – 271
3.0 (very fine)	25	58	136	0.26 – 406
4.0 (silt)	5	0.12	n a	n a

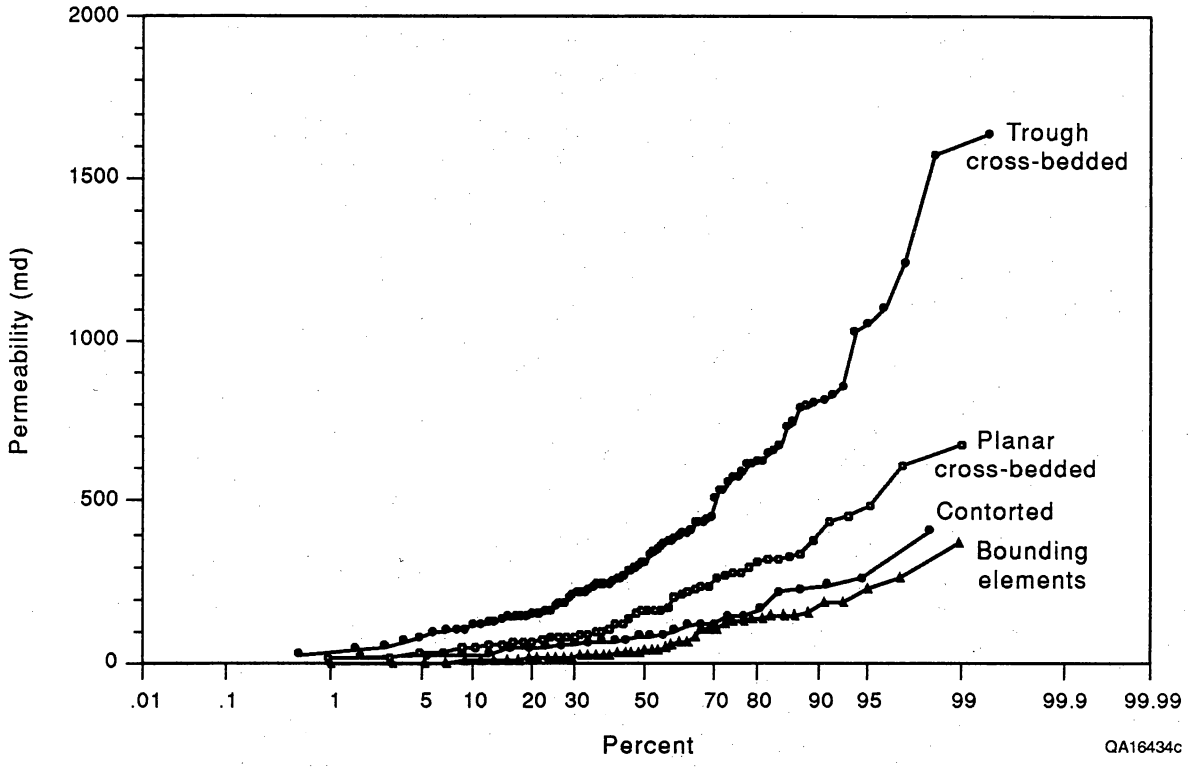

Figure 7. Cumulative permeability plot for trough crossbedded, planar crossbedded, and contorted strata, and for bounding elements. Plot is constructed from statistical data shown in Table 4.

md (mean = 115 md). Planar crossbedded strata have intermediate permeabilities, ranging from 18 to 674 md (mean = 197 md). Trough crossbedded strata are the most permeable and range from 31 to 1,638 md (mean = 409 md). Overall, the permeability histogram for the entire distributary channel complex best fits a log-normal distribution with a range of more than four orders of magnitude (mean = 297 md; Fig. 8).

Permeability Variation

F- and T-test results on transformed data indicate that although the permeability class of each group is significantly different (greater than 99-percent confidence level), considerable overlap exists. Much of the overlap between groups can be associated with grain size, sorting, and mineralogical variation. Grain size displays an interesting influence on permeability (Fig. 9 and Table 4). Permeability shows a predictable increase with increasing grain size from very fine through medium-grained sandstone. However, average permeability decreases as grain size increases beyond medium-grained sandstone. This trend is presumed to be due to the poor sorting and an increased presence of mud clasts, distorted into pseudomatrix, associated with these sediments. The presence of clay rip-up clasts, particularly within the trough crossbedded stratal type, causes a dramatic decrease in permeability. Thus, within each stratal type permeability also varies as a function of grain-size distribution. For example, in the planar crossbedded sandstones grain size ranges from fine to medium. As a result we observe within the planar crossbedded stratal type an increase in permeability with increasing grain size. However, in the trough crossbedded facies in general the opposite is true—increasing grain size results in decreased permeability.

Within each stratal type permeability variation is partitioned according to individual units. The coefficient of variation (C_v), defined as the ratio of the sample standard deviation to the sample mean, is used as an indicator of variability that is not sensitive to the sample mean. Figure 10 compares the C_v of permeability groups of different

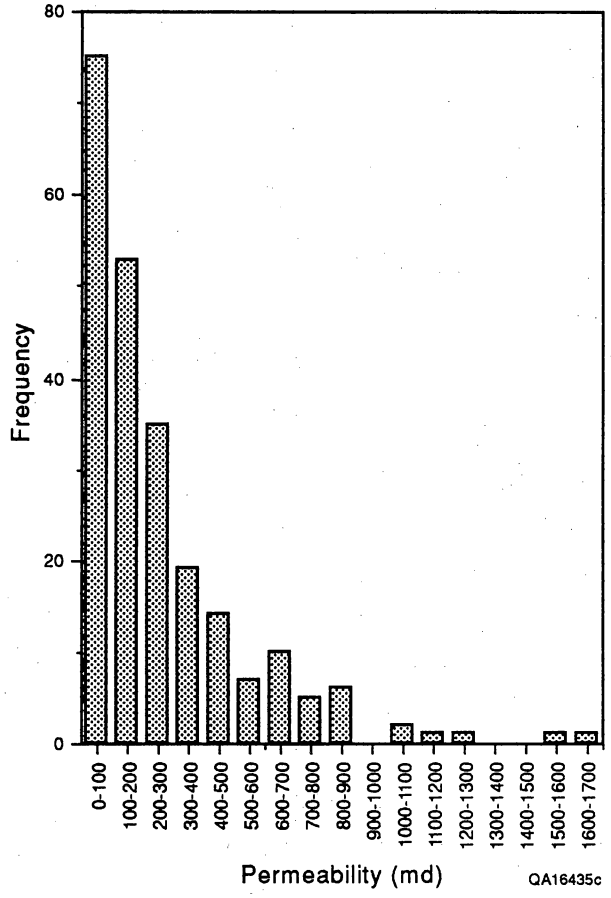

Figure 8. Permeability histogram for all samples from the South Muddy Creek distributary channel complex. The total of 226 measurements best fits a log-normal distribution.

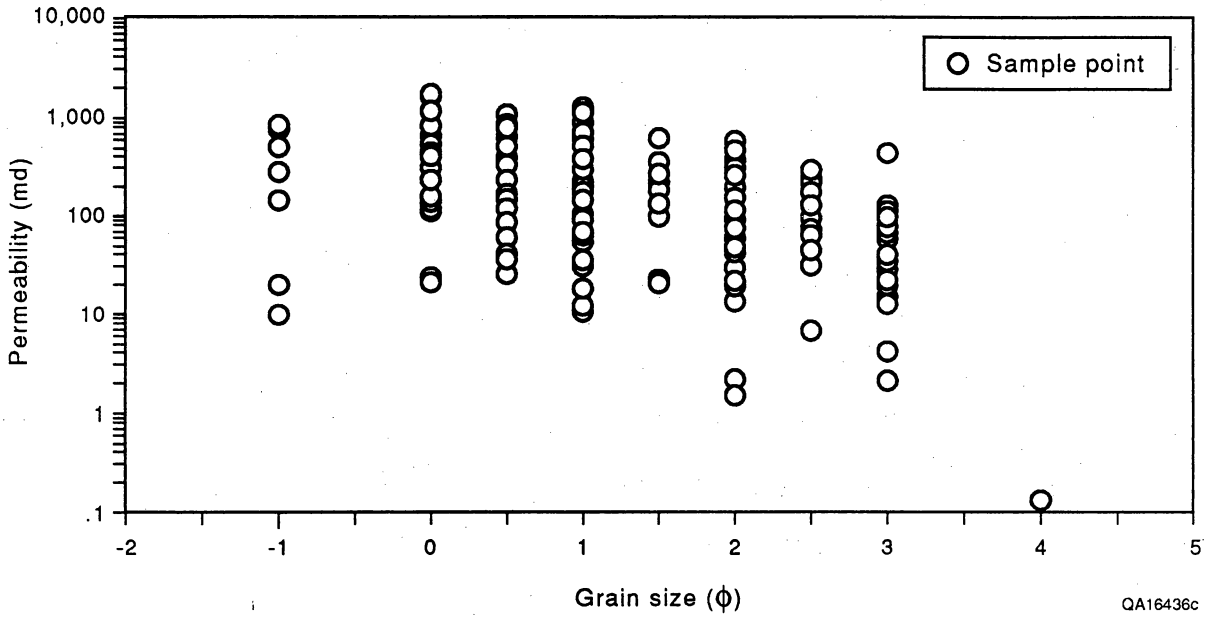

Figure 9. Plot of permeability values versus grain size for distributary channel sandstones. Plot is constructed from statistical data shown in Table 4.

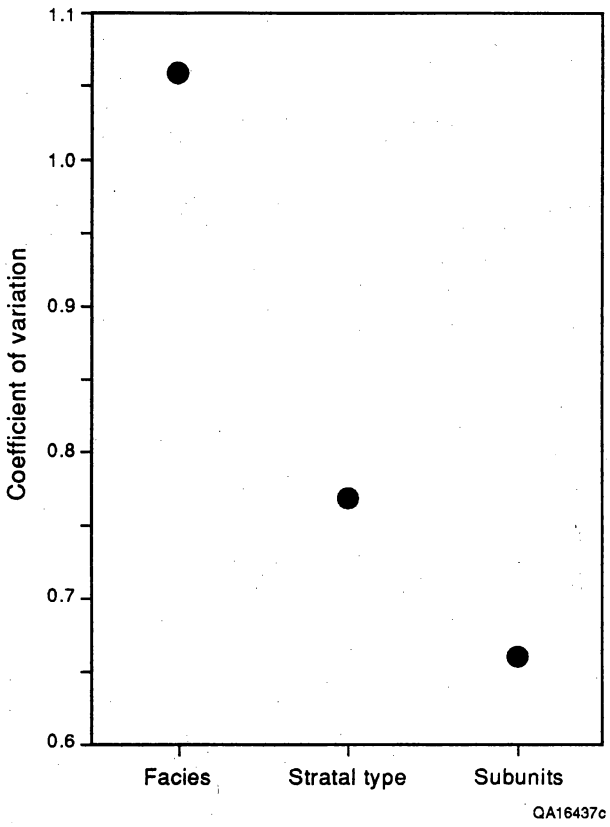

Figure 10. Plot of coefficient of variation (Cv) versus scale of sample group showing that variation decreases as the size of the feature being measures becomes smaller.

scales and shows that C_v decreases significantly when permeability measurements are disaggregated, first according to stratification type and then according to individual bedded units within stratal types. This indicates that the variability between lithological units is greater than within lithological units. Additionally, the C_v is relatively constant for the contorted, planar crossbedded, and trough crossbedded units, suggesting that sample standard deviation increases with sample mean.

Permeability Trends

Figure 11 displays an idealized vertical sequence and permeability profile for the meandering distributary channel complex in south Muddy Creek. Within the trough crossbedded lithofacies permeability displays an erratic but upward-increasing trend due to poor sorting and the presence of clay rip-up clasts in the lower part of the channel. The highest permeability zone within the distributary channel facies is associated with the medium-grained, trough crossbedded stratal type located within the middle to upper part of the channel. Several vertically increasing trends may be present due to the superposition of stacked channels. Permeability often shows a decrease across the boundary between the trough and planar crossbedded stratal types. In planar crossbedded sandstones an erratic upward-decreasing permeability profile results because of an upward decrease in grain size. Within this facies dramatic permeability decreases are associated with lateral accretion surfaces. In the contorted strata that cap the sequence, permeability is relatively uniform and often displays a slight increase relative to lower units. The lithologic and permeability characteristics of the Ferron stratal type are summarized in Table 5.

Permeability Correlation

To determine how far permeability values and distributions can be extrapolated in a reservoir model, two approaches were taken to examine the permeability structure. One method is visual correlation

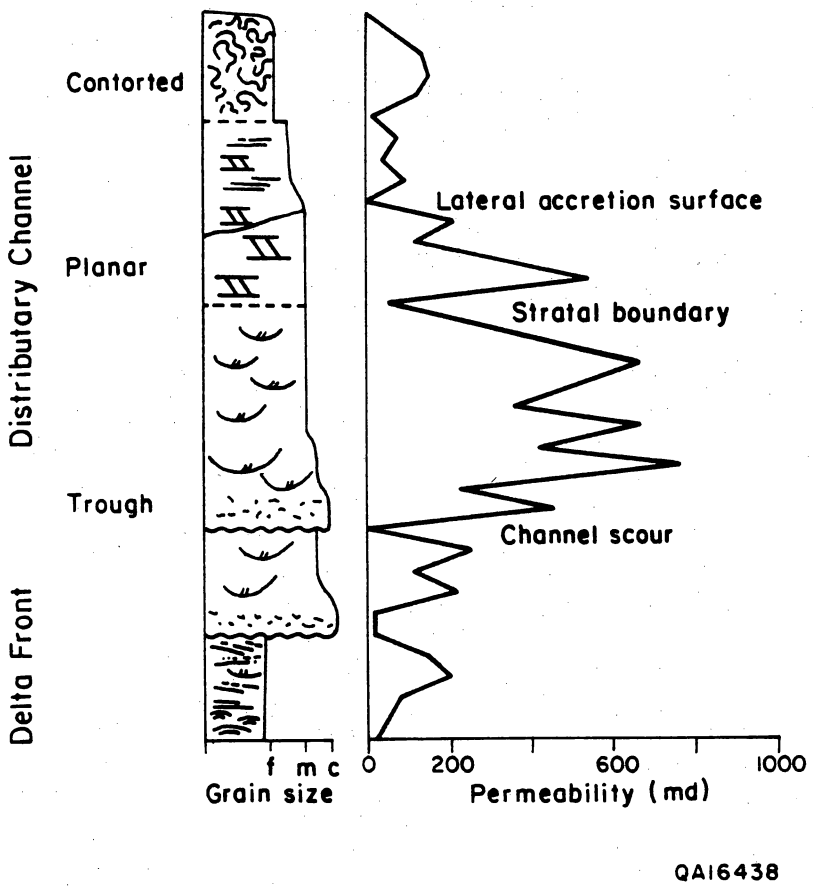

Figure 11. Idealized vertical sequence of depositional environments and stratification types, and corresponding permeability profile for delta-front and distributary channel sandstones in South Muddy Creek Canyon.

Table 5. Permeability characteristics of component facies.

Facies	Geological characteristics	Permeability characteristics
Contorted	Uniform grain size (vf–f). Bounding surfaces consist of silt or sand-on-sand contacts. Approximately 5 × 500 ft.	Low to intermediate permeability. Uniform profile. Variation due to bounding surfaces.
Planar cross-bedded	Upward-fining grain size (f–m). Sand-on-sand bounding surfaces. Approximately 10 × 750 ft.	Intermediate permeability. Erratic upward-increasing profile. Variation due to grain-size variation and bounding elements.
Trough cross-bedded	Upward-fining poorly sorted, grain size (m–vc). Clay rip-up clasts common along channel scour. Approximately 15 × 1,200 ft.	High permeability. Erratic upward-decreasing profile. Variation due to poor sorting and rip-up clasts.
Bounding elements	Occur as channel scours and lateral accretion surfaces. 100 to 400 ft in lateral extent and inclined 5 to 10 degrees.	Lowest permeability class, often one to two orders of magnitude less than associated facies.

of permeability profiles; the second involves application of the variogram technique. Both methods indicate the lateral and vertical continuity of zones with similar permeabilities.

Profile Correlation.—Stalkup and Ebanks (1986) and Dreyer and others (1990) used permeability profiles to evaluate the lateral continuity of permeability zones. This method can be used to visually compare the continuity of permeability profiles and see if any correlation exists with adjacent profiles.

Figure 5 is a cross section showing the lateral and vertical extent of lithofacies, bounding elements, and permeability from the South Muddy Creek window. Permeabilities were measured at 1-ft intervals along vertical transects spaced 120 to 160 ft apart. Adjacent profiles show similar trends of upward-increasing and -decreasing permeability relative to lithofacies boundaries, indicating that different stratal types are characterized by gross permeability layering. These permeability units can be traced over distances of 500 to 1200 ft.

Crosscutting elements, such as lateral accretion surfaces display good correlation across the cross section and disrupt lateral continuity within stratal types. Vertical profile trends indicate the stratal types are composed of permeability subintervals on the order of 1 to 5 ft thick. However, these subintervals displayed a very poor correlation between profiles. The limited degree of correlation of these subintervals indicates that permeability zones within stratal type are lenticular. Laterally, permeability displays an increasing trend toward the central part of the channel, particularly within the trough crossbedded stratal type.

Variograms.—Permeability variation in permeable media can be described by two components, correlation and randomness (Goggin, 1988). The variogram is a statistical tool used to estimate the spatial variability of a property such as permeability, that is, how laterally or vertically correlatable a given permeability measurement may be. It expresses the similarity or dissimilarity on average between data pairs some distance (h) apart. In particular, a variogram provides an estimate of the distance over which permeabilities are correlated, or alternatively, provides an indication of the absence of correlation in

the data. A variogram is calculated by summing the squares of the differences of all data pairs separated by a distance (h) and dividing this sum by the number of pairs. This value is then plotted on the ordinate of a graph, and the distance between pairs is plotted on the abscissa.

In this model the range of influence of a property is the distance at which the variogram function becomes constant (correlation ceases), and the sill is the value at which the function levels off (approximates the global sample variance). When $h = 0$ the variogram should approach zero, but when h is large enough so that the data are not correlated, the variogram approaches the sample standard deviation. In general, experimental variograms do not go through the origin, an effect known as the nugget effect. This effect may be attributable to (1) measurement error or (2) correlation on a distance smaller than the smallest lag distance.

Two grids were constructed to determine the spatial distribution of permeability according to stratification type and the nature of small-scale permeability variation. The largest grid (40 × 40 ft; 2-ft sample interval) was located to sample the three dominant stratification types: contorted bedding at the top, planar crossbedding in the middle, and trough crossbedding at the base (Fig. 12). A smaller grid (6 × 6 ft with sample interval of 0.33 ft) was located entirely within the planar crossbedded facies.

Figure 13 shows the horizontal variograms for the contorted, planar and trough crossbedded stratal type based on the 40 × 40 ft sampling grid. The results indicate that the range that permeability is spatially correlated (horizontally) depends on the stratification type. Within the planar and trough crossbedded facies permeability measurements were spatially related over a distance of 12 and 18 ft, respectively. However, in the contorted strata there is no apparent range of spatial correlation. Nearly all ordinate values in this facies approximate the total variance of the population. This observation may reflect the fact that primary depositional features that influence the permeability distribution have been highly disrupted.

A considerable amount of unexplained variation (nugget effect) exists within the experimental variograms. The nature of this

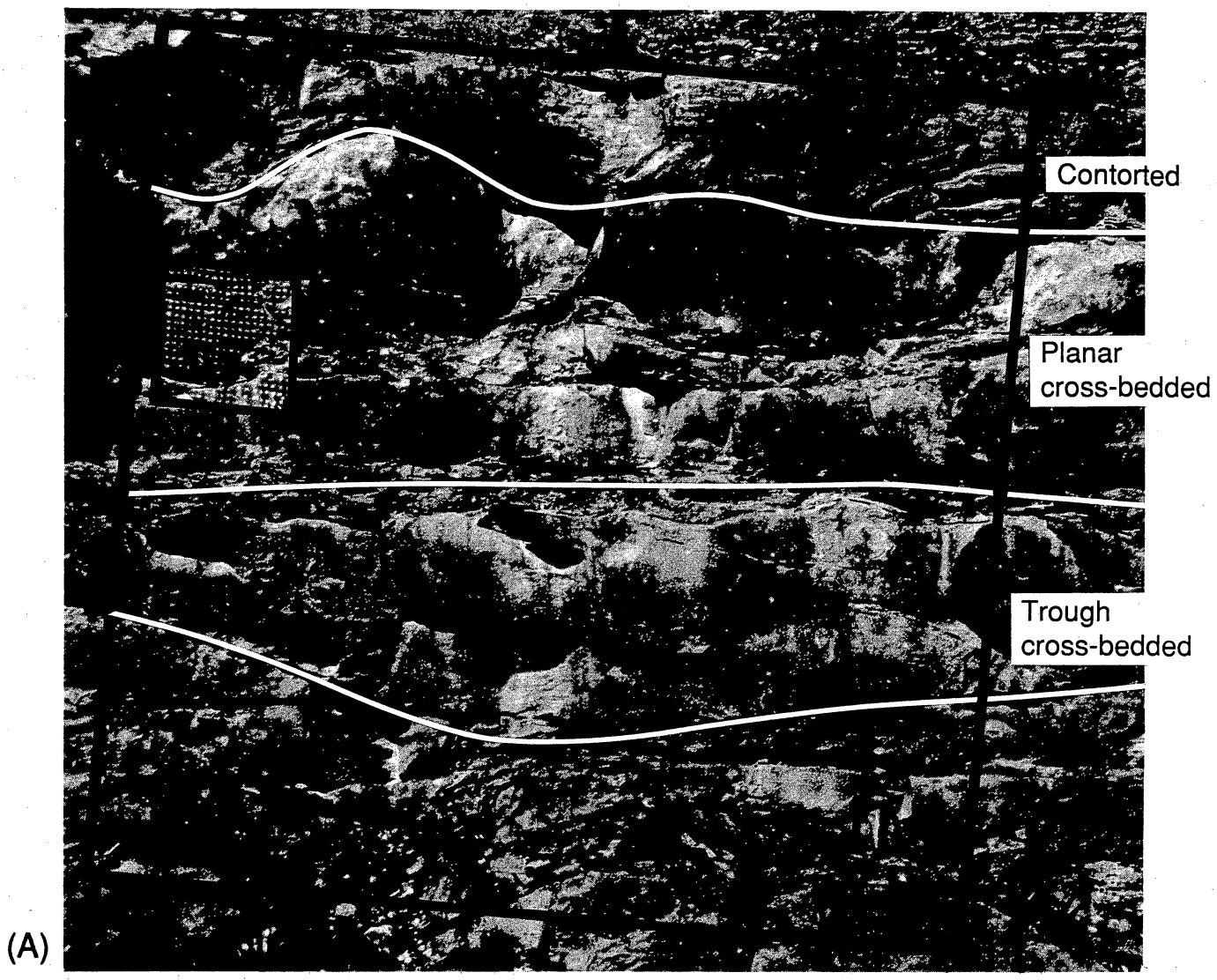

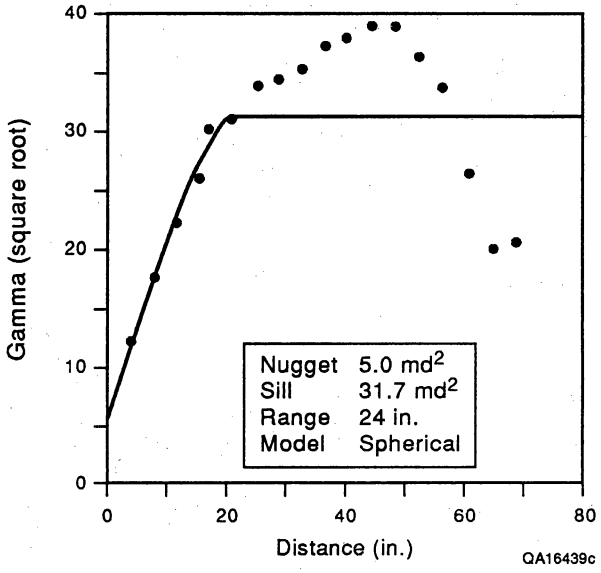

Figure 12. (A) Photograph of 40 × 40 ft grid and embedded 6 × 6 ft grid showing relations of stratification types and grid positions. (B) Horizontal semivariogram for measurements from the 6 × 6 ft grid showing a correlation length of approximately 2 ft.

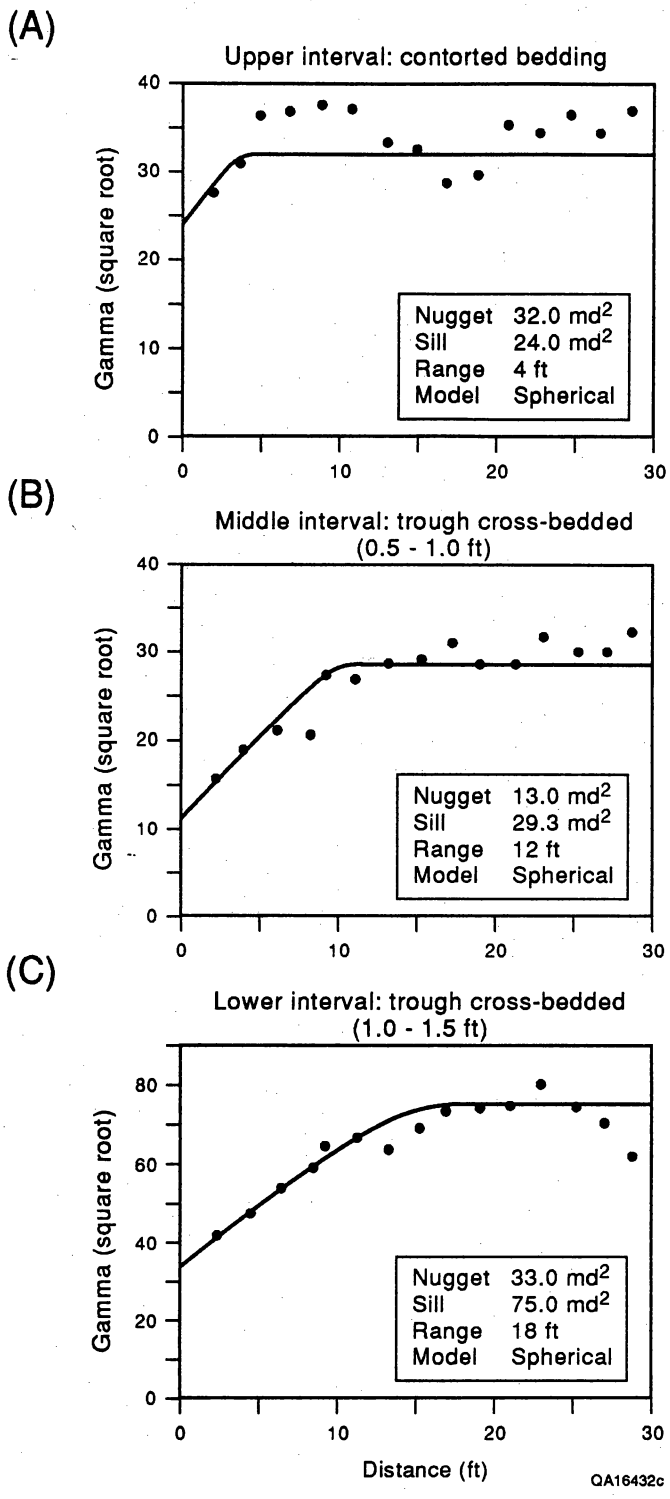

Figure 13. Horizontal semivariograms for permeability measurements on the 40 × 40 ft grid classified by stratification type: (A) Unit having contorted bedding has a correlation distance of approximately 4 ft. (B) Planar crossbedded unit has a correlation distance of approximately 12 ft. (C) Trough crossbedded unit has a correlation distance of approximately 18 ft.

variation was analyzed by refining the sample interval. At the smallest point spacing measured, the range of influence is reduced to 2 ft (Fig. 12). Given that the detailed grid was analyzed entirely within the boundaries of a planar crossbedded unit, this abrupt decrease in range indicates the permeability distribution is scale dependent.

Summary of Permeability Characteristics

Several generalizations can be made regarding permeability values measured in Ferron sandstones. We will continue to investigate all levels of permeability characteristics during future studies so appropriate values, relations, and distributions can be input into reservoir models. Evaluation of how these permeability attributes and distributions relate to gas mobility awaits further progress in the measurement of petrophysical properties and the pore-level modeling aspects of the project.

1. Permeability characteristics display a close correspondence to each of the three major stratification types. Highest permeabilities occur in the trough crossbedded stratal type, whereas lowest permeabilities are associated with bounding elements.
2. Within stratal type permeability variation is related to grain size, sorting, and mineralogy. Within a homogeneous lithology permeability is further partitioned between bedding units.
3. Vertical trends in permeability are predictable. Trough crossbedded strata display an upward-increasing trend, planar crossbedded strata display an upward-decreasing trend, and contorted strata display no trend.
4. Comparison of permeability profiles shows that permeability groups based on stratal types can be correlated over hundreds of feet. However, permeability subzones within stratal groups displayed little correlation at this scale.
5. Variogram analysis demonstrates the permeability structure to be dependent on stratal type and sampling scale. At a sampling

interval of 2 ft the trough crossbedded sandstone showed the greatest lateral correlation length (18 ft) and the contorted beds the least (less than 4 ft). Within the planar crossbedded strata lateral correlation length was dependent on the sampling scale. At a sampling interval of 2 ft the correlation length was 12 ft, whereas at a sampling interval of 0.33 ft the correlation length was 2 ft. This demonstrates the scale-dependent nature of the correlation length and suggests that the permeability structure may be fractal. This subject will be a topic of investigation in the second year of the project.

6. Highest permeabilities occur toward the central part of the channel and decrease toward the channel margins.

SIGNIFICANCE OF RESULTS AND APPROACH FOR THE 1991 RESEARCH YEAR

The first year of this study not only yielded a large amount of data, it also provided a test of whether our fundamental approach to the problem of carrying information from outcrop to gas reservoir and then to reservoir model is valid. On the basis of results obtained thus far, we think our general research strategy is sound and we anticipate only minor changes in our plan of investigation. The significance of first-year findings to the goals of this project and anticipated modifications to our methodology for the second and third years of work are described in the following sections.

Confirmation of Predictability of Architectural Elements

Analysis of the architecture of distributary and delta-front sandstones in this retrogradational deltaic system has demonstrated that depositional patterns can be defined on the outcrop. Delta-front sandstones are vertically heterogeneous but laterally continuous over typical gas well spacings. In contrast, the distributary system is characterized by both lateral and vertical heterogeneity and by spatial variation in geometric and dimensional attributes. Distributary sand belts are composite sand bodies composed of

amalgamated, laterally accreted point-bar sandstones. Landward in the distributary system sand belts display similar widths (1,200 ft) and are composed of thin and wide, laterally accreted, sigmoidally shaped point-bar sandstones. Apparent width-to-thickness ratios of the accretion-foreset-bounded sand bodies average 481. Seaward in the distributary system, accretion-foreset-bounded sand bodies are comparatively narrower but are twice as thick. Apparent width-to-thickness ratios average 211.

Because of the encouraging results obtained from the architectural analysis, we plan to continue this subtask during year 2 of the project.

Delineation of Hierarchy of Bounding Elements

A step toward the definition of effective seals in reservoir analogs is the delineation of the hierarchy of bounding elements that separate and bound analogous productive components. Bounding elements spanning four levels of variability from the depositional systems scale to the mesoscale (on the order of less than 10 ft) have been recognized. Preliminary results suggest that as the scale of the feature decreases so does does the effectiveness or ability of the surface or element to act as a reservoir seal. Great emphasis will be placed on the definition of geometric and petrophysical attributes of these bounding surfaces during the next 2 years of the project.

Diagenetic Effects on Petrophysical Properties

Work during the first year of this study concentrated on establishing the petrographic character of various facies and bounding elements. Our next major task is to seek out permeability anomalies within and between facies and to examine the sandstones to determine what causes the extreme variation in permeability that we have observed. This will be the main focus of petrographic studies during the second and third years of this study.

Permeability Structure

Progress has been made toward defining the flow units that compose the deltaic sandstones. Analysis of permeability structure indicates that stratal types define distinct permeability groups that are the basis for definition of flow units. Stratal types do have not discrete permeability values, however, as there is variation internally within each group as well as overlap between groups. This finding is consistent with the original concept of flow units as defined by Hearn and others (1984) and Ebanks (1987).

Variability within, and overlap between, these stratally constrained permeability groups will be investigated in more detail in year 2 of the project. Key concerns are whether the variability is random or structured and if the variability is structured whether the structure is a product of diagenesis, or alternatively, proximity to flow boundaries.

Scales of Permeability Variation

We plan to modify the sampling program to explore correlation lengths of permeability values in various lithofacies. First, based on results of examination of permeability variation in the detailed grid and in borehole core, we propose to reduce the vertical sampling interval to 3 inches to capture vertical permeability variation. Second, there are four potential options to address lateral permeability variation: (1) to adjust spacing between vertical profiles to correspond to geologic structure (to ensure that profiles intersect the same feature more than once) rather than arbitrarily spacing sections at 100- to 200-ft intervals; (2) to undertake large-scale grids with spacings every 10 ft on selected windows; (3) to halve the distance separating transects until appropriate correlation lengths are obtained; and (4) to measure permeability laterally between transects in key stratal types. Favored options at present are a combination of options (1) and (3). This combination will be tested during the first month of the 1991 field season on the Picture Flats window.

LABORATORY PETROPHYSICAL PROPERTY MEASUREMENTS

Jon Holder and K. E. Gray
Earth Sciences and Engineering Laboratory

INTRODUCTION

Activities during the first year of the experimental program have been directed towards the implementation, operational verification, and calibration of the facilities to be used for these measurements. Suites of measurements were carried out on specimens from five blocks of Ferron outcrop material, selected as representative geological facies, to assess the range of anticipated measurements and to determine the appropriate procedures to be used for the bulk of the experimental testing. In this section of the report, the laboratory measurement systems are described, results from the initial set of measurements on the five blocks of Ferron material are presented and discussed, and the test procedures and the anticipated sequence of laboratory activities during the second project year are outlined.

LABORATORY MEASUREMENT SYSTEMS

The bulk of the laboratory measurements for the testing program are being carried out in an apparatus being leased from the Earth Technology Corporation (TETC); a cross-sectional view of the triaxial vessel is given in Figure 14. It is a triaxial testing vessel with capabilities for simultaneous pore fluid circulation and measurements of permeability, electrical resistivity, and static and dynamic moduli, on triaxially-loaded 2 1/8 inch by 4 inch cylindrical test specimens. Axial load is applied by a hydraulic ram, collar-coupled to the pressure vessel. Differential axial load is indicated by the output of a load cell in series with the loading

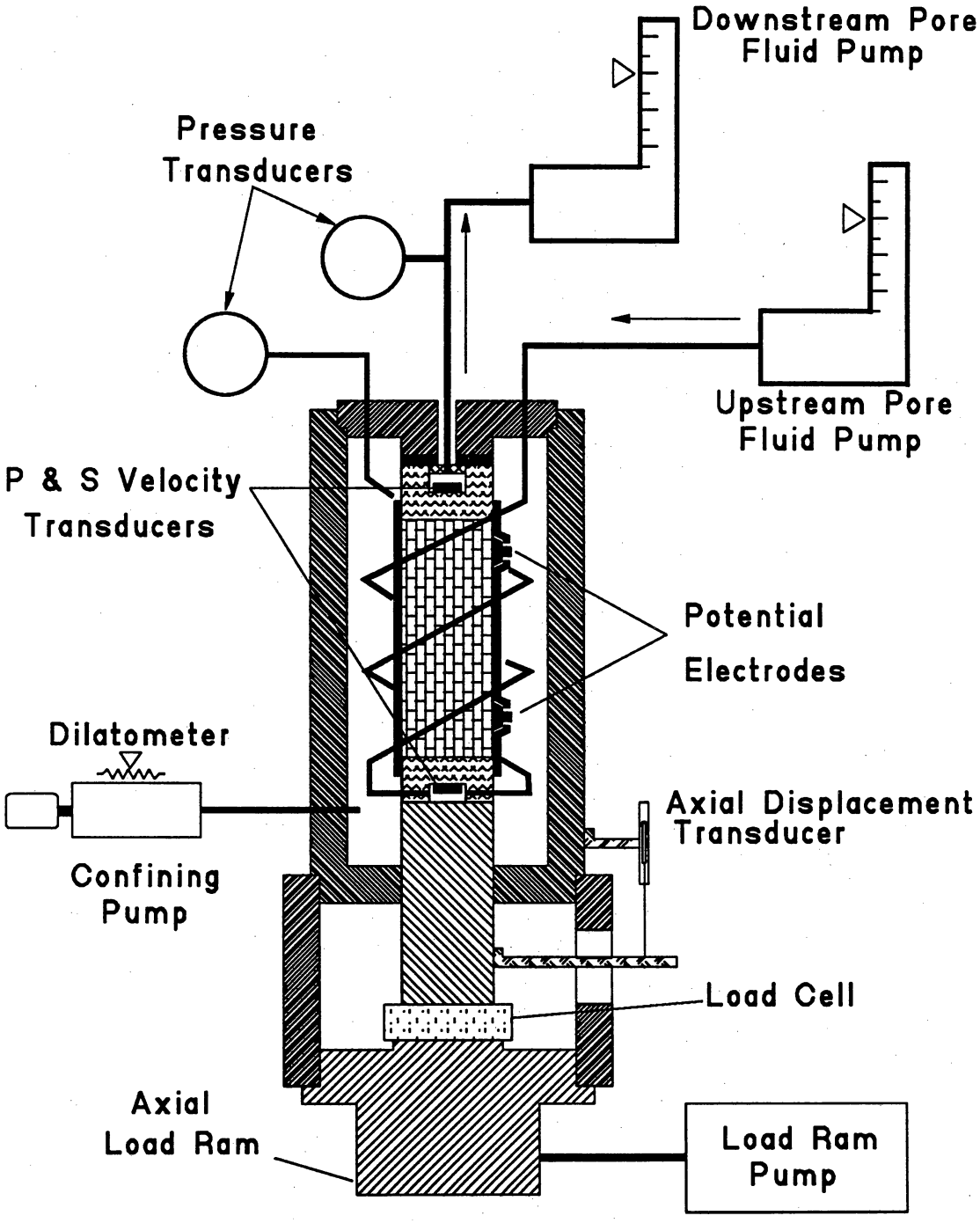

Figure 14. View of TETC triaxial testing apparatus, with liquid pore fluid circulation system.

piston. An in-line equalizer compensates for the axial force due to the confining pressure, and for the change in confining fluid volume due to the movement of the axial load piston into the vessel. Axial strain is determined from the output of a linear transducer connected between the vessel wall and the loading piston. Confining, pore, and load-ram pressures are applied by motor-driven syringe pumps. A linear displacement transducer is attached to the confining fluid pump to monitor changes in total specimen volume. Liquid pore pressure and circulation control is provided by separate motor-driven syringe pumps up- and downstream from the specimen, and the pressures are measured by independent up- and downstream pore pressure transducers. The calibrated indicators of pore fluid pump volume are used to monitor changes in pore volume or, for two-phase pore fluid flow, the relative saturation of the pore volume. Permeability measurements are carried out under constant flow conditions, using the up- and downstream transducers and direct measurements of fluid flow volumes; permeabilities as low as a few tens of nanodarcys can be measured in this system. All transducer outputs are input to a microcomputer-based data acquisition system, which also provides closed-loop servo-control of confining pressure, axial load, and up- and downstream pore pressure. The pore liquid syringe pumps also have internal provision for servo-control at a constant flow rate.

The heat-shrink teflon material used for jacketing the specimen is impermeable to both air and liquid; a light coat of silicone glue is applied to the outer specimen surface to prevent bypass of pore fluid between the jacket and specimen. The specimen end caps house ceramic transducers for the generation and detection of pulses for shear and compressional wave velocity measurements along the axis of the specimen. The top end cap is electrically isolated from the vessel in order that the end caps can serve as electrodes for the application of a uniform axial electric current in the specimen, for electrical resistivity measurements. The resistivity measurements are carried out in a four-terminal configuration, using the electrical feed-through contacts along the circumference of the specimen as the potential electrodes. An a-c phase-sensitive detection system

operating at a frequency of one kilohertz is used for the potential measurements, so that only the in-phase contributions from the resistive processes within the specimen are measured. The resistance of the specimen is determined directly by comparison with the potential drop across a calibrated standard resistance. Details of the specimen assembly and the measurement instrumentation for electrical resistivity determinations are given in Donath et al. (1988).

The permeability, k, in millidarcy, is determined from measured values of flow rates (Q, in milliliters per hour) and the differences (δp, in pounds per square inch) between the indicated pressures at the upper and lower ends of the specimen (length, l_S, in inches and cross-sectional area, A, in square inches):

$$k = \frac{K_p \cdot \mu \cdot l_s \cdot Q}{A \cdot \delta p} \tag{1}$$

where μ is the viscosity (in centipoise) and K_p is a constant (4.08 for the units used here). The temperature-dependent viscosity values for de-ionized water and 6% brine were taken from the measurements carried out in this laboratory. The formation factor, F, is determined from the measured sample resistance, R, in kilohms, the cross-sectional area of the specimen, the distance l_r, in inches, between the potential electrodes, and the pore fluid resistivity, rf, in ohm-meters:

$$F = \frac{25.4 \cdot R \cdot A}{l_r \cdot r_f} \tag{2}$$

Because of the in-line pressure equalizer in the TETC system, the differential axial stress (total stress minus confining pressure, p_C) is given directly by the ratio of the indicated load cell output to the cross-sectional area of the specimen. Axial strain is given by the ratio of the specimen length change, indicated by the axial displacement transducer output, to the specimen length the measurement pressure. Corrections for apparatus distortion with

axial load and confining pressure are applied to the displacement transducer outputs; standardized procedures for the determination of the correction factors in triaxial deformation apparatuses are described in Donath and Güvin (1971). Again because of the confining fluid equalizer, the change in total specimen volume is equal to the change in indicated confining fluid volume (after correction for apparatus distortion due to axial load changes), and the volumetric strain is the ratio of this volume change to the initial specimen volume. The static Young's modulus, E_S, is the slope of the axial stress-strain curve, and Poisson's ratio, σ_S, is the ratio of radial strain (one half of the volumetric strain minus the axial strain) to axial strain.

The transit times for the calculations of the compressional and shear mode wave velocities, v_p and v_S, are determined from oscilloscope readings of the time interval between the input pulse initiation at the top of the specimen and the first indication of signal arrival at the bottom transducer. This total travel time is then corrected for the propagation time of the wave through the end platens of the apparatus; the determination of the travel time corrections is discussed in the following sub-section. The dynamic Young's modulus, E_d, is determined, in millions of pounds per square inch, from

$$E_d = 1.35 \times 10^{-2} \cdot \mathrm{P}\, v_s^2 \cdot \frac{(3\, v_p^2 - 4\, v_s^2)}{(v_p^2 - v_s^2)}, \tag{3}$$

where P is the specimen density, in grams per milliliter, and the numeric factor is to accommodate velocities expressed in thousands of feet per second. The dynamic Poisson's ratio, σ_d, is determined from

$$\sigma_d = \frac{(v_p^2 - 2\, v_s^2)}{(v_p^2 - v_s^2)}. \tag{4}$$

In addition to the TETC measurement system, several other systems are used in the program of studies for supplementary measurements, particularly during this initial phase of apparatus

configuration and system calibration. Reference zero-pressure brine permeability measurements are frequently carried out in benchtop permeameters, one designed for one-inch diameter plugs and the other for two-inch diameter test specimens. The two-inch diameter permeameter chamber can accommodate specimens up to 2 1/8 inches in diameter, and several of the permeameter measurements were carried out on the same test specimen used in for testing in the TETC system. Permeability, deformation, and deformation measurements have been carried out at various confining and pore pressures in a Simultaneous Property System (SPS), a triaxial testing apparatus with provisions for radial pore fluid flow through two-inch diameter cylindrical test specimens (Evans, 1973).

A significant part of the activities during the first year of this project has been the design, construction, and calibration of ancillary pore-fluid system components for nitrogen circulation through the specimen, for simultaneous measurements of petrophysical properties in partially saturated specimens. The flow diagram of the two-phase flow system is shown in Figure 15. The flow of dry nitrogen from a nominal 2,000 psi tank is controlled and metered by a control unit, prior to its introduction into the specimen. For two-phase flow measurements, the nitrogen is saturated under pressure with water in the humidifier. Brine is supplied at a constant flow rate by the upstream pore fluid syringe pump. The water-saturated nitrogen and the brine flow through separate lines to the lower specimen end platen, and the fluids flow independently to the pore-fluid supply input at the center of the platen. The two fluids are mixed and flow together through the system of spreader ports in the bottom assembly, before they travel into the specimen. The air/brine mixture flows from the specimen to the separator vessel, from which separate lines connect nitrogen and brine to their respective downstream metering and back-pressure regulation systems. The brine flows into the downstream syringe pump operating at the

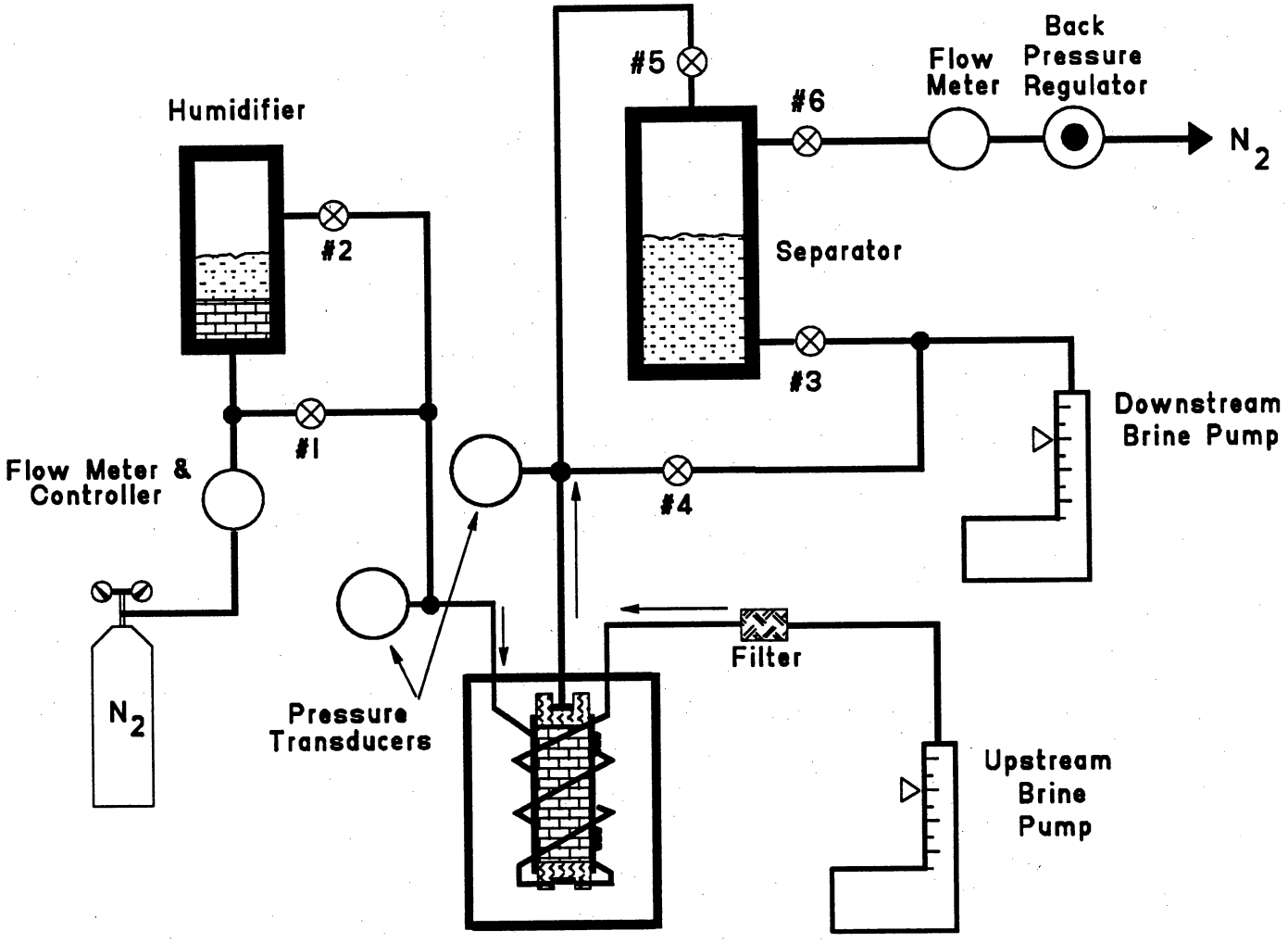

Figure 15. Two-phase pore fluid system.

same flow rate as the upstream brine pump. An electrical sensor in the separator vessel is used to maintain the fluid volume at a constant level, and the variations in brine saturation in the pore volume is determined by the indicated up- and downstream pump volumes. The downstream gas flow is routed through a flow meter calibrated for water-saturated nitrogen, and then to a gas back-pressure regulator which determines the downstream pressure for both nitrogen and brine. The indicated valves #1 - #6 provide for single-phase flow of dry nitrogen, water-saturated nitrogen, or brine through the specimen, for the determination of absolute permeabilities.

RESULTS AND DISCUSSION

The first-year laboratory activity has been directed towards apparatus calibration, verification of system performance, and a preliminary survey of material behavior for representative Ferron outcrop samples. The specific objectives of these measurements were:

1) apparatus calibration;
2) documentation of measurement resolution and system accuracy;
3) survey of anticipated material response; and
4) determination of appropriate test conditions.

The survey measurements were carried out for liquid (brine and de-ionized water) saturated specimens. Apparatus shakedown tests and system calibration measurements were carried out with circulation of de-ionized water, brine, dry nitrogen, water-saturated nitrogen, and nitrogen/brine mixtures through the pore fluid system.

The test material for this phase came from five blocks of Ferron sandstone. Material descriptions for the five blocks are given in Section A of this report. The block designations are:

Block #1 - Shore face;
Block #2 - Bioturbated;
Block #3 - Cross-bedded;

Block #4 - Ripple laminated; and

Block #5 - Top of upper channel.

Specimens of Sciota sandstone, a fine-grained quarry sandstone from Ohio, were also used for some of the system shakedown tests; this material has been extensively tested in other projects within the laboratory, and provides a useful standard for characterization of permeability and mechanical property measurements. Specimens were cored in the laboratory from blocks of either the Ferron or Sciota sandstone, and the specimens ends were ground flat and parallel in a lathe. For all liquid-saturated tests, the specimens were evacuated and then saturated in a desiccator prior to installation in the test apparatus.

Preliminary Shakedown Tests

Initial permeability measurements were carried out for three specimens from Block #1 of the Ferron outcrop. This shore face deposit was used for the shakedown tests because its permeability was expected to be intermediate between the 'reservoir' and 'seal' flow units. Permeability measurements were carried out in the benchtop permeameter, at nominal atmospheric conditions, and in the TETC apparatus at several pressures up to an effective pressure corresponding to a depth of 10,000 feet. In addition, the formation factor was determined from the electrical resistivity measurements carried out in the TETC apparatus. Both brine and de-ionized water were used as the pore fluid for these initial measurements. Permeability measurements were also carried out on two specimens of the Sciota sandstone, in the benchtop permeameter and in the TETC unit.

Results for these initial tests are summarized in Table 6. In this and all subsequent tables, the tabulated entries for each specimen are listed in the chronological order in which they were measured. All specimens were nominal two-inch diameter cylinders,

Table 6. Permeability and resistivity shakedown tests.

Spc #	Por (%)	Pc (kp)	Pp (kp)	k (md)	F	Pore Fl.	App
Ferron Block #1							
3	15.4	0.2	0.0	7.1		Brine	Prmetr
2	15.4	0.2	0.0	7.2		Brine	Prmetr
				4.5		D-I Wtr	
4	16.5	4.0	3.8	10	10	D-I Wtr	TETC
		4.0	3.0	9	7		
		4.0	2.0	10	9		
		2.0	1.0	10	6		
		2.0	1.8	11	6		
		0.3	0.1	11	7		
4A	16.5	0.3	0.1	11.2	19.1	Brine	TETC
		1.2	1.0	11.4	18.7		
		2.0	1.0	11.4	20.2		
		0.2	0.0	12.0			
4A	16.5	0.2	0.0	10.8		Brine	Prmetr
				7.6		D-I Wtr	
Sciota							
1	19.2	0.2	0	2.5		Brine	Prmetr
1	19.2	0.3	0.1	2.5		Brine	TETC
		1	0.8	2.2			
		2	1	2			
		1.1	0.1	2.1			
2	19.3	1.1	0.1	2.8		Brine	TETC
		2	1	2.7			
		4	1	2.6			
		6	1	2.4			

approximately four inches in length. Specimen 4A was a four-inch section cut from specimen number 4, and the orientation of the axis, and hence the flow direction, of test specimen 4 was perpendicular to that of specimens 2, 3, and the specimen used in the SPS System. The agreement between brine permeabilities determined independently for specimen 4 in the TETC and bench-top permeameter provides a quantitative indication of the reliability of permeability determinations in the TETC apparatus.

Over the range of pressures considered there are only minor variations in permeability and formation factors with pressure. There is an indication of some permeability reduction with time, a likely consequence of compaction. There is a significant variation between brine and de-ionized water permeabilities, and the formation factors for de-ionized water are highly variable and significantly lower than those for brine. It is likely that these variations are associated with the clay content in the material, and all subsequent measurements in the program utilize a 6% brine solution, for a pore fluid with a reasonable electrical conductivity and minimum interaction with expandable clays.

The indicated agreement between permeabilities determined for the Sciota materials with the TETC and bench-top permeameter gives further support for test system accuracy. Earlier permeability determinations for specimens taken from the same four- by eight- by one-foot quarry block as the specimens included in Table 6, carried out in connection with other in-house programs (unpublished), have an average value of 2.5 millidarcy.

The apparatus transit time corrections for velocity measurements are generally determined from measurements of total travel times through test specimens with known wave velocities. This procedure was carried out using a steel calibration specimen in the TETC apparatus, but a supplementary test was also used to verify the travel time correction. In this procedure a set of velocity measurements was carried out for three different confining pressures, first in a four-inch long Sciota sandstone, and then in a 2.6 inch-long specimen segment which was cut from the original specimen. The apparatus travel times for the shear and

compressional mode waves are corresponding values extrapolated to a zero specimen length. The calibration results for the TETC system, shown in Figure 16, yield well-behaved values for the two travel time corrections, which are more precise and more accurate than those determined from the steel calibration specimen.

Several shakedown tests for static and dynamic moduli determinations were carried out using Sciota sandstone specimens, to document measurement system reliability by comparison with the large body of existing in-house measurements on this material. The results from one of the Sciota sandstone tests, at several pore and confining pressures, and for one of the Ferron specimens from Block #1, at two confining pressures, are summarized in Table 7. The previous static measurements of Young's modulus and Poisson's ratio, at confining and pore pressures of 4 kpsi and 2 kpsi, respectively, average to 3 Mpsi and 0.15, respectively, in good agreement with the Table 7 data. The representative stress-strain data for two separate deformations of a Ferron Block #1 specimen shown in Figure 17 illustrate that the measurement system is very repeatable, and that measurement resolution is adequate for quasi-elastic moduli determinations in which axial strains are confined to less than 0.2 percent to avoid dilatant behavior. Previous dynamic modulus measurements for this block of Sciota sandstone were not available for comparison. The velocity measurements in the TETC system were very repeatable between different tests on the same specimen (± 0.1 %) and different specimens (± 1 %) of the same material, and, based on the trends seen in the data for both Sciota and Ferron material in Table 7, we feel confident in the reliability of the dynamic measurements.

Survey Measurements

All of the specimens of shore face (Block #1) material were used in the preliminary shakedown tests, the results from which are

Figure 16. Travel time variations with specimen length for Sciota sandstone.

Table 7. Shakedown tests for moduli measurements in the TETC apparatus.

TEST PRESSURE		STATIC MODULI		DYNAMIC MODULI	
Confining (kpsi)	Pore (kpsi)	E (Mpsi)	P.R.	E (Mpsi)	P.R.
Ferron Block #1:					
6.0	1.0	3.80	0.10	5.3	0.22
2.0	1.0	3.00	0.22		
Sciota Sandstone:					
1.1	0.1	2.2	0.14	3.6	0.26
2.0	1.0	2.3	0.17	3.5	0.26
4.0	1.0	2.8	0.15	4.0	0.24
6.0	1.0	3.2	0.18	4.3	0.24

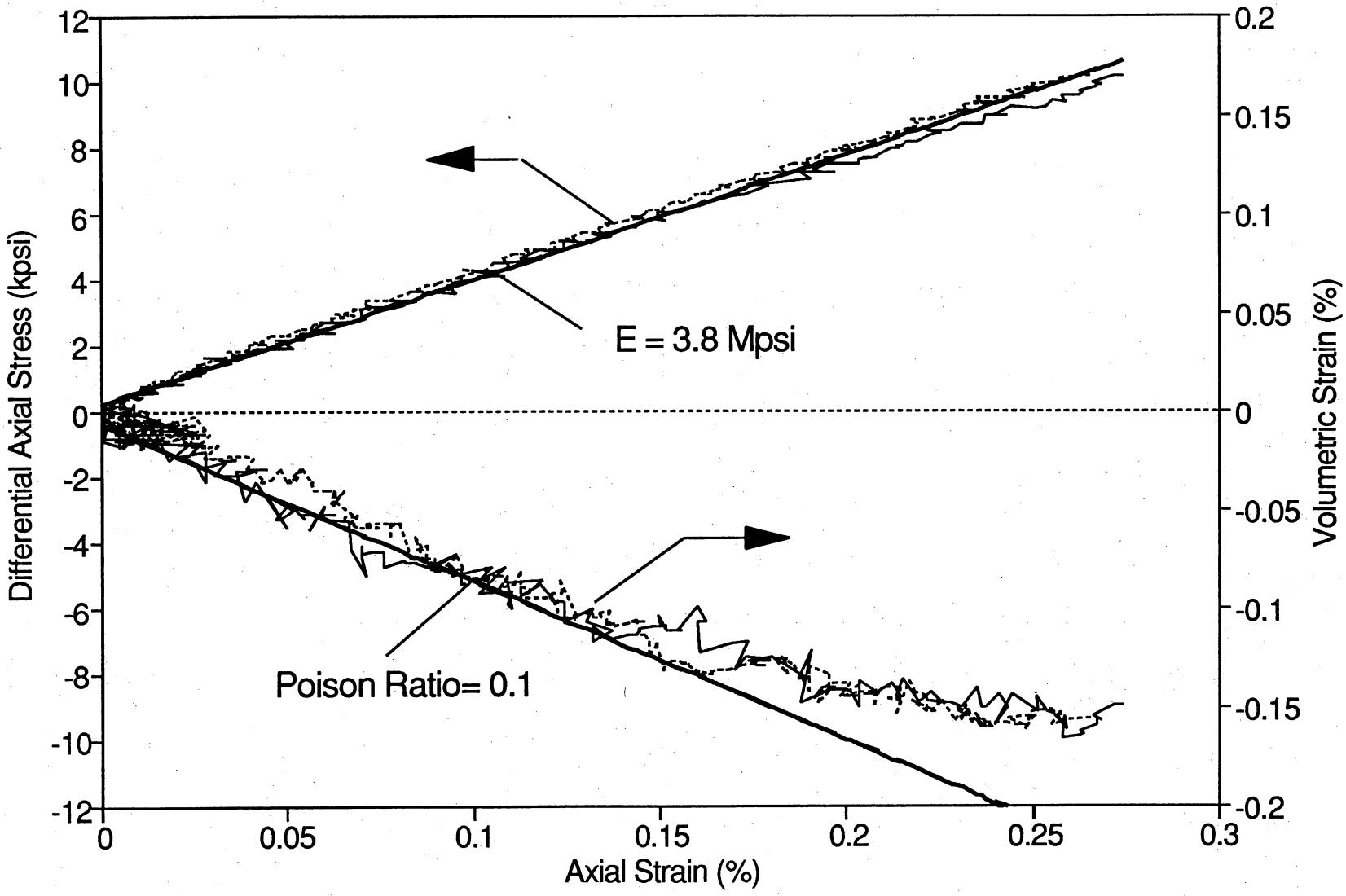

Figure 17. Static deformation test results for Ferron Block #1–4. Pc = 6 kpsi, Pp = 1 kpsi.

summarized in Tables 6 and 7. Following these shakedown tests, the following sets of survey tests were carried out on specimens of the remaining four initial blocks of Ferron material. With exceptions as noted, the survey tests included porosity, permeability, formation factor, and static and dynamic moduli measurements at nominal bench-top, reservoir, and one or two intermediate test pressures. All these survey tests were carried out for brine-saturated specimens. Results from the tests are summarized in Table 8.

The bioturbated material (Block #2) was characterized by numerous void spaces with dimensions ranging from sub-millimeters to over one centimeter. These voids present a significant problem in the preparation of the triaxial test specimens, because their presence on or near the specimen wall invariably leads to jacket rupture. Specialized specimen preparation procedures, in which surficial void spaces are filled with a sealing material prior to jacketing, were developed to minimize the rupture problems in future testing. Unfortunately Block #2 contained only enough material for the preparation of three specimens, all of which were at least partially contaminated with oil from the confining fluid system prior to the completion of testing. The only successful set of measurements for this material, which are included in Table 8, were those of permeability and formation factor under nominal atmospheric conditions. It is important to stress that this material is very heterogeneous over dimensions similar to the test specimen size; the formation factor in particular is probably very sensitive to the spatial relationships of potential electrodes and large-scale voids. If material of this nature is encountered in the main body of material for the laboratory measurement study, it will be necessary to carry out a number of measurements, using different electrode arrangements on the same specimen and using different test specimens, in order to quantitatively assess the variability and to determine suitable average values.

The cross-bedded material of Block #3 is considerably less permeable than that of either of Block #1 or #2; its formation factor is significantly higher, and its porosity significantly lower, than that

Table 8. Summary of Ferron Block #2 – Block #5 test survey results.

Spc #	Por. (%)	Pp (kpsi)	Pc (kpsi)	Perm. (md)	F	E(st) (Mpsi)	E(dy) (Mpsi)	PR(st)	PR(dy)	Apparatus, Flow Orient.
BLOCK #2: Bioturbated										
1	11.6	0.1	0.3	6.7	26.8					TETC
BLOCK #3: Cross-Bedded										
3	11.1	0.1	0.3	0.15	28.5	1.6	3.5	0.24	0.32	TETC,
		1.0	4.0	0.13	24.0	2.0	3.5	0.30	0.32	Parallel
		1.0	4.0	0.10	28.7	2.5	4.0	0.21	0.31	
3	11.1	0.1	0.3	0.15						"
2	14.4	0.0	0.1	0.13						Prmetr., Perpen.
2	14.4	0.1	0.3	0.15	25.1					TETC, Perpen.
3	11.1	1.0	1.1	0.08	34.5	2.0	4.6	0.27	0.30	TETC, Paral.
		1.0	4.0	0.08	38.7	2.2	4.9	0.18	0.26	
BLOCK #4: Ripple Laminated										
1	16.1	0.1	1.1	0.59	25.5		2.9		0.34	TETC,
		0.1	3.1	0.49	23.3		3.5		0.33	Parallel
		0.1	5.1	0.43	21.3		3.9		0.31	
		1.0	6.0	0.40	22.2	3.3	3.9	0.17	0.30	
		1.0	4.0	0.35	21.0	3.0	3.6	0.22	0.32	
		1.0	2.0	0.40	20.2	2.3	3.0	0.27	0.33	
2	15.7	1.0	6.0	0.04	28.7	2.0	4.1	0.15	0.26	TETC, Perpen.
3	15.9	1.0	6.0	0.05	29.9					"
		1.0	2.0	0.06	24.4					
4	15.9	0.0	0.1	0.16						Prmetr., Perpen.
5	16.1	0.0	0.1	0.45						Prmetr., Paral.
BLOCK #5: Top of Upper Channel										
2	18.8	0.1	0.3	25.9	14.0					TETC, Perpen.
3	17.9	0.1	0.3	91.2						TETC,
		0.1	1.1	74.2	18.6	1.4		0.23		Parallel
2	18.8	1.0	1.1	5.1	14.4	1.5	4.5	0.23	0.10	
		1.0	2.0	4.1	14.5	1.5		0.32		"
		1.0	6.0	4.7	18.0	2.6	4.4	0.12	0.22	
4		0.0	0.1	76.5						Prmetr., Paral.
5		0.0	0.1	61.5						Prmetr., Perpen.

of the Block #1 material. The limited amount of data for the permeabilities and formation factors do not indicate a strong dependence on effective stress, as shown in Figure 18, although there is a trend towards decreasing permeability and increasing formation factor with effective stress. The moduli, shown as a function of effective pressure in Figure 19, also do not vary substantially with measurement pressure, although it is important to note that modulus measurements were not carried out for the nominally unconfined state. Laminations were clearly evident in this material, and there appeared to be a preferential orientation plane for the laminations. However, the cross-bedding is apparently significant even at the scale of specimen dimensions, because none of the properties listed in Table 8 exhibit a strong anisotropy. The final set of results listed for specimen number 3 in Table 8 were determined after the sample had been triaxially deformed in two earlier sets of tests, and it is likely that the somewhat lower permeability and higher formation factor values listed for this test are consequences of the cumulative non-elastic deformations in the earlier tests.

The Block #4 material exhibited the greatest degree of permeability and formation factor anisotropy of all material tested in this initial survey, and the permeabilities of specimens for which flow was perpendicular to the laminations of dark, clay-filled layers had the lowest permeabilities. The permeabilities for flow parallel to the predominant direction of lamination in the block are still lower by an order of magnitude than those for the shore face material, although the porosities and formation factors of the two materials are similar. The permeabilities and formation factors show no strong dependence on test pressure, as indicated in Figure 20. The moduli variations with pressure, shown in Figure 21, are more substantial.

The Block #5 material, from the top of an upper channel, is a very poorly cemented, high-porosity material. Its fragile nature is reflected in the considerable scatter in permeability values listed in Table 8. The change of more than an order of magnitude in permeability is likely to be the result of sand-grain re-arrangement during the modest deformations used for the static moduli

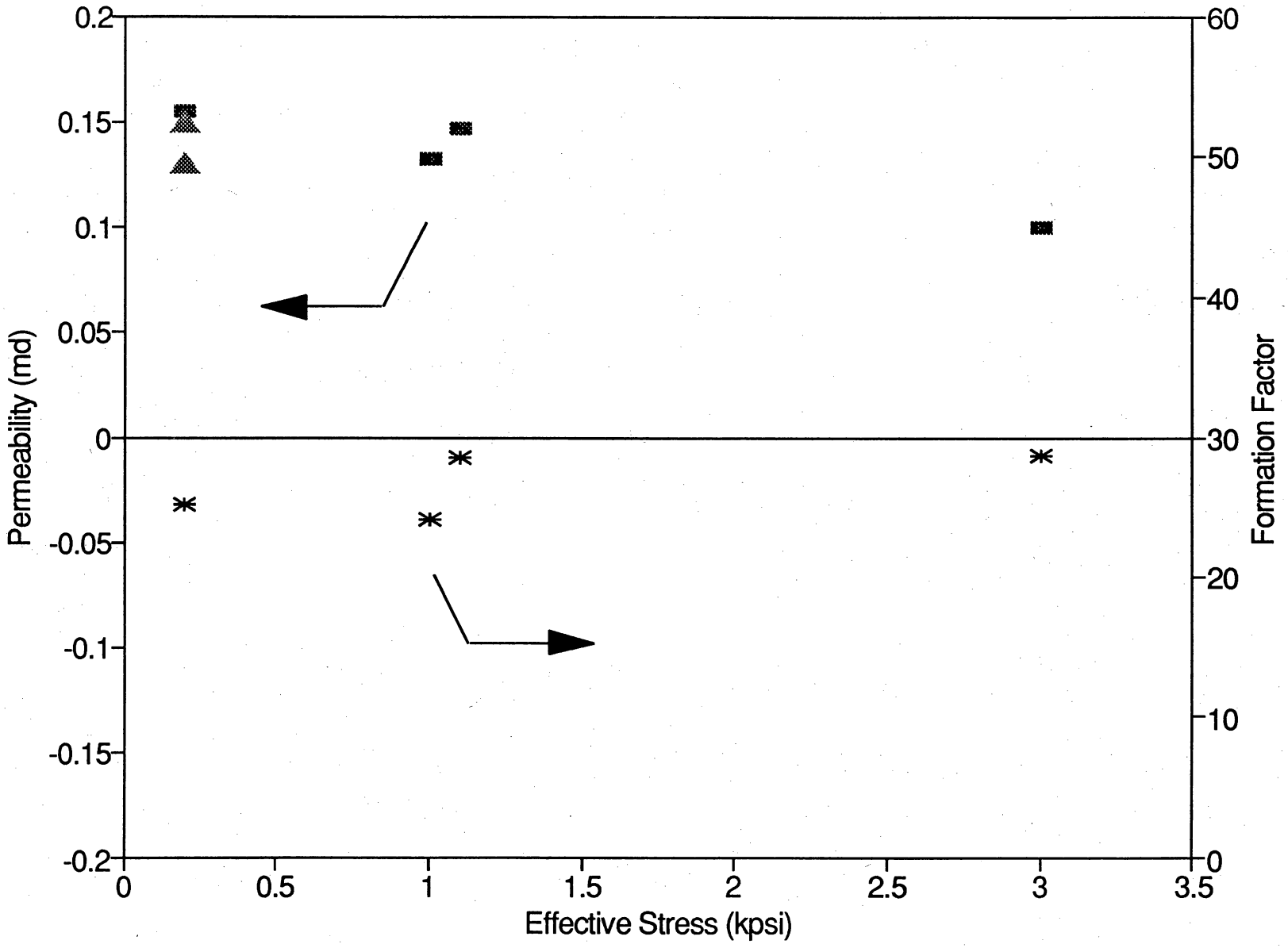

Figure 18. Effective stress dependence of permeability and formation factor in Block #3 (crossbedded) material.

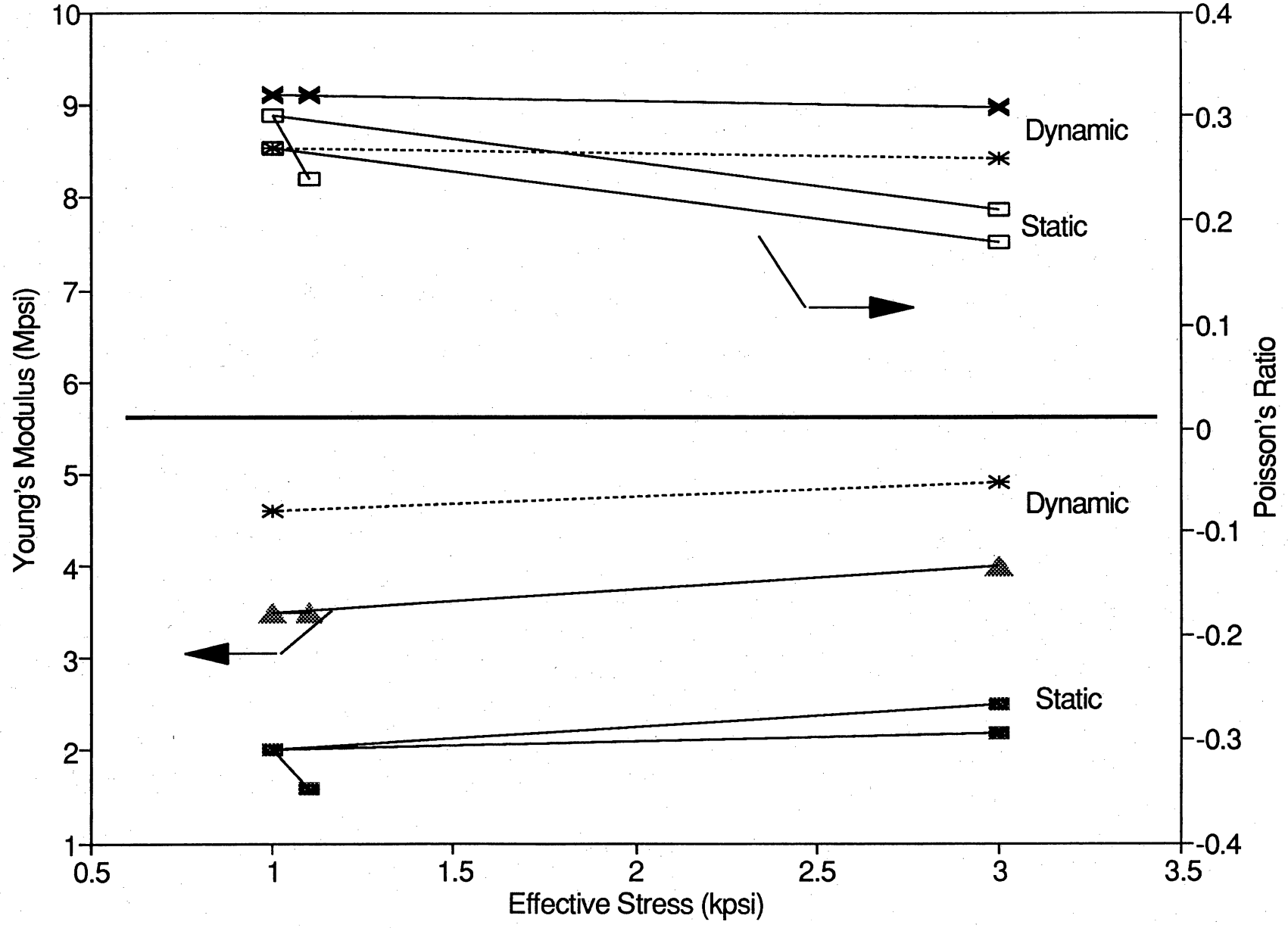

Figure 19. Effective stress dependence of moduli in Block #3 (crossbedded) material.

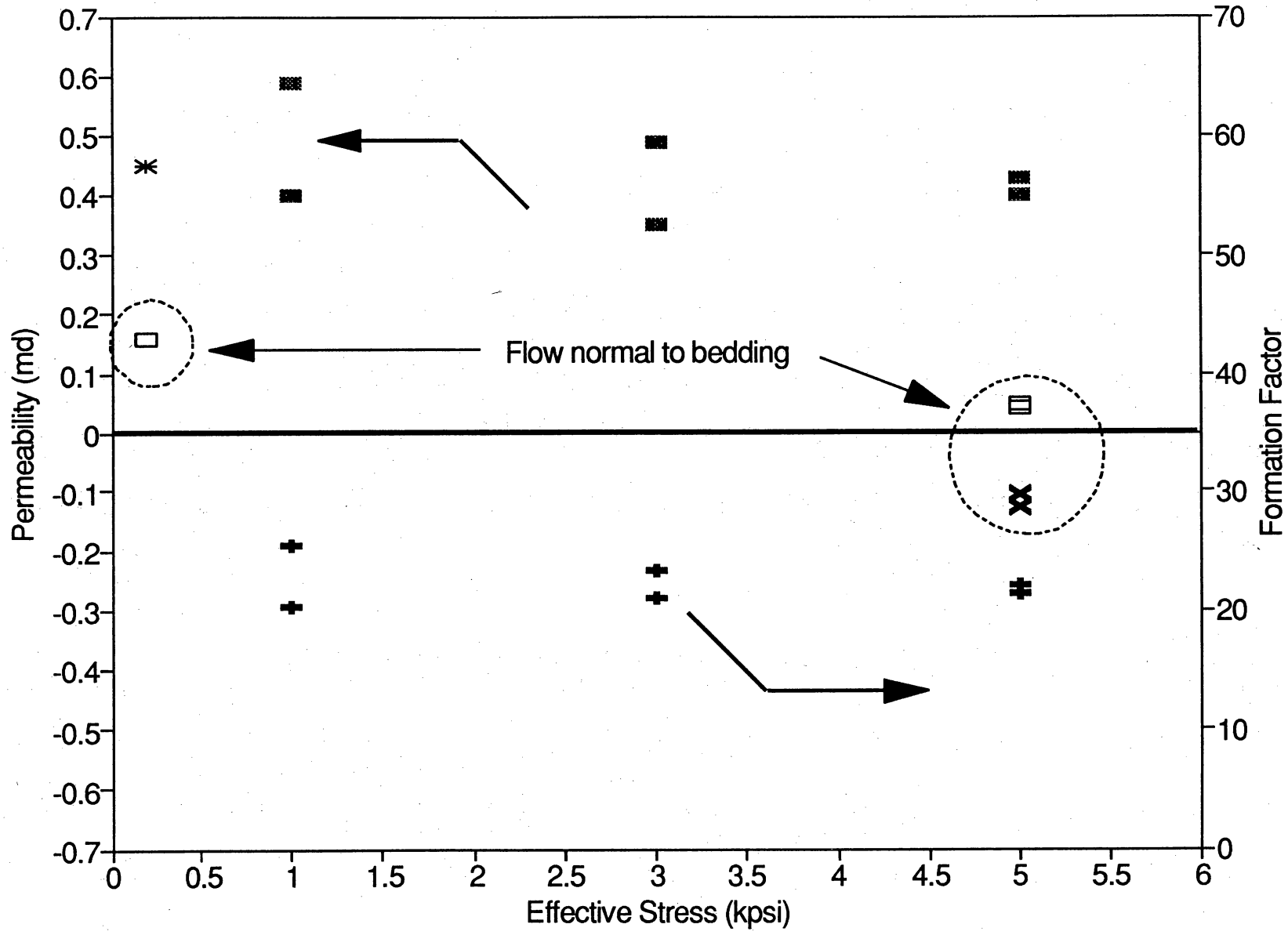

Figure 20. Effective stress dependence of permeability and formation factor in Block #4 (ripple laminated) material. Values correspond to flow parallel to laminations except where noted.

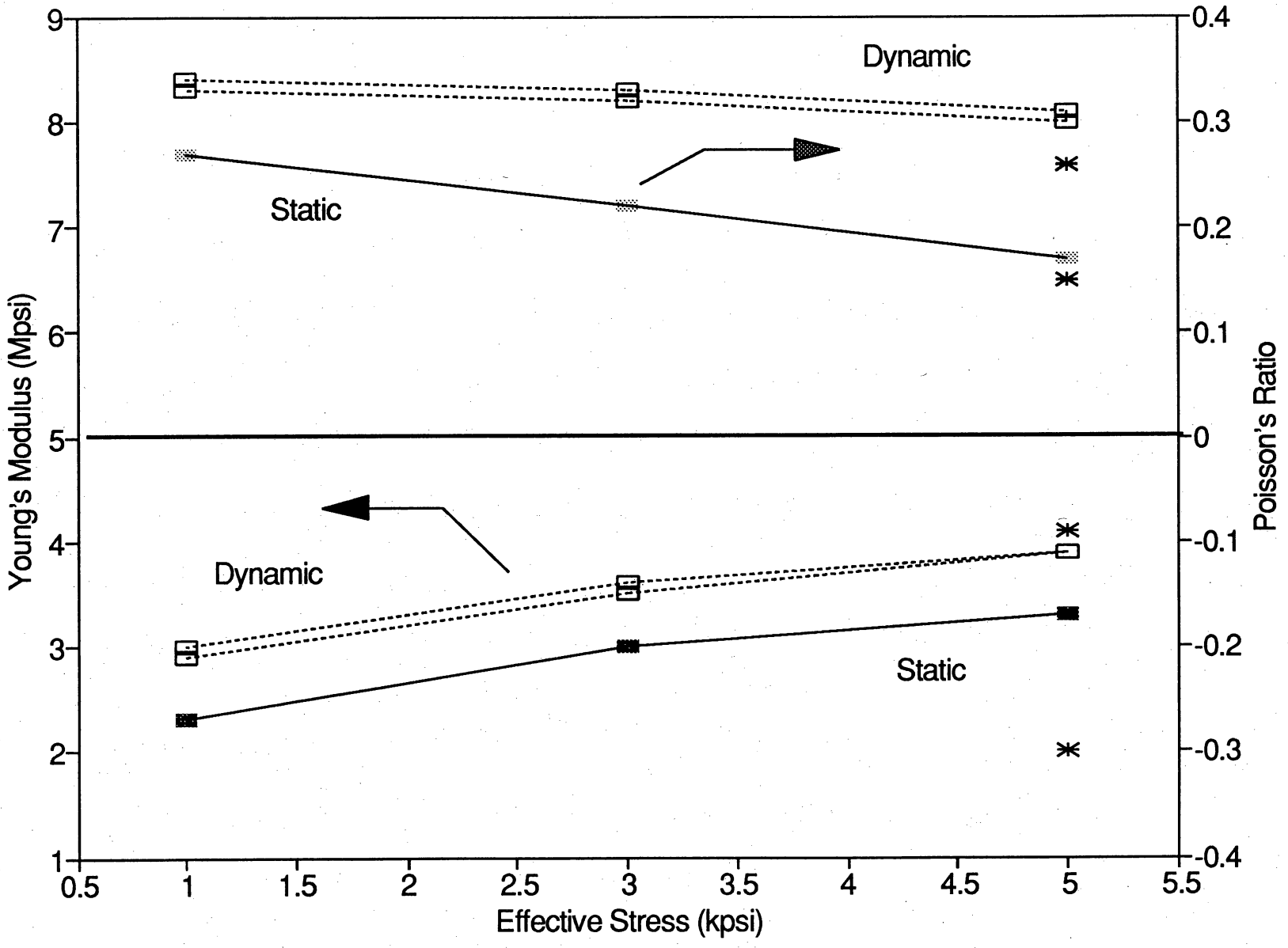

Figure 21. Effective stress dependence of moduli in Block #4 (ripple laminated) material. Values indicated by * are for specimen axis normal to laminations.

measurements; the second set of tests for specimen number 2 were determined following an initial set of deformations during the first test set. If this is the case, the material is very sensitive to non-hydrostatic deformations, since the maximum axial strain used in the initial set of deformations was less than 1%. Unfortunately there was not sufficient Block #5 specimen material to confirm this behavior, but subsequent testing will be carried out on similar material in the batch of blocks gathered for the next phase of measurements.

The time- and pressure-dependent trends noted for the Block #1 shakedown tests are generally found in all the survey measurements. Namely: 1) the permeabilities and formation factors show only minor variations over the range of pressures utilized; 2) all the measured properties give some indication of compaction during the course of the tests; and, 3) beyond this time variation, the data generally follow an effective stress behavior. A summary of averaged values for tests on the five initial blocks of Ferron material is given in Table 9. Two entries are listed for Block #4, corresponding to flow parallel and perpendicular to the laminations, and for Block #5, corresponding to the undeformed and deformed specimen behavior.

Also listed in Table 9 are average values of minipermeameter readings carried out by the BEG, on the same blocks from which the laboratory test specimens were taken. The overall trends in laboratory and minipermeameter results are consistent with one another, and, in the low-permeability cases, the statistical spread in minipermeameter data overlaps the laboratory data. The laboratory results are consistently lower than the minipermeameter averages, however, and are below the indicated statistical spread for the high-permeability materials. The discrepancy is not of major consequence; the values show the widest variation for very high permeabilities, where both the minipermeameter and laboratory measurements indicate that these facies are well into the regime of flow units. Attempts to resolve the remaining differences between minipermeameter and laboratory measurements will be carried out over the next year. In particular, minipermeameter measurements

Table 9. Averaged values from survey laboratory measurements on brine-saturated Ferron material, and minipermeameter measurements on the blocks from which the laboratory specimens were taken.

	Porosity (%)	k(brine) (md)	k(miniprm) (md)	F	E(st) (Mpsi)	E(dyn) (Mpsi)	PR(st)	PR(dyn)
BLOCK #1: Shore Face	15-17	11.5	25 +/- 6	19.3	3.8	5.5	0.1	0.2
BLOCK #2: Bioturbated	11-12		22 +/- 36					
BLOCK #3: Cross-Bedded	11-14	0.14	0.5 +/- 1.2	26.6	2.5	3.7	0.2	0.3
BLOCK #4: Ripple Lamin.	16		0.5 +/- 0.5					
Parallel flow		0.44		22.3	3.3	3.9	0.20	0.30
Perpendicular flow		0.05		27.7	2.0	4.1	0.15	0.25
BLOCK #5: Upper Ch. Top	18-19		315 +/- 94					
Undeformed		75		18.6	2.6	4.5	0.15	0.2
Deformed		5		15.6				

will be carried out on the test specimens used for the laboratory tests.

Two-Phase Flow Measurements

The system diagramed in Figure 15 is fully operational, and the necessary calibrations for nitrogen- and nitrogen/brine flow have been carried out. Shakedown tests were repeated, using nitrogen and nitrogen/brine flow in one of the Block #1 specimens used in the initial brine-saturated shakedown tests. The measured absolute permeabilities, static moduli, and shear wave velocities are the same, within the scatter of experimental measurements, for brine and nitrogen saturated specimens; the compressional mode velocity for the brine-saturated specimen is larger than that for the nitrogen-saturated specimen by approximately 10%. Several measurements carried out with dry and water-saturated nitrogen show no discernible variation with moisture content.

ANTICIPATED SECOND-YEAR ACTIVITIES

Twenty three blocks of Ferron material have been obtained, and the full suites of simultaneous petrophysical property measurements will be carried out on specimens from these blocks during the second year of the project. We anticipate that approximately twenty additional blocks will be added to this material, and the combined sets of measurements on this material will comprise the bulk of laboratory measurements to be carried out; the first of the test specimen measurement suites is underway. For each of the specimens a matrix of tests will be carried out, which has been established on the basis of the survey measurements described above. The test matrix is described in the following discussion.

The pressurization and circulation of pore fluid, particularly a gas, is considerably less complicated for pressures lower than 2,000 psi, while some elements of fluid flow measurement and analysis are simplified for pressures greater than a few hundred psi. The survey measurements indicate that the permeabilities and formation factors

in the Ferron material are relatively independent of confining pressure, and the somewhat larger variations in moduli follow an effective stress law. Accordingly, the body of laboratory measurements in the remainder of the program will be carried out using a pore pressure of approximately 1,000 psi, and a confining pressure of approximately 6,000 psi. This effective pressure corresponds to an underground depth of about 10,000 feet, which is representative of Texas Gulf Coast reservoirs that are of ultimate concern to the program. As indicated in the discussion of the initial shakedown tests, a 6% brine solution will be used as the pore liquid for all tests.

The network modeling activity requires laboratory petrophysical property data as a function of pore fluid saturation. Because of the times required for equilibration and measurements at each test condition, we anticipate that measurements will be carried out for only three to four levels of saturation for each specimen. The saturation values must include the gas or brine saturated end limit, for absolute permeability determinations. Although the absolute permeability should be independent of the fluid type, permeability determinations will be carried out using both nitrogen and brine flow. This provides for two independent permeability determinations, and for the measurements of dynamic moduli for saturations with two different fluids. In addition to the measurements at the two saturation conditions, the data set will include measurements for at least three partial saturation values: irreducible water and residual air saturations, because these values are experimentally convenient to determine, and one intermediate saturation value involving the simultaneous flow of both fluid phases. With minor variations, the following test procedures are being used for the simultaneous laboratory measurements.

In order to carry out the absolute gas permeability determinations, the measurements commence with a dry specimen. Preliminary measurements have given no indication of variations of gas permeability with gas humidity, and test specimens will begin at room-humidity conditions. The initial gas permeability is determined following an overnight equilibration period, during

which several pore volumes of dry nitrogen are flowed through the specimen. Dynamic moduli measurements are carried out during the saturated nitrogen flow. At least for the first few specimens, the flow of dry nitrogen will be followed by a period of water-saturated nitrogen. The system valving (Figure 16) is such that this change can be made without interrupting the pore fluid flow, and provides a direct indication of any variations in permeability or flow meter performance due to water vapor content in the circulating gas.

The nitrogen-saturated measurements are followed immediately by the brine-saturated measurements. This sequence facilitates the determinations of saturation values by mass balance. The saturation procedure is as follows. The upstream brine pump is pressurized and stabilized, and the initial indicated volume of brine in the pump is recorded. The pore downstream pore fluid line, which is on the top of the test specimen (Figure 16) is disconnected at its junction to the pressure vessel. A vacuum line is attached, and the specimen and the upstream pore fluid system up to the valve connecting the (pressurized) upstream brine pump are evacuated for approximately one hour. The gas humidifier is valved out of the pore fluid system. The valve to the upstream pump is opened, and, with the downstream (specimen top) end of the pore fluid system still being evacuated, the upstream pump injects brine at a rate of 20-80 milliliters per hour into the bottom of the test specimen. This process is continued until a stead flow of brine is observed coming into the (transparent) vacuum line at the top of the specimen. The brine injection is stopped and the vacuum line is removed; the volume of pore fluid remaining in the line is carefully measured. The downstream pore fluid line is re-connected, and, with the separator vessel valved out of the pore fluid system, the system is pressurized (to the same pressure as used for the initial pump volume measurement), stabilized for approximately one hour, and the final pump volume is recorded. The pore volume, and initial brine volume in the specimen, is given by the difference between initial and final pump volumes, minus the measured volume of fluid remaining in the vacuum line and the (calibrated) volume of the pore fluid components used during the saturation.

When the specimen saturation is complete, the downstream brine pump is valved into the pore fluid system and pressurized, and flow of brine through the specimen commences. After the flow has stabilized, absolute permeability, dynamic moduli, and electrical resistivity measurements are carried out on the brine saturated specimen. The specimen resistivity measurements serve as the reference values for subsequent saturation exponent determinations. Samples of brine are extracted downstream from the specimen near the conclusion of the brine-saturated measurement sequence, on which resistivity measurements are carried out. This resistivity reflects alterations in pore fluid chemistry that may take place within the specimen, and is used for all formation factor determinations for the specimen.

At this point the system is prepared for two-phase flow. Typically, the upstream brine pump is refilled and the downstream pump is emptied. Brine flow through the brine-saturated specimen is resumed, and, while maintaining the brine flow, the separator and gas humidifier vessels are valved into the system. The system is stabilized, the level of the air-brine interface in the separator is adjusted to the reference value, and the initial volumes of brine in the up- and down-stream pumps are recorded for use in subsequent determinations of brine saturation. Nitrogen flow is initiated, and rates of nitrogen and brine flow are adjusted so that the pressure drop across the specimen remains below approximately 10% of the mean pore pressure; the gas flow is also restricted to values less than that calculated for the onset of turbulent flow in the pores. When the system stabilizes, gas and brine relative permeabilities, the formation factor, and the dynamic moduli are measured. The magnitude of the brine saturation is determined from the indicated volumes of the up- and down-stream brine pumps, together with the initial pump volumes. If the system stabilizes within a few hours, a second set of flow rates are used to set up another level of partial saturation. For each period of stable flow, permeability, resistivity, and dynamic moduli measurements are carried out.

Following the two-phase flow measurements, brine flow from the upstream pump is stopped, the nitrogen flow rate is re-adjusted.

When the system re-stabilizes, at irreducible water saturation, the set of permeability, resistivity, dynamic moduli, and brine saturation determinations are carried out. Nitrogen flow is then stopped, and the brine flow is restarted. Flow is continued until the system is stabilized, at residual gas saturation, typically overnight. The set of permeability, resistivity, and dynamic moduli are carried out. After this suite of measurements is completed, a triaxial deformation is carried out to determine the static moduli of the specimen at residual gas saturation. The static moduli are not sensitive to the partial saturation value, and one set per specimen should provide an adequate description of mechanical behavior.

At the conclusion of the suite of measurements on the specimen in the triaxial vessel, the partially-saturated specimen is removed and weighed. The specimen is then fully re-saturated with brine and re-weighed, to determine the specimen density and to confirm the initial estimate of specimen porosity from the mass flow calculations.

PORE-LEVEL MODELING FOR SCALING PETROPHYSICAL PROPERTIES

Mark Miller
Center for Petroleum and Geosystems Engineering

INTRODUCTION

The ability of a reservoir rock to act as either a seal or flow unit depends upon more than simply gas permeability. Potential reservoir seals may be fully saturated with water at native reservoir conditions, but drain water and become permeable to gas when certain threshold capillary pressures are reached. Drainage relative permeabilities can dramatically alter the effective permeability of a rock during water drainage. Imbibition relative permeabilities control the rate of water influx and the amount of subsequent trapped gas. In addition, detailed petrophysical evaluation of reservoir rocks ultimately depends in large part upon well log measurements, the most important of which is the evaluation of water saturation through electrical logging.

Because the more complex petrophysical properties are so expensive and time-consuming to measure, it is not likely that a sufficient number of these measurements will ever be made in a single reservoir that is statistically significant. These measurements are not likely to even cover the entire range of rock types that are present in a given reservoir. A key objective of this project is thus to develop transformation functions between gas reservoir petrophysical properties (including porosity, permeability, cementation factor, saturation exponent, capillary pressure, and relative permeability) and geologic heterogeneity structure in fluvio-deltaic reservoirs. Defining the variability of petrophysical properties both within and between different rock facies is necessary for reservoir modeling studies to optimize operational strategies for gas reservoirs. One important aspect of how this research program is different from others in the past is that we are focusing on the variability of a large number key petrophysical data.

The premise of this work is that geologic information can be related to petrophysical properties through the use of pore-level network models. These models, which simulate transport and storage properties of porous media at the pore scale, provide a theoretical link between pore structure and petrophysical measurements. It is our hypothesis that pore-level simulators which have been "tuned" to replicate a large number of simultaneous petrophysical property measurements can then be used to develop transformation functions for generating theoretical statistical distributions of the important petrophysical properties both within and between rock facies.

By having statistical distributions of petrophysical properties, it will then be possible to begin to address the scale-dependence of these properties in order to define effective reservoir-scale properties. This task will be accomplished by simulating volumes of rock within which petrophysical properties of interest are distributed according to the transformations developed in this study.

APPROACH

Our first year's work has been to develop and test a pore-level simulator for use in this study. The model is largely complete, with the exception of validation of relative permeability and relative conductivity measurements. Initial sensitivity studies indicate that certain petrophysical properties are more closely coupled to average pore sizes, while other properties are more closely coupled to pore size distributions. This is an important result, that if verified in subsequent studies, will provide a means to verify our hypothesis that a single model realization can be matched against a wide variety of petrophysical properties.

Once the simulator has been completely validated, it will be used for the following:

- *Matching of laboratory petrophysical property measurements with one set of pore network parameters for each sample.*

The purpose of this work will be to first define what types of pore parameters are necessary to completely describe the petrophysical properties of a single piece of core material. Our initial sampling has focused on sampling a wide variety of facies types. Depending upon the speed at which samples can be measured, we will also focus on the variability of samples within each important facies.

One issue that will to be addressed is the issue of uniqueness of model matches. Although we recognize this as a possibility, the uniqueness issue will diminish with increasing number of petrophysical properties matched by the same set of pore parameters. And although we will be addressing this issue through sensitivity studies, it is anticipated that it is probably more likely that we will have the opposite problem — i.e., that even a single match of all petrophysical properties may be difficult.

The matching process will be guided by petrographic studies being conducted by the BEG. This will help both in achieving matches and also in dealing with non-uniqueness issues. We believe it highly unlikely that matches of data, consistent with thin section observations, will still remain non-unique.

- *Relating pore-level characteristics to geologic features.*

The next phase of the work will be to relate the quantitative pore-level parameters to geology. Basically the task here will be to to determine what ranges of values of pore-level parameters are correlated with depositional and diagenetic features. The goal of this task will be to be able to utilize geologic observations and extrapolations to determine pore-level parameters that can then be used to generate petrophysical properties. Although we will not have a large number of all of the petrophysical measurements, there will be on the order of 10^4 minipermeameter measurements. Because permeability will be correlated with the other petrophysical measurements through network parameters, this will allow us to define the theoretical geostatistical variability of all of the petrophysical properties.

A key issue to be addressed from the start of this project will be sample selection. That is, on what basis do we select the limited number of samples on which to measure petrophysical property suites. Our approach to sample selection has been to first define the geostatistics for permeability within a particular facies and then to select samples representing both averages and extremes.

- *Defining the petrophysical nature of flow and bounding units.*

This, of course, is the final outcome of the petrophysical work on this project. This task will be to utilize geologic observations and extrapolations combined with petrophysical property transformations to begin to address whether a particular facies unit potentially acts as a barrier or not. This, of course, depends upon effective petrophysical properties at reservoir scales.

Although a precise determination of sealing characteristics depends upon how a unit behaves in concert with other units at the reservoir scale, there is still much to be learned by examining effective flow properties of different rock units using simplified flow patterns. To this end, we will address the scale problem using one-dimensional flow calculations through reservoir rock with volumes on the order of size as both: a) STRATAMODEL grid blocks, and b) anticipated continuity of geologic units. These rock volumes will have petrophysical properties stochastically assigned on the basis of minipermeameter statistics, geologic interpolation, and the petrophysical property transformations determined from network modeling studies.

- *Defining flow and bounding units in the subsurface.*

Extrapolation of the results of this study to the Lake Creek field will be undertaken in the final stages of this research program. Although the data set, both geologic and quantitative, will not be as large for Lake Creek, we plan to extend the Ferron outcrop results by adjusting the pore-level parameter transformations between the outcrop and the subsurface. Previous studies (Stalkup and Ebanks,

1986) have suggested that outcrop and subsurface geostatistics may be different in magnitude, but general spatial trends remain. We should thus be able to develop similar correlating relationships for Lake Creek by utilizing whatever core data and special core tests are available to adjust the correlations to subsurface conditions. Depending upon the availability of time for petrophysical measurements, it may be deemed desirable to perform some complete petrophysical measurements on Lake Creek core samples.

Review of Pore Modeling Approaches

Pore level network models use an approximate pore structure consisting of a network of stochastically-distributed effective pore dimensions and properties. Using appropriate physical laws, network models can then be made to replicate measurements made at the macroscopic scale. Historically, statistical and bundle of tubes models have been utilized for such purposes, however, these models have been found to fall short of replicating key phenomena, such as hysteresis and phase trapping. Hysteresis effects are important in gas reservoirs because of the differ flow processes that occur — drainage being the process resulting in the initial state of the reservoir, and imbibition occurring during water influx and coning.

Bundle of tubes models (Dullien, 1979; Fatt, 1956a; Mohanty and Salter, 1982) appear to have been the first approach at representing pore structure. However, these models are not physically similar to actual pore structures. As a result, they are not able to exhibit such properties as hysteresis and phase trapping.

Statistical models have also been developed (Lin and Slattery, 1982). These models also lack three-dimensional interconnections between pores. Thus, nonzero irreducible wetting phase and residual nonwetting phase saturations characteristic of capillary pressure curves, phase trapping, and mass conservation and pressure continuity at interconnections are not precisely modeled.

Bond percolation theory results (Chandler *et al.*, 1981; Wong, 1988; Thompson *et al.*, 1987) have been applied to fluid flow in porous media. However, the two problems — bond percolation and

flow in porous media — are similar but not identical. The bond percolation problem is static, as either a percolating cluster is present or one is not. Also, the probability that a bond is present (conducting fluid) is equal for all bonds. Clearly, this is not true for porous media because of accessibility; pores only become accessible as adjacent ones do. Invasion percolation, which can even model trapping, has also been used. However, among other things, it does not have the flexibility to allow pore bodies in the network.

It has been demonstrated by numerous researchers (Chatzis and Dullien, 1977; Dias and Payatakes, 1986a; 1986b; Dullien, 1979; Fatt, 1956a; Hopkins and Ng, 1986; Lin and Slattery, 1982; Mohanty and Salter, 1982; Touboul *et al.*, 1987) that network models do exhibit the observed properties of porous media. Fatt (1956a,b,c) introduced the concept of modeling a porous medium by a pore network. He used a two-dimensional regular network of randomly-distributed capillary throats with nodes that had no volume. He used both uncorrelated throat lengths and capillary throat lengths that were inversely proportional to their radii.

Fatt's model qualitatively represented observed behavior of capillary pressure, relative permeability, relative resistivity, and the saturation exponent in an actual porous medium. He illustrated his model using square and single, double, and triple hexagonal patterns and found that the results were less affected by the pattern than they were by the throat radius distribution. Fatt demonstrated his network using only up to about 400 pore throats, since his calculations were done manually.

Fatt began his capillary pressure calculations with the network 100% wetting phase saturated. He used the Laplace equation, assuming a contact angle of zero, for determining when invasion of nonwetting phase occurred in the network:

$$P_c = \frac{2\sigma}{r} \tag{1}$$

where,

P_c = capillary pressure, $m/L/t^2$

σ = interfacial tension, m/t^2

r = pore throat radius, L

Fatt allowed the nonwetting phase to invade from all four sides of the two-dimensional pore network and assumed that the wetting phase could always escape to the outside of the network through thin films along pore walls. This assumption of no trapping of wetting phase results in an irreducible wetting phase saturation of zero. This is a shortcoming of Fatt's work that can easily be overcome if appropriate trapping mechanisms are assumed.

The process of nonwetting phase invasion (drainage) was carried out by finding the wetting phase saturated pore throats adjacent to a nonwetting phase saturated pore throat that could be invaded by nonwetting phase with the smallest increase in capillary pressure. Due to the Laplace equation, this was equivalent to finding the accessible pore throat with the largest radius. Initially, this meant determining the pore throats on the edge of the network with the largest radius. Any interior pore throats then accessible through these largest pore throats that were of larger radius were also invaded. When no more invasion could occur because all wetting phase saturated pore throats adjacent to nonwetting phase saturated pore throats were of smaller radius, the process was repeated. Eventually the capillary pressure reached a value such that the smallest pore throat was able to be invaded and the network was 100% nonwetting phase saturated. Since Fatt simulated mercury injection experiments, irreducible wetting phase saturation was zero.

Fatt made relative permeability measurements using the Hagen-Poiseuille equation for laminar flow of a Newtonian fluid in a circular tube:

$$q = \frac{\pi}{8\mu} \frac{r^4}{L} \Delta P \qquad (2)$$

where,

q = flow rate, L^3/t

μ = fluid viscosity, m/L/t

L = pore throat length, L

ΔP = pressure drop across the pore throat, $m/L/t^2$.

Fatt used an analog computer of resistors with the resistances determined from Ohm's law:

$$I = \frac{1}{R} \Delta V \tag{3}$$

where,

I = current, I

R = resistance, W

ΔV = voltage drop across the resistor, V.

The conductance of the resistor is proportional to r^4/L for the pore throat. Therefore, with a random throat radius distribution and either a random or nonrandom throat length distribution, the representative resistor in the analog resistor network is proportional to L/r^4.

After constructing the resistor network, Fatt used the same nonwetting phase invasion process as in his capillary pressure measurements. When a pore throat was invaded by nonwetting phase, that resistor was removed from the wetting phase resistor network and placed in an identical resistor network for the nonwetting phase. The wetting phase relative permeability was calculated as the resistance of the wetting phase resistor network at a particular wetting phase saturation divided by the resistance of the resistor network at 100% wetting phase saturation, i.e., with all of the network resistors in place. Note that the nonwetting phase relative permeability was zero until a continuous chain of resistors was formed in the nonwetting phase resistor network. Again, because trapping of the wetting phase was not allowed, the endpoint wetting phase relative permeability was always one.

To determine relative resistivity, R_t/R_o, Fatt used another form of Ohm's law to determine resistance values for the resistor network. This form is

$$I = \frac{\pi}{r}\frac{r^2}{L}\Delta V \tag{4}$$

where r is the resistivity of the saturating fluid. The proportional resistance of a representative resistor is therefore given by L/r^2. The determination of relative resistivity was then performed exactly as was that of relative permeability. Graphing relative resistivity vs. wetting phase saturation on a log-log plot gave a straight line whose slope was the negative of the saturation exponent, as given by Archie's equation (Jorden and Campbell, 1986):

$$\frac{R_o}{R_t} = S_w^{\,n}. \tag{5}$$

Fatt found that saturation exponents determined using the network were in the range of 2 to 4. Fatt did not study hysteresis effects.

Simon and Kelsey (1971, 1972) used the network model concept to investigate the ability of a network of pores to match recovery and effluent composition vs. pore volumes injected (PVI) data for miscible displacement of a core. Unlike Fatt, they allowed only one entrance face and an opposite exit face. Three pore throat radius distributions were used in their work: single radius, uniform, and Gaussian. As in Fatt's work, their model assumed nodes with no volume. They presented two papers, dealing with equal- and unequal-viscosity displacements.

In an equal-viscosity displacement, flow rates through each pore throat and node pressures are constant under a constant inlet to outlet pressure drop. The flow rates were represented by the Hagen-Poiseuille equation and material balance was maintained at each node. A set of linear equations resulted since there is no capillary effect in a miscible process. The pressures were then calculated from the system of linear equations and the flow rates

were found using these pressures. Assumptions of plug flow and instantaneous mixing at each node were made. Breakthrough time was found using pore throat velocities and PVI to breakthrough was calculated using total flow rate, breakthrough time, and total network pore volume. Distribution parameters were varied until the PVI to breakthrough value matched that of core data. Using a double hexagonal network with 100 to 1000 pores, Simon and Kelsey were able to match linear core PVI to breakthrough data.

In an unequal-viscosity linear miscible displacement, some pore throats contain composition interfaces. Because of this, Simon and Kelsey used volume-averaged viscosities. This also causes flow rates and pressures in the network to change. Nevertheless, Simon and Kelsey found that they could also match unequal-viscosity displacement data in cores.

Simon and Kelsey also used the network model to match miscible displacement data for a quarter five-spot pattern with a diamond configuration. They were able to match sweep efficiencies expected from theory.

Wardlaw and Taylor (1976) used a network model to study the effect of pore throat and pore body distribution on capillary pressure curves. Their model was a two-dimensional hexatriangular network of rectangular shape, with only the left and right faces permeable to fluid. They simulated a drainage experiment using the Laplace equation to control invasion. They did not allow the wetting phase to be trapped. They then simulated imbibition and again used the Laplace equation to control the emptying of a pore by the nonwetting phase. Wardlaw and Taylor did obtain a nonzero residual nonwetting phase saturation by permitting that phase to empty a pore only if it had a continuous path out of the sample. This situation where nonwetting phase became trapped in a pore because it was no longer connected to the exit by nonwetting phase is termed "snap-off." They concluded that during drainage the fact that many pores were not accessible to invasion when the capillary pressure became high enough for them to be invaded only delayed invasion. However, if a pore, because of snap-off, was not emptied when the

capillary pressure was reduced to its threshold level, it would never empty and became part of the residual nonwetting phase.

Chatzis and Dullien (1977) studied both two- and three-dimensional networks. They used the coordination number, the total number of pore throats (bonds) connected to one pore body (node), to characterize a network pattern. They defined a cumulative probability, Pc, by

$$P_C = \frac{\sum_{j=1}^{k} N_j}{\sum_{j=1}^{n} N_j} \qquad (6)$$

where Nj is the total number of pores of size j (pores were only allowed to be an integer size), k is the size of pores being invaded when breakthrough occurs, n is the total number of pore sizes, with 1 being the largest pore size and n the smallest. They obtained cumulative probability values for different network lengths until the critical probability was determined. The critical probability is that which would apply to a network of infinite length. They found that a network of about 40 pore segments deep was sufficient to simulate an infinite-length network. They also found that the product of the coordination number and the critical probability did not depend on the geometry of the network, only on its dimension. The products were 2 and 1.5 for two- and three-dimensional networks, respectively. Bond percolation theory data was used to approximate three-dimensional network results because of good agreement with breakthrough data and with two-dimensional differential saturation data. No actual three-dimensional calculations were done.

Chatzis and Dullien concluded that two-dimensional networks could not be used to simulate three-dimensional networks because of their differing properties. One discrepancy is that bicontinua cannot exist in a two-dimensional network. They also found that the best three-dimensional results were obtained when the volume fraction of pores of a certain size was proportional to the diameter of those

pores. They noted that porosities in the 20 to 40% range could not be described if the pore throat lengths were made either directly or inversely proportional to their diameters.

Lin and Slattery (1982) presented a three-dimensional network model that could correlate drainage and imbibition capillary pressure data, single-phase permeability, relative permeability to both the wetting and the nonwetting phases, irreducible wetting phase saturation, and residual nonwetting phase saturation. It could also quantify hysteresis loops for both capillary pressure and relative permeability. Their model assumed sinusoidal pore throats with a Beta distribution of throat radii. The throat shape is shown in Fig. 22.

In Fig. 22, the ratios A/r_n and L/r_n were denoted as A* and L* and were made constant. Throat lengths were computed using a power law relationship of the throat radii:

$$L_t = L_{t,max} \left(\frac{r_n}{r_{n,max}} \right)^a \tag{7}$$

where,

$L_{t,max}$ = maximum throat length in the network, L

$r_{n,max}$ = maximum throat radius in the network, L

L_t = individual throat length, L

r_n = individual throat radius, L

a = free parameter.

They define a unit throat as that part of a throat from z=0 to z=L which then has volume V_u and pressure drop ΔP_u. The volume of a throat and the pressure drop across it are then considered to be directly proportional to its length as a fraction of the unit length L, i.e.:

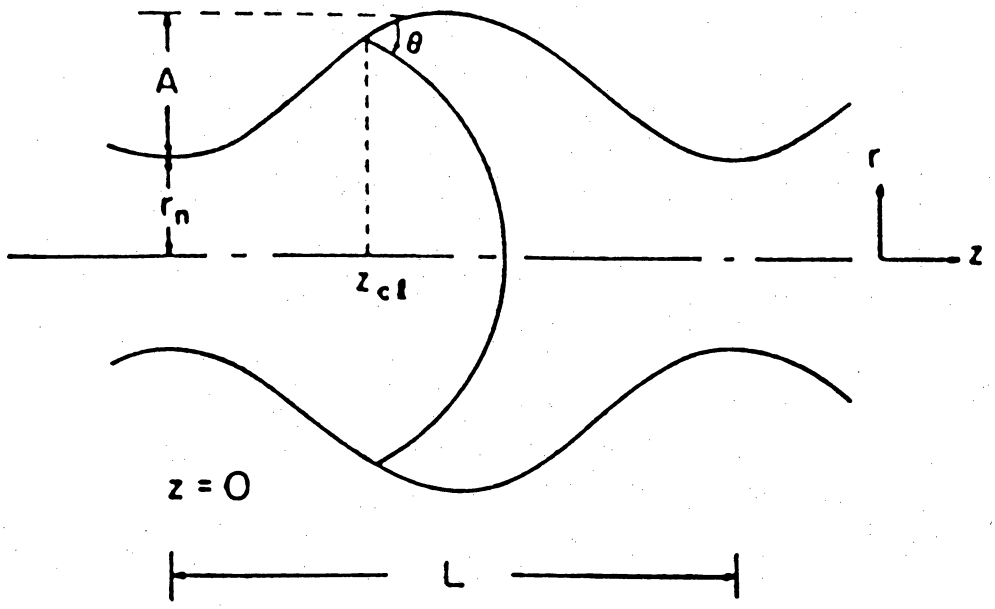

Fig. 22. Schematic of sinusoidal pore (Lin and Slattery, 1982)

$$V_t = V_u\left(\frac{L_t}{L}\right) \tag{8}$$

$$\Delta P_t = \Delta P_u \left(\frac{L_t}{L}\right). \tag{9}$$

They used nodes with no volume and a coordination number of 12 (face-centered cubic network). The coordination number was varied by assigning all pores for which a generated random number between zero and one was less than $1 - \frac{n}{12}$, where n is the new coordination number.

A pore throat was allowed to be displaced when it met the following conditions: a) the imposed capillary pressure (using equations similar to the Laplace equation with zero contact angle) was such that it could be invaded, b) the displacing phase was continuous from the throat inlet to the network inlet, and c) the displaced phase was continuous from the pore outlet to the network outlet. Capillary forces were assumed to dominate viscous forces. Trapping was allowed when a pore throat (or group of pore throats) filled with the displaced phase was completely isolated by the displacing phase. They performed drainage experiments starting from 100% wetting phase saturation and then simulated imbibition experiments from irreducible wetting phase saturation. They found that they could match both drainage and imbibition capillary pressure curves reasonably well.

In performing permeability calculations, the pressure drop across the unit pore throat was assumed to be given by (Neira and Payatakes, 1979):

$$\Delta P_u = -\frac{q\mu C}{\pi r_n^3} \tag{10}$$

where C is the constant $\Delta P_1^*/L^*$ with ΔP_1^* taken from Fig. 1 of Neira and Payatakes (1979). This equation neglects inertia as well as entrance and exit effects. Equations 7, 9, and 10 can be combined to define a dimensionless flow rate:

$$q^* = -\frac{q\mu C\, L_{t,max}}{\pi L^*\, \Delta P_N\, (r_{n,max})^4} \tag{11}$$

$$= -(\Delta P_t^*) \left(\frac{r_n}{r_{n,max}}\right)^{4-a} \tag{12}$$

where,

$$\Delta P_t^* = -\frac{\Delta P_t}{\Delta P_N} \tag{13}$$

with ΔP_N the pressure drop across the network. To calculate pore throat flow rates and node pressures, the following equation must be satisfied at each node of the given network:

$$\sum_{j=1}^{12} \left[-\Delta P_t^* \left(\frac{r_n}{r_{n,max}}\right)^{(4-a)}\right]_j = 0 \tag{14}$$

This equation results in mass being conserved and the pressure being single-valued at each node. Permeability is found from Darcy's law:

$$k = -\frac{\mu\, L_N\, u}{\Delta P_N} \tag{15}$$

where,

k = single-phase permeability, L^2

u = volumetric flux, L/t

L_N = length of a side of the cubic network, L

with L_N given by

$$L_N = \left(\frac{1}{\phi} \sum_{ALL} V_t \right)^{\frac{1}{3}} \tag{16}$$

where ϕ is porosity. Volumetric flux is found from

$$u = \frac{1}{L_N^2} \sum_{PLANE} (q \cos \vartheta) \tag{17}$$

with PLANE denoting only those pore throats which are intersected by a plane perpendicular to the direction of u and ϑ the angle between the pore throat axis and the direction of u. Relative permeability can be calculated using:

$$k_{ri} = \frac{q^*_{Ni}}{q^*_N} \tag{18}$$

where k_{ri} is the relative permeability to phase i, and q^*_N is given by:

$$q^*_N = \sum_{PLANE} (q^* \cos \vartheta) \tag{19}$$

and q^*_{Ni} by

$$q^*_{Ni} = \sum_{PLANE} (q^*_i \cos \vartheta) \tag{20}$$

where q^*_i indicates only those pore throats filled with phase i. A simplification results when V^*_N, defined by:

$$V_N^* = \sum_{ALL} \left(\frac{r_n}{r_{n,max}}\right)^{a+2} \tag{21}$$

is introduced. Now,

$$k^* = \frac{C\,k}{L^*} \left\{ \frac{\left(1+A^*+\frac{3}{8}(A^*)^2\right)(L_{t,max})^4}{\pi^2\,\phi\,(r_{n,max})^{10}} \right\}^{\frac{1}{3}} \tag{22}$$

$$= q_N^* (V_N^*)^{-1/3}. \tag{23}$$

Runs were then made with set values for the free parameters a, A^*, L^*, $r_{n,max}$, $L_{t,max}$, etc. ΔP_N was set equal to one. First, pore throat radii were assigned. Next, V_N^* was found using Eq. 21. Equation 14 was solved to determine the node pressures using Gauss-Seidel iteration. Dimensionless flow rates could then be calculated from Eq. 12. Dimensionless single-phase permeability could then be found from Eq. 23 after obtaining q_N^* from Eq. 19. For relative permeability, capillary pressure was increased in small increments and fluids were distributed according to the invasion and trapping mechanisms stated earlier. At each capillary pressure, flow rates were solved for and q_N^* and q_{Ni}^* were found from Eqs. 19 and 20, respectively. Relative permeability to phase i was then determined from Eq. 18. This process, as with capillary pressure calculations, was done several times and averaged to obtain appropriate results.

Payatakes (1982) utilized the network concept to study the movement of oil ganglia during immiscible displacements. However, his network used constricted-tube type pore throats instead of cylindrical capillaries. This constricted-tube type throat, or unit cell as Payatakes deems it (Fig. 23), is a portion of a sinusoidal tube and

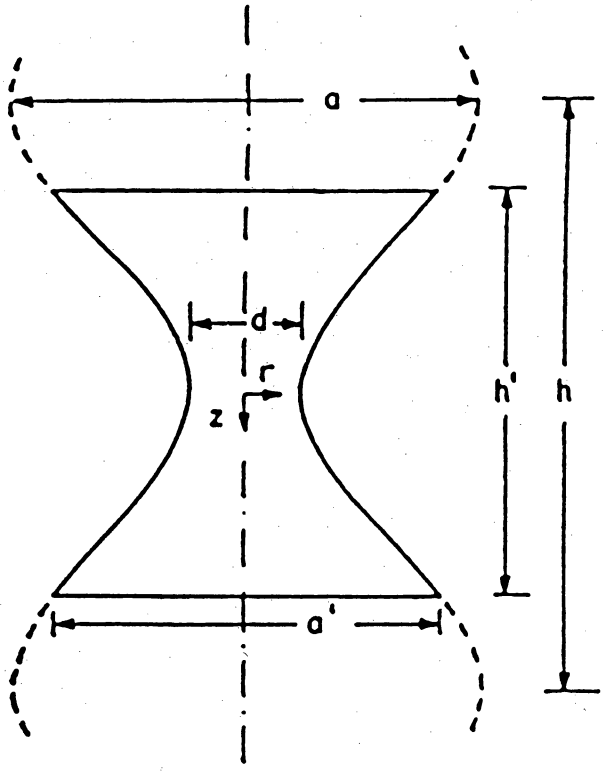

Fig. 23. Schematic of unit cell (Payatakes, 1982)

is represented by five parameters: maximum diameter a, entrance diameter a', minimum diameter d, length h', and wavelength h. He defined a conceptual elemental void space (CEVS) as a node together with the near-halves of the six unit cells attached to that node. Figure 24 illustrates the network.

Payatakes states that constricted-tube throats are superior to cylindrical capillaries for two reasons. First, for a cylindrical capillary, it is not possible for a phase interface in a throat that is not at equilibrium to adjust itself in that same throat and come to equilibrium. The interface may then have to move through several throats to finally achieve equilibrium. The constricted-tube throats allow for the interface to possibly come to equilibrium in the same throats. His second reason is that pressure drops calculated for cylindrical capillaries do not accurately account for those in pore throats which strongly converge and diverge. These objections, however, can be easily overcome by considering assigned cylindrical pore throat radii to be effective values that yield threshold capillary pressures as well as appropriate flowing pressure drops.

Payatakes accounted for moving interfaces within a pore throat using work done by Rillaerts and Joos (1980). They found that the difference between the cosine of the dynamic contact angle and the cosine of the intrinsic contact angle was proportional to the square root of the average velocity. For a constricted-tube throat, the average velocity is a function of position in the throat. Therefore, provision for a moving interface could be made. The "quasistatic" motion of a single oil ganglion under a pressure gradient was modeled. Starting with a pressure gradient too small to cause the ganglion to be mobilized, the pressure gradient was increased. Interfaces on the border of the ganglion react to this. Those on the downstream end gain higher curvature due to the higher capillary pressure. This results because the pressure in the ganglion remains constant while the wetting phase pressure is reduced. Wetting phase pressure is increased on the upstream end and therefore the capillary pressure is decreased, resulting in lower curvatures on this

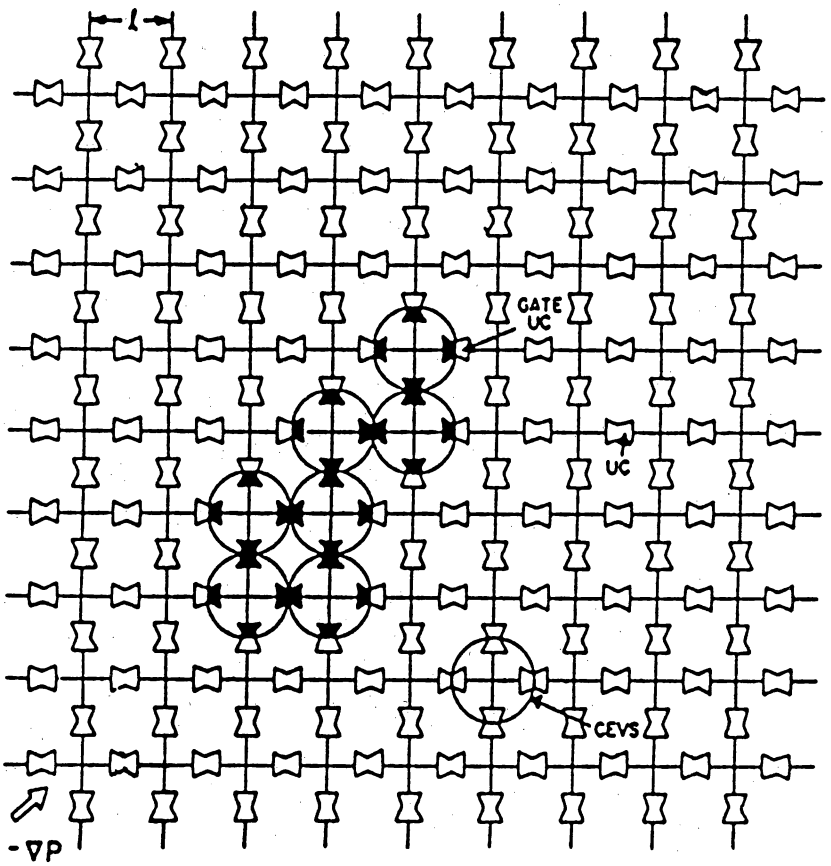

Fig. 24. Schematic of network of unit cells (Payatakes, 1982)

end. Invasion was instigated by increasing the pressure gradient until a rheon took place. A rheon is a combination of one or more xerons, invasions of nonwetting phase into throats occupied by wetting phase, and one or more hygrons, which are the opposites of xerons. A ganglion is allowed to fissure into two daughter ganglia if a hygron occurs at a location where the ganglion is only one unit cell thick. Movement of the ganglion is controlled by the maximum appendix mobility factor, β_{KI}, defined by:

$$\beta_{KI} = \frac{\Delta L_{KI} \cos \vartheta_{KI}}{J_{dr,I}(\vartheta_r) - J_{lb,K}(\vartheta_a)} \tag{24}$$

where ΔL_{KI} is the straight-line distance between throats I and K (which are both on the border of the ganglion with I downstream, K upstream), ϑ_{KI} is the angle between the straight line from K to I and the direction of macroscopic pressure gradient, $J_{dr,I}$ is the drainage curvature (a function of ϑ_r, the receding contact angle), and $J_{lb,K}$ is the lower bound of the imbibition curvature. $J_{lb,K}$ is estimated using:

$$J_{lb,K} = 4 \cos \frac{\vartheta_a}{a_K} \tag{25}$$

where,

ϑ_a = advancing contact angle

a_K = maximum diameter of unit cell K.

Now, mobilization and stranding (no movement) are determined by

$$N_{Ca} = \frac{\mu_w v_f}{\sigma_{ow}} > \frac{k_{rw} k}{\beta_{KI}} \quad \text{for mobilization} \tag{26}$$

$$N_{Ca} = \frac{\mu_w v_f}{\sigma_{ow}} < \frac{k_{rw} k}{\beta_{KI}} \quad \text{for stranding} \tag{27}$$

where,

N_{Ca} = capillary number,

μ_w = wetting phase viscosity, m/L/t

v_f = wetting phase velocity, L/t

σ_{ow} = interfacial tension, m/t^2.

Payatakes found that until a ganglion became stranded, it underwent fissure every 5 to 50 rheons. All of the daughter ganglia, which were much smaller than the ganglia with which they fissured, eventually became stranded unless the capillary number was high enough that even a 1-CEVS ganglion kept moving.

Mohanty and Salter (1982) used a network model to calculate capillary pressure, relative permeability, and dispersivity. They used a three-dimensional cubic arrangement of pore throats with pore bodies at the nodes. They used the Weibull distribution to determine pore throat and pore body radii. Pore body volumes were assumed to be proportional to the cube of their radii. Pore throat volumes were neglected in saturation calculations. Pore throat lengths were considered to be proportional to some power of the throat radii.

Nonwetting phase fluid was only allowed in a pore throat if it was also present in both adjoining pore bodies. Wetting phase fluid, however, was allowed in any pore throat regardless of the state of the adjoining pore bodies. It was assumed to be present in films or in the nooks and crannies of a throat. The volume fraction of wetting phase in a pore throat in which nonwetting phase is present, f_p, is given by

$$f_p = f_n \left\{ 1 - \exp\left(-\frac{2\sigma}{P_c} \right) \right\} \tag{28}$$

where f_n is the volume fraction of nooks and crannies, and σ/P_c has units of microns. The conductivity of wetting phase in pore throats in which nonwetting phase is also present is C/F^4 where C is the

conductivity of the throat when only wetting phase is present and F is the ratio of the throat radius to the effective radius of the nooks and crannies.

Invasion was controlled by the Laplace equation, where

$$P_c \geq \frac{2\sigma}{r_t} \tag{29}$$

must be satisfied for a xeron to take place and

$$P_c < \frac{2\sigma}{r_b} \tag{30}$$

for a hygron to take place. A "choke-off," where the wetting phase is sucked into a throat and the nonwetting phase in that throat then splits into two parts, was allowed to occur whenever the critical radius ratio, r_c, defined by:

$$r_c = \frac{r_b}{r_t} \tag{31}$$

was greater than 3.

Pseudostatic displacements were modeled assuming viscous forces were negligible. Dynamic displacements, where viscous forces are important, were also done. In this case, three fluid fractions are recognized: 1) flowing fraction, 2) dendritic fraction, and 3) isolated fraction. The flowing fraction conducts fluid and viscous forces are present. The dendritic fraction branches off of the flowing fraction but "dead-ends." The pressure in a dendritic branch is uniform and equal to the pressure at the point where it is connected to a flowing branch. The pressure in the isolated fraction is not related to applied pressures.

Koplik and Lasseter (1984, 1985) show that Fatt's analog resistor network procedures can be condensed into a two-step analog effective medium process. They note that the pressure drop across a pore throat is given by:

$$\Delta P = \frac{q\mu}{g_{ik}} \tag{32}$$

where $1/g_{ik}$ is analogous to resistance. They consider one pore throat where all of the random conductances, g_{ik}, in the rest of the network have been changed to an effective conductance, g_m. They calculate the pressure gradient across the one pore throat assuming its conductance is both g_m and then is random. Requiring that the pressure gradient for g_m be equal to the average pressure gradient for g random gives:

$$\left\langle \frac{g - g_m}{g + \left(\frac{z}{2} - 1\right) g_m} \right\rangle = 0 \tag{33}$$

where z is the average coordination number and the brackets indicate the average over all possible values of g. They found that this approximation is good to ±5%. They derived an equation estimating the average velocity. Macroscopic permeability was then calculated using this equation and Darcy's law.

For two-phase flow, they model pressure drop across a throat which contains a moving interface with:

$$\Delta P = -\frac{q\mu_1}{g_1} + P_c - \frac{q\mu_2}{g_2} \tag{34}$$

where 1 and 2 represent wetting and nonwetting phases, respectively, and g_i is the conductance of the region filled with phase i. They used a similar equation for pore bodies which contained interfaces. They note that the capillary pressure terms represent moving batteries in an electrical network analogy. They can then solve for pressures and fluxes in the pores. They use the fluxes to compute the average velocity for each interface, v_α, and, for a given time step, Δt, move the interface $v_\alpha \Delta t$. The pressures and fluxes are then computed again for the new fluid distribution. This process is then repeated as desired.

Koplik and Lasseter found that for small capillary numbers, it was possible to obtain zero or negative capillary pressure at the entrance of a pore body, because of the large size difference. When the viscous pressure gradient in this region was not "large," there would be no flow. This situation was represented in the electrical analogy by a pair of differently-biased diodes in parallel. Because of the difficulty in resolving this situation, they were only able to use about 100 pores in their two-dimensional network.

Koplik et al. (1984) used effective medium theory and similar techniques to calculate both permeability and conductivity. Using rock thin sections to get pore sizes, their results were off by factors of 10 and 2, respectively.

In 1986, Dias and Payatakes (1986a,b) used the network of Payatakes (1982) to study the immiscible displacement of a nonwetting phase by a wetting phase. The basic pore is shown in Fig. 25. In this model, the unit cell has been divided into compartments to allow for the invasion of wetting phase into the throat by stages. As in Payatakes (1982), the nodes have no volume.

They arbitrarily number the throats (or branches) from 1 to N_b and the nodes (or pores) from 1 to N_p and present the flow and material balance equations in matrix form. The following equation is then solved to determine the instantaneous pressure in each of the pores:

$$\mathbf{Yp} = \mathbf{AGv_s} \tag{35}$$

where $\mathbf{Y}$ is the node conductance matrix of dimensions N_p x N_p, $\mathbf{p}$ is the pressure solution vector of length N_p, $\mathbf{A}$ is the reduced incidence matrix of dimensions N_p x N_b which reflects node-throat connections, $\mathbf{G}$ is the branch conductance matrix, a diagonal matrix of order N_b, and $\mathbf{v_s}$ is a capillary pressure source vector of length N_b. The branch flow rate vector, $\mathbf{q}$, is computed by:

$$\mathbf{q} = \mathbf{G}\,(\mathbf{A}^T\mathbf{p} - \mathbf{v_s}). \tag{36}$$

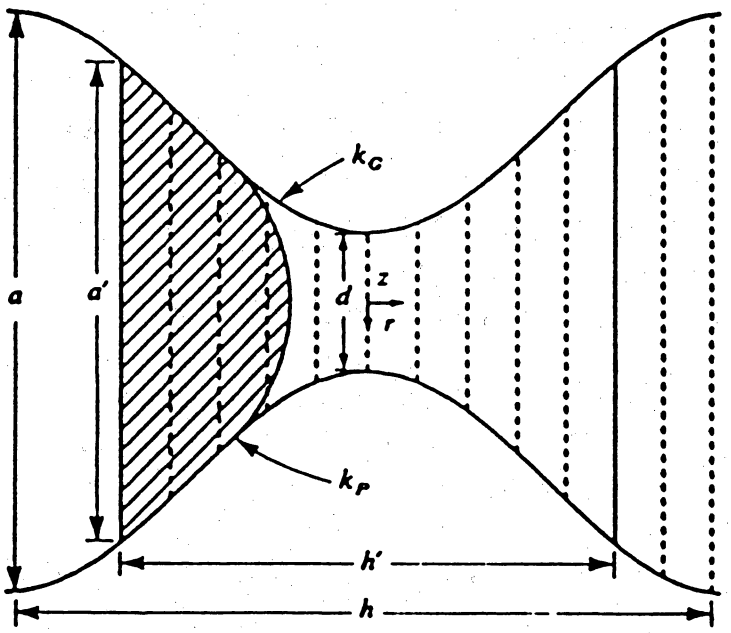

Fig. 25. Schematic of compartmentalized unit cell (Dias and Payatakes, 1986a)

Periodic boundary conditions were used for the sides of the network and a "tail" of pores was added to more accurately model constant capillary number conditions. The 15 x 30 pore network they chose was augmented by the tail to a 15 x 40 network. Xerons, hygrons, pinch-offs, rupturing of a ganglion into daughter ganglia, and stranding of ganglia were all modeled.

Most recently, Touboul, Lenormand, and Zarcone (Touboul *et al.*, 1987); Lenormand *et al.*, 1988) compared results from micromodel experiments and stochastic models with those of their network model. An immiscible drainage process was used and all of the methods were two-dimensional.

Their network model consisted of spherical pores arranged in a square two-dimensional lattice connected by equal-length throats. Both the pores and throats were given uniform radius distributions between maximum and minimum values. Therefore, five parameters constrain the network: the average radius and distribution width for both the pores and throats, and the distance between pores.

No mixing was allowed and Laplace's equation was used to handle capillarity. For flow in a throat, Poiseuille's equation was used:

$$q_{ij} = \frac{\pi r_{ij}^4}{\mu_{ij}} (P_i - P_j - P_{ij})^+ \qquad (37)$$

where,

q_{ij} = flow rate from pore i to pore j, L^3/t

r_{ij} = radius of throat connecting pore i to pore j, L

P_i = pressure in pore i, $m/L/t^2$

P_j = pressure in pore j, $m/L/t^2$

P_{ij} = pressure drop across interface (if present) in throat joining pore i to pore j, $m/L/t^2$

μ_{ij} = an effective viscosity for the fluid in the throat connecting pores i and j, m/L/t

where + indicates that the result of $(P_i-P_j-P_{ij})^+$ is either positive or taken as zero. The effective viscosity, μ_{ij}, is given by

$$\mu_{ij} = \mu_1 + \frac{(a_i+a_j)(\mu_2-\mu_1)}{2} \tag{38}$$

where,

μ_1 = viscosity of the wetting phase fluid, m/L/t

μ_2 = viscosity of the nonwetting phase fluid, m/L/t

a_i = volume fraction of nonwetting phase fluid in pore i

a_j = volume fraction of nonwetting phase fluid in pore j.

[Note that it appears that there is an error in Touboul *et al.* (1987) which has been corrected in Lenormand *et al.* (1988). Their Eq. 5 in Touboul *et al.* (1987) has the pressure term as $(P_i-P_j+P_{ij})^+$.]

Due to the positive rule for the flow rate equation in throats containing menisci, the system of equations to be solved is nonlinear. The time step was limited to the smallest time needed for the nonwetting fluid to fill a pore and hence, reach a pore throat. Touboul *et al.* used a 100 x 100 network in order to obtain a size similar to that of the micromodel. They state that their simulations were "extremely computer-time consuming."

Three patterns were evident in their simulations: capillary fingering, viscous fingering, and stable displacement. These were found to occur in conditions which depended on viscosity ratio and capillary number and matched the micromodel results.

The stochastic models they used, invasion percolation, diffusion-limited aggregation (DLA), and anti-DLA, were in agreement with network results. Invasion percolation theory was found to emulate stable displacement. However, DLA and anti-DLA could only

describe the limits of the regions of viscous and capillary fingering, respectively.

High performance computing is a must for efficient execution of reasonably-sized network models. Many researchers' networks have been two-dimensional and of small size — usually on the order of a few hundred to a thousand pores. For a three-dimensional network with many pores, a prohibitive amount of computing time would be required unless a powerful computer is used with code optimized for that computer. As Aldag (1989) states, supercomputers are making feasible the simulation of many complex phenomena which formerly were impossible.

Scaling Issues

All petrophysical properties are scale dependent. Reservoir rocks are heterogeneous beginning at the pore scale up to any scale of interest. Even core plug measurements should be thought of as being "effective" properties that reflect the "average storage" and transport properties of the combined individual pores. The scale dependency of petrophysical properties is based principally upon reservoir heterogeneity.

The question of scale arises either when measurements made at one scale are compared to measurements at another scale (e.g., core-plug vs. well-test permeabilities), or when measurements are made at a scale that is impractical to be utilized (e.g, utilizing core-plug information in reservoir simulation models). An excellent discussion of some of the primary issues regarding scale can be found in Haldorsen (1986). He points out, for example, that the volume sampled by a sonic log measurement encompasses on the order of 103 core plugs, and the volume sampled by a pressure transient test contains on the order of 1012 core plugs.

The question of scale also arises in attempting to interpolate information between wells and in the prediction of hydraulic unit continuity. Sparse information (measured only at or near wells) must often be utilized to create an entire picture of the internal architecture of a reservoir. When so little information is available,

geological methodologies can be used to create a reservoir picture consistent with observations and knowledge of the depositional and diagenetic factors that created reservoirs.

Reservoir heterogeneities also lead to scale-dependent anisotropies, even when the medium is isotropic at smaller scales (Lake, 1988). A good example of this is the horizontal/vertical permeability anisoptropy that is created by laminated shales. Even if sand member permeabilities are isotropic, vertical permeability is reduced to a much larger extent than horizontal permeabilities. The point is that information about the exact distributions of very small scale properties may need to be very precisely known in order to arrive at accurate large scale values.

There are, of course, multiple scales of variability in a reservoir. Each most probably must be understood in order to develop a consistent picture of petrophysical property variability. Core plug measurements within a given rock type are distributed in some manner, as are rock types within facies and facies within flow units. It is inconceivable that the scale issue will be ultimately resolved without a consideration of each of the different scales of variability.

The sparseness of actual data creates a great deal of difficulty in discerning petrophysical property variability. Even in a very detailed outcrop study (e.g. Goggin, *et al.*, 1988) sampling is extremely limited in comparison to the entire volume of interest. And in actual reservoir situations, key petrophysical data (such as capillary pressures) are seldom measured on more than a few samples, representing a miniscule fraction of the entire reservoir.

In addition, it is very difficult to test whether an approach to averaging from one scale to another is valid. Since larger scale measurements are so inaccurate and expensive to obtain, seldom is enough statistical information gathered at the larger scales (e.g., seismic measurements, pressure transient tests) to be able to make good comparisons between actual scale-dependent measurements.

The question that arises then is precisely how is the scale issue to be addressed. Scale averaging has already progressed from averaging techniques based on simple statistical approaches (e.g., Dykstra and Parsons, 1948) through more sophisticated approaches

based on detailed measurements (e.g., Arya *et al.*, 1988; Lake *et al.*, 1989) or geostatistics (e.g., Begg *et al.*, 1989; Hewett and Behrens, 1989).

Although more recent approaches show a great deal more sophistication and knowledge about geostatistical issues and the relationship between geologic features and petrophysical measurements, all essentially address the scale issue by starting with a model (or an exact description) of the variability of petrophysical properties within a volume of interest. Some averaging model is then applied to this variability model to arrive at a scaled average. Although the variability and averaging models have become more sophisticated, the basic approach remains essentially the same.

The key components of scale averaging models utilized by different researchers seems to be of the following form:

1. A variability model that conceptually describes how petrophysical properties are spatially distributed

2. Petrophysical property statistics, i.e., the appropriate geostatistical parameters that yield actual observed distributions

3. An averaging algorithm to determine larger scale values from the stochastically distributed small scale values

4. A method for validating the scale-up procedure

The variability model is a key component in reservoir characterization studies. A number of approaches have be tried, ranging from the simplest statistical approaches (e.g., log-normal permeability distributions) to more complex approaches based upon large scale geostatistical and descriptive geological information (e.g., Goggin, 1988).

A good approach to the creation of variability models seems to be one that combines descriptive geologic information with quantitative geostatistics. Although a purely statistical approach may work in some circumstances (e.g., Hewett and Behrens, 1989), important pieces of information are lacking that will undoubtedly be

of need in developing as precise a picture as possible of interwell variability. Geological concepts and approaches provide information that is unavailable through the blind application of statistics. The character of the interwell space is governed by depositional and diagenetic forces that are present in many settings. The geoscientist is in a position to provide important interpolation and extrapolation methods based upon knowledge of primary depositional features and subsequent diagenesis. The question, however, is what type of variability model is appropriate that encapsulates geologic knowledge in a way to produce the correct scale-averaged petrophysical properties. This seems to be a central problem in reservoir characterization.

The development of new and better variability models will require the use of advanced geological concepts to address scales of variability that have not historically been comprehensively addressed. But it is only through an understanding of the forces that created reservoir heterogeneity can we hope to discern its nature in sparse data systems. Outcrop and modern sediment studies, both descriptive and quantitative, play key roles in this step of the process. Technical and economic barriers to fine-scale description and quantification in subsurface reservoirs impede any meaningful results, without some sort of well-defined analog with which to compare and contrast. Although it is often expressed that the connection between surface outcrops and subsurface measurements is, at best, tenuous, it is only through understanding the variability in the outcrop that observed variability in the subsurface can be well understood.

The determination of geostatistical parameters is more straightforward than the creation of variability models. Once a variability model is created that appears to match observations, even in a subsurface environment, we believe that sparse data can be utilized to at least estimate geostatistical parameters that will yield distributions of properties within the reservoir consistent with observations. It remains to be seen, of course, whether the generated distributions do indeed match larger scale observations.

Appropriate averaging models are used for this purpose. Averaging models can range from the simple to the extremely complex. Generally storage properties, such as porosity, can be averaged quite simply on an arithmetic basis, since a given volume is the sum of all individual volumes. Transport properties, such as permeability and electrical resistivity, on the other hand, can be averaged only by knowing in some sense how transport is going to occur through both the large scale volume and through the individual small scale volumes. Very complex approaches are required (e.g., Kasap, 1990) to precisely determine large scale transport properties, usually relying on some sort of simulation approach. This is the approach we will utilize in the present study, except that we will rely on simple one-dimensional flow fields over limited rock volumes. This approach should provide initial information on averaging that can later be utilized by more detailed reservoir-scale simulation studies.

The last step in the scale-up process is, of course, validation. Although this is a key step in determining whether a particular approach is valid, it is also a step that is extremely difficult to accomplish, principally because of the difficulty in making large scale measurements with any certainty and in enough detail to provide meaningful comparisons. There are both technical and economic barriers to making such comparisons. The one area in which some comparisons might be made is through detailed analysis of log vs. core data and the comparison of log and core data with individual well pressure and rate performance.

Perhaps the best way to verify scale-up procedures at the larger interwell scales is through the utilization of reservoir performance models. Since such models require scale-averaged data and require the interpolation of interwell data, if their performance can be made to replicate actual reservoir performance (through a history matching process, for example), this at least provides some evidence of appropriate averaging procedures.

Validations in the subsurface will necessitate the use of stochastic approaches, since deterministic small scale values will be be unavailable to utilize in an averaging model. Conditional

simulations are one approach to this problem, by generating different realizations consistent with known data and expected variability of petrophysical properties between wells.

RESULTS

Pore Network Model

Network models reported by others in the literature have been research tools, used principally to investigate the relationships between pore structure characteristics and petrophysical properties. Although the model being used for the present study has this same goal, there are some important differences in how the model will be applied.

First of all, the model needs to replicate, with a single set of pore parameters, the petrophysical properties being measured in the Earth Sciences and Engineering Laboratory — porosity, permeability, capillary pressure, relative permeability, formation factor, and saturation exponent. Secondly, the model will be utilized to address, in part, the problem of scaling of petrophysical data. Thus, results of the model will have to be generated in a stochastic sense. That is, within a given rock facies, stochastic distributions of pore parameters that have been correlated against permeability measurements will be utilized to generate stochastic distributions of all petrophysical properties. This will be an extremely intense application of such models, requiring as much computational efficiency as can be achieved.

We could not identify any models reported in the literature that addressed all of the petrophysical properties of interest in any comprehensive manner. There appeared little evidence that others' models could adequately replicate simultaneous property measurements over a wide range of values. Our model has been constructed in such a way as to achieve a great deal of flexibility in being able to alter pore-level physics, while retaining a sufficient degree of simplicity to allow for large-scale stochastic modeling.

Our experiences in adapting others' codes to vector/parallel processing has proven that it is often far easier to formulate models from scratch with advanced computing in mind. Many man-months of effort are often needed to vectorize a code for maximum efficiency. And since our model is based on approaches already utilized by others (Lin and Slattery, 1982 and Mohanty and Salter, 1982) and based on previous work done at The University of Texas (Tendo, 1984; Mishra, 1990), we believe the most efficient approach has been to do our own coding, but based on others' algorithms.

The model is one in which the transport and storage properties of the permeable medium are represented by a three-dimensional system of effective cylindrical pore throats and spherical pore bodies. Pore parameters utilized to represent the system currently consist of:

1. Average effective pore throat diameter
2. Average effective pore throat length
3. Average effective pore body diameter
4. Dimensionless pore throat diameter distribution function (2 parameters)
5. Dimensionless pore throat length distribution function (2 parameters)
6. Dimensionless pore body diameter distribution function (2 parameters)
7. A parameter to represent the relationship between effective pore lengths and bulk orthogonal lengths.

Pore-level physics are modeled with the following assumptions:

1. There is no mixing of gas and water phases.
2. Phase distributions are determined by assuming that capillary forces dominate viscous forces (pseudostatic displacements). Threshold capillary pressure is given by:

$$P_c = \frac{4\sigma\cos\theta}{d_t} \tag{39}$$

Either trapping, where part of a phase can be cut off from both the inlet and outlet ends of the network, or no trapping can be specified.

3. Flowing pressure drops only occur in pore throats. An approximate linear equation relating laminar gas flow rate and pressure drop is assumed:

$$\dot{m} = \frac{M_g}{RT}\frac{\pi d_t^4 \Delta P^2}{256\mu L} \tag{40}$$

4. For resistivity calculations, only the aqueous phase is assumed conducting (This may later need to be adjusted to account for the presence of conducting clays). Current passing through each throat is according to Ohm's law, with zero voltage drop assumed in each node:

$$I = \frac{\pi d_t^4 \Delta V}{16 R_w L} \tag{41}$$

A major advantage to the approach outlined above is the fact that the resulting equations are linear. We thus expect much benefit to be gained by advanced computational approaches.

Most of the present effort continues to be that of model validation. The primary difficulty is that previous researchers have made other assumptions in the network model, e.g., that there are no bodies or that the throats are noncylindrical. This is being addressed.

There is still, at present, some question as to whether there is a problem with the nonwetting phase relative permeability. Current thought is that the model is working correctly but that the trapping assumption may be flawed. Investigations are continuing.

Sensitivity Studies

In this research period, preliminary sensitivity studies of the effects of pore dimensions on the petrophysical parameters have been initiated. For a 3-dimensional network model, the porosity, absolute permeability and formation factor can be expressed in the following dimensionless forms:

$$\phi = \frac{\pi}{6} \frac{f_l^3}{f_v} \phi_D \tag{42}$$

$$k = \frac{\pi}{2592} \frac{\lambda^3 f_l^4 (1-f_v)^2}{f_v^2 (1-\lambda f_l)^3} \frac{\langle d_b \rangle^2 \langle d_{bD}^3 \rangle^2}{\langle d_{tD}^2 l_{tD} \rangle^2} [k_D] \tag{43}$$

$$\frac{1}{F} = \frac{\pi}{18} \frac{\lambda^2 f_l^3 (1-f_v)}{f_v (1-\lambda f_l)^2} \frac{\langle d_{bD}^3 \rangle}{\langle d_{tD}^2 l_{tD} \rangle} \left[\frac{1}{F_D}\right] \tag{44}$$

where,

$$f_l = \frac{\langle d_b \rangle}{\lambda \left[\langle l_t \rangle + \langle d_b \rangle \right]} \tag{45}$$

$$f_v = \frac{2 \langle d_b \rangle^3 \langle d_{bD}^3 \rangle}{9 \langle d_t \rangle^2 \langle l_t \rangle \langle d_{tD}^2 l_{tD} \rangle + 2 \langle d_b \rangle^3 \langle d_{bD}^3 \rangle} \tag{46}$$

$$k_D = \left\langle \frac{d_{tD}^4}{l_{tD}} P_D \right\rangle_{entrance} \tag{47}$$

$$\frac{1}{F_D} = \left\langle \frac{d_{tD}^2}{l_{tD}} V_D \right\rangle_{entrance} \tag{48}$$

$$\phi_D = \langle d_{bD}^3 \rangle \tag{49}$$

$$P_D = \frac{P_1 - P_i}{P_1 - P_2} \tag{50}$$

$$V_D = \frac{V_1 - V_i}{V_1 - V_2} \tag{51}$$

d_b = pore body diameter, L
d_{bD} = dimensionless pore body diameter, $d_b/\langle d_b \rangle$
d_t = pore throat diameter, L
d_{tD} = dimensionless pore throat length, $d_t/\langle d_t \rangle$
F = formation factor, dimensionless
F_D = dimensionless formation factor
f_l = average pore body diameter per pore unit bulk length, dimensionless
f_v = pore body volume per total pore volume, dimensionless
k = permeability, L^2
k_D = dimensionless permeability
l_t = pore throat length, L
l_{tD} = dimensionless pore throat length, $l_t/\langle l_t \rangle$
P_D = dimensionless pressure
V_D = dimensionless voltage
ϕ = porosity, dimensionless
ϕ_D = dimensionless porosity
λ = effective orthogonal bulk length per unit pore length, dimensionless
$\langle\ \rangle$ = mean

Subscripts:

1 = entrance
2 = exit
t = throat
b = body
D = dimensionless

In this formulation, dimensionless pore parameters are normalized to the mean values of the parameter. This normalization was done so that the effects of mean pore size could easily be distinguished from effects due to pore size distributions. Dimensionless permeability, formation factor, and porosity were also defined such that the effect of pore size distribution is encapsulated in the dimensionless quantity, while the effects of mean pore size are encapsulated in the remaining factors. The morphological arrangement of the pores enters into the analysis through the calculation of pressure (permeability) and voltage (formation factor) and then averaging the flux over some plane, in our case the entrance plane.

Since effects due to mean pore size can be algebraically calculated in this formulation, sensitivity studies have initially concentrated on the effects of pore size distributions on the dimensionless quantities. The Beta probability density function was used to characterize these distributions:

$$f(x) = \frac{(\alpha+\beta+1)!}{\alpha!\beta!}\, x^{\alpha}(1-x)^{\beta}, \qquad o \le x \le 1 \tag{52}$$

This function was selected because of its simplicity (only two parameters) and its flexibility in producing different pore distribution function shapes. Other functions can be utilized in the model should this become necessary to match petrophysical property measurements. Initially only symmetric distributions have been studied, although the Beta function is capable of non-symmetric shapes.

To see the effects of different distributions, we have varied the distributions by changing α and β values to achieve a wide range of standard deviations. Three cases were studied:

	Case		
	1	2	3
α,β	0	2	15
σ	0.8919	0.5533	0.2480

where σ is the standard deviation:

$$\sigma = \sqrt{\langle f^2(x)\rangle - \langle f(x)\rangle^2} \tag{53}$$

As σ increases distribution in effect becomes "fatter." The three cases were chosen such that they represent uniform, medium and narrow distributions. Figure 26 shows the three different distributions.

Figures 27 and 28 show the effect of pore size distributions on dimensionless permeability and dimensionless formation factor, respectively. Note that, as expected, the sensitivity curves have similar shapes and magnitudes. It should be noted that completely uniform pore size distributions would result in dimensionless permeability and formation factor equal to one. Therefore the effect of pore size distribution on these functions is at most a factor of three.

Figure 29 shows the effect of pore size distribution on dimensionless porosity. Note that this too is theoretically one for a uniform pore size distribution, but increases to approximately two for high standard deviation distributions.

Figure 30 shows the effect of pore size distribution on an important parameter determined from capillary pressure curves. Swanson (1981) correlated permeability against the point on a

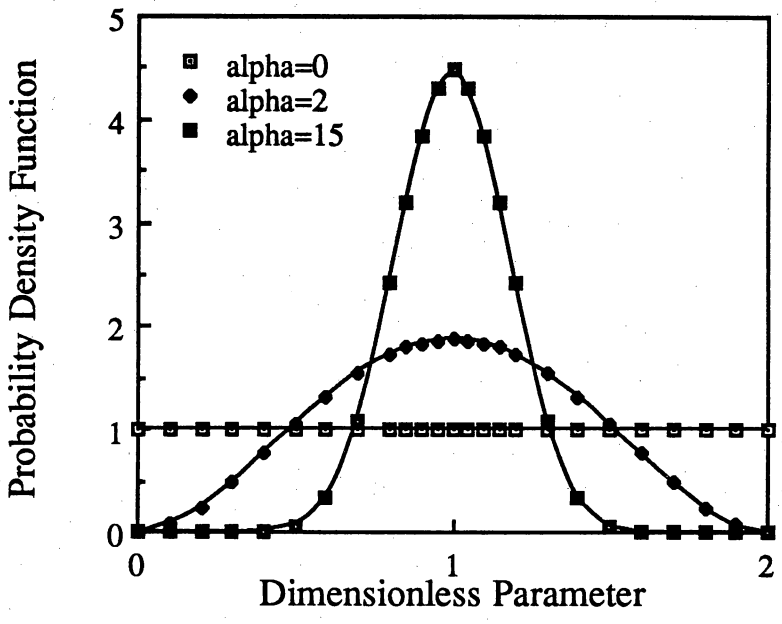

Fig. 26. Probability density functions for sensitivity study

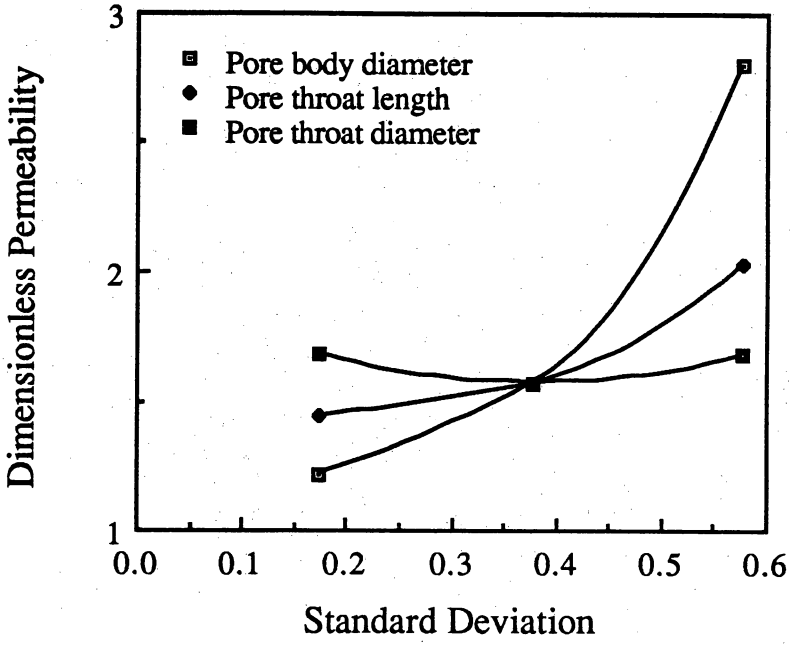

Fig. 27. Dimensionless permeability vs. parameter standard deviation

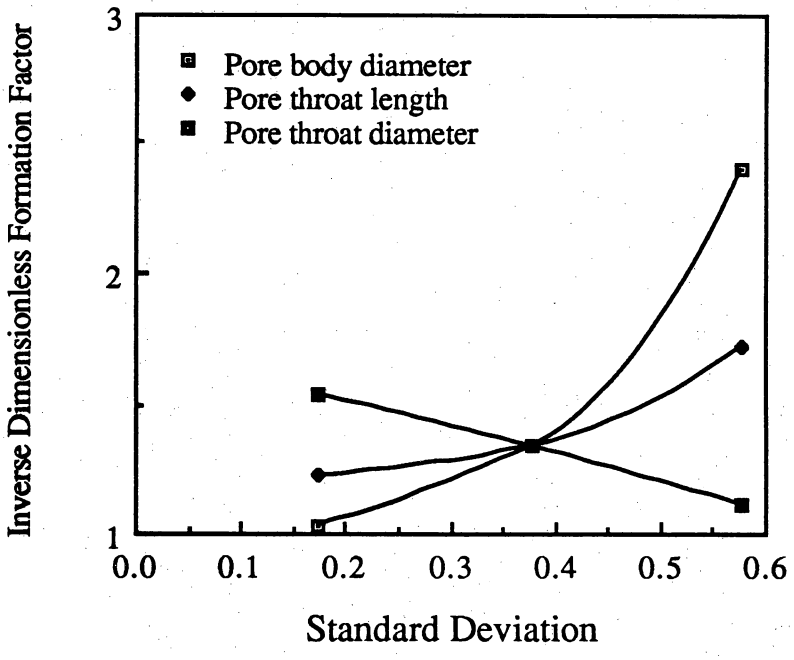

Fig. 28. Inverse dimensionless formation factor vs. parameter standard deviation

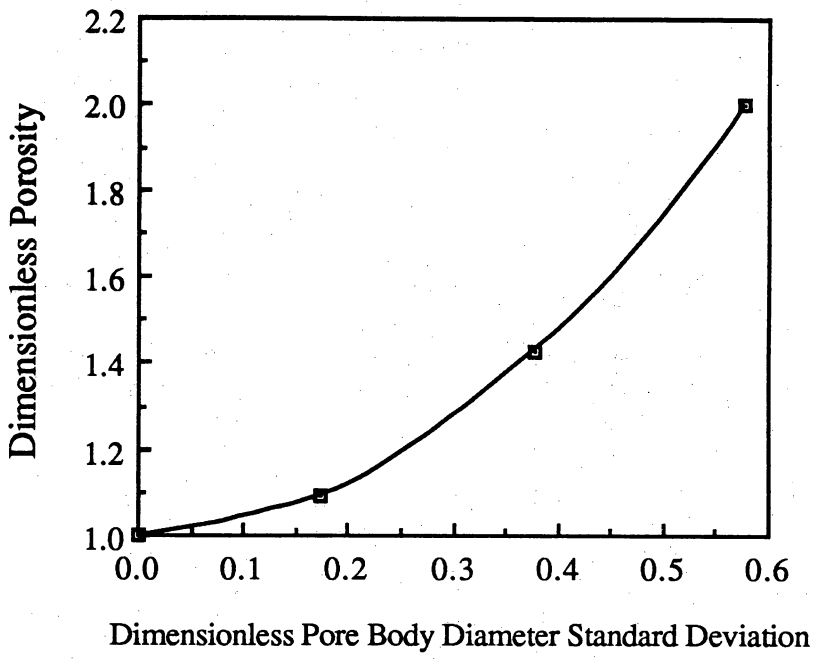

Fig. 29. Dimensionless porosity vs. dimensionless pore body diameter standard deviation

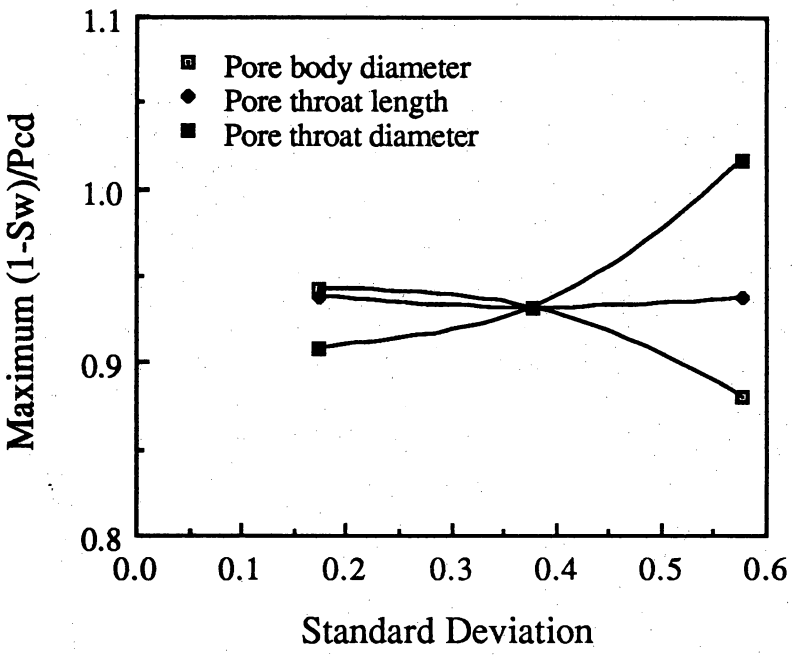

Fig. 30. Dimensionless Swanson (1981) point vs. parameter standard deviation

mercury intrusion capillary pressure curve at the maximum value of $\frac{(1-S_w)}{P_c}$. Note that this point is also one for a uniform pore size distribution. The effect of pore size distribution is restricted to changing this value by only at most 10%. We have not as yet studied the effect of pore size distributions on the shape of capillary pressure curves.

Initial results of the sensitivity studies are encouraging in that the effects of pore parameter distributions on permeability, formation factor, and porosity are fairly small. This means that most of the distribution effects probably will be reflected in relative permeability and resistivity vs. saturation curves. This is welcome news, since it would appear to allow us to decouple the effects of pore size and pore size distributions on different petrophysical properties.

ANTICIPATED 1991 RESEARCH PROGRAM

Now that the network model is essentially complete, our next task will be to "tune" the model to actual petrophysical property measurements from the Earth Sciences and Engineering Laboratory on Ferron outcrop material. We anticipate that the better part of 1991 will be spent on this process.

Our first task will be to determine how best to approach this matching process. In particular we will need to determine how pore parameters affect petrophysical properties and how petrophysical properties are interrelated through pore parameters. This will be accomplished by further sensitivity and correlating studies, covering the entire range of possible pore parameters. Completion of the sensitivity work will also help us address whether uniqueness will be a problem. By the end of 1991 we will thus be in a position not only to have matched all of the laboratory measurements, but also to have addressed the full range of model response.

We also plan in 1991 to begin the scaling studies. The goal for 1991 will be to construct one or more appropriate averaging models. Our approach will be to formulate simple two-phase (gas and water)

one-dimensional flow models of parallelepiped volumes of reservoir rock, within which petrophysical properties can be stochastically distributed. By flowing multiphase mixtures through the blocks and then mathematically integrating both fluid and electrical current flow, we can determine effective properties for these large-scale volumes. We will attempt to utilize existing reservoir simulation models available at The University of Texas; however, we anticipate that some simple model development will be necessary for this task.

Whether a particular facies unit acts as a barrier or not depends upon rock property continuity and how the unit interacts with nearby units in a reservoir context. Exact determination of flow barriers and baffles can thus probably best be studied with reservoir-scale flow models, which are out of the scope of the present study. However, the simple one-dimensional flow calculations will allow us to determine appropriate averaging methods to get up to the STRATAMODEL grid block scale, and perhaps to begin to formulate preliminary estimates of sealing or non-sealing capability of the various rock facies.

CONCLUSIONS

Results of the first year of study of the role played by depositional and diagenetic processes in defining between-well or macroscale reservoir heterogeneity have proved to be most encouraging. The fundamental premise of the study, that architecture of sandstone bodies is quantifiable and hence predictable, has withstood outcrop scrutiny and statistical testing. Accompanying petrophysical and pore-network studies have established the validity of baseline testing and calibration of equipment and have developed a pore-level simulator that is capable of modeling absolute and relative permeability, porosity, saturation, and capillary pressure. Integration of these various scales of data, from macroscale outcrop-architectural studies to the petrologic and petrophysical analyses at the microscopic scale, will facilitate development of realistic, three-dimensional predictive reservoir models that will define patterns of subsurface flow, areas of inadequate reservoir drainage, and untapped reservoir compartments in fluvial-deltaic reservoir analogs.

REFERENCES

Aldag, J. E., 1989, The impact of supercomputers: global, pervasive, positive: The International Journal of Supercomputer Applications, v. 3, no. 2, p. 3–5.

Arya, A., Hewett, T. A., Larson, R. G., and Lake, L. W., 1988, Dispersion and reservoir heterogeneity: Society of Petroleum Engineers, Reservoir Engineering, p. 139–148.

Begg, S. H., Carter, R. R., and Dranfield, P., 1989, Assigning effective values to simulator gridblock parameters for heterogeneous reservoirs: Society of Petroleum Engineers, Reservoir Engineering, p. 455–463.

Chandler, M. A., Kocurek, G. A., Goggin, D. J., and Lake, L. W., 1989, Effects of stratigraphic heterogeneity on permeability in eolian sandstone sequence, Page Sandstone, northern Arizona: American Association of Petroleum Geologists Bulletin, v. 73, no. 5, p. 658–668.

Chandler, R., Koplick, J., Lerman, K., and Willemsen, J. F., 1981, Capillary displacement and percolation in porous media: Ridgefield, Conn., Schlumberger-Doll Research report.

Chatzis, I., and Dullien, F. A. L., 1977, Modelling pore structure by 2-D and 3-D networks with application to sandstones: Journal of Canadian Petroleum Technology, v. 16, no. 1, p. 97–108.

Dias, M. M., and Payatakes, A. C., 1986a, Network models for two-phase flow in porous media: part 1. immiscible microdisplacement of non-wetting fluids: Journal of Fluid Mechanics, v. 164, p. 305–336.

_____ 1986b, Network models for two-phase flow in porous media: part 2. motion of oil ganglia: Journal of Fluid Mechanics, v. 164, p. 337–358.

Donath, F. A., and Guvin, Necip, 1971, Data reduction in experimental rock deformation: Contributions to Geology, v. 10, p. 89–123.

Donath, F. A., Holder, Jon, and Fruth, L. S., 1988, Simultaneous hydraulic/physical parameter measurement on rock specimens subjected to triaxial conditions: Advanced Triaxial Testing of Rock, American Society for Testing and Materials STM 977, p. 143–154.

Dullien, F. A. L., 1979, Porous media: fluid transport and pore structure: New York, Academic Press, 396 p.

Dreyer, T. A., Scheie, A, and Walderhaug, O., 1990, Minipermeameter-based study of permeability trends in channel sand bodies: American Association of Petroleum Geologists Bulletin, v. 74, no. 4, p. 359–374.

Dykstra, H., and Parsons, R. L., 1948, The prediction of oil recovery by waterflooding: Los Angeles, presented at the American Petroleum Institute spring meeting on Secondary Recovery of Oil in the U.S.

Ebanks, W. J., 1987, Flow unit concept—integrated approach to reservoir description for engineering projects: American Association of Petroleum Geologists Bulletin, v. 71, no. 5, p. 551–552.

Evans, W. M., 1973, A system for combined determination of dynamic and static elastic properties, permeability, porosity, and resistivity of rocks: The University of Texas at Austin, Ph.D. dissertation.

Fatt, I., 1956a, The network model of porous media: 1. capillary pressure characteristics: American Institute of Mining, Metallurgical, and Petroleum Engineers, Transactions, v. 207, p. 144–159.

_____ 1956b, The network model of porous media: 2. dynamic properties of a single size tube network: American Institute of Mining, Metallurgical, and Petroleum Engineers, Transactions, v. 207, p. 160–163.

_____ 1956c, The network model of porous media: 3. Dynamic properties of networks with tube radius distribution: American Institute of Mining, Metallurgical, and Petroleum Engineers, Transactions, v. 207, p. 164–181.

Goggin, D. J., 1988, Geologically-sensible modeling of the spatial distribution of permeability in eolian deposits: Page Sandstone (Jurassic), northern Arizona: The University of Texas at Austin, Ph.D. dissertation, 418 p.

Goggin, D. J., Chandler, M. A., Kocurek, G. A., and Lake, L. W., 1988, Patterns of permeability in eolian deposits: Society of Petroleum Engineers, Formation Evaluation, p. 297–306.

Haldorsen, H. H., 1986, Simulator parameter assignment and the problem of scale in reservoir engineering, *in* Lake, L. W., and Carroll, H. B., Jr., eds., Reservoir characterization: Orlando, Academic Press, p. 293–340.

Hearn, C. L., Ebanks, W. J., Tye, R. S., and Ranganathan, V., 1984, Geological factors affecting reservoir performance of the Hartzog Draw field, Wyoming: Journal of Petroleum Technology, v. 38, no. 8, p. 1335–1344.

Hewett, T. A., and Behrens, R. A., 1989, Scaling laws in reservoir simulation and their use in a hybrid finite difference/streamtube approach to simulating the effects of permeability heterogeneity: presented at the

Second International Reservoir Characterization Technical Conference, Dallas.

Hopkins, M. R., and Ng, K. M., 1986, Liquid-liquid relative permeability: network models and experiments: Chemical Engineering Communication, v. 46, p. 253–279.

Jones, J. R., Scott, A., and Lake, L. W., 1987, The geological aspects of reservoir characterization for numerical simulation, Mesaverde meanderbelt sandstone, Northwestern Colorado: Society of Petroleum Engineers Formation Evaluation, March, p. 97–107.

Jorden, J. R., and Campbell, F. L., 1986, Well logging II—electric and acoustic logging: New York, Monograph Series, Society of Petroleum Engineers, v. 10, p. 30.

Kasap, E., 1990, Analytic methods to calculate an effective permeability tensor and effective relative permeabilities for cross-bedded flow units: The University of Texas at Austin, Ph.D. dissertation.

Kittridge, M. G., 1988, Analysis of areal permeability variations—San Andres Formation, New Mexico: The University of Texas at Austin, Master's thesis, 361 p.

Koplik, J., and Lasseter, T. J., 1984, One- and two-phase flow in network models of porous media: Chemical Engineering Communications, v. 26, p. 285–295.

_____ 1985, Two-phase flow in random network models of porous media: Society of Petroleum Engineers Journal, p. 89–100.

Koplik, J., Lin, C., and Vermette, M., 1984, Conductivity and permeability from microgeometry: Journal of Applied Physics, v. 56, no. 11, p. 3127–3131.

Lake, L. W., 1988, The origins of anisotropy: Journal of Petroleum Technology, p. 395–396.

Lake, L. W., Kasap, E., and Shook, M. 1989, Pseudofunctions—the key to practical use of reservoir description: presented at the Second International Conference on North Sea Oil and Gas Reservoirs, Trondheim, Norway.

Lenormand, R., Touboul, E., and Zarcone, C., 1988, Numerical models and experiments on immiscible displacements in porous media: Journal of Fluid Mechanics, v. 189, p. 165–187.

Lin, C-Y., and Slattery, J. C., 1982, Three-dimensional, randomized, network model for two-phase flow through porous media: American Institute of Chemical Engineers Journal, v. 28, no. 2, p. 311–324.

Mishra, B., 1990, Determination of porosity, permeability, and capillary pressure with a three-dimensional network model of porous media: The University of Texas at Austin, Master's thesis, 132 p.

Mohanty, K. K., and Salter, S. J., 1982, Multiphase flow in porous media: 2. pore-level modeling: Society of Petroleum Engineers Paper 11018.

Neira, M. A., and Payatakes, A. C., 1979, Collocation solution of creeping Newtonian flow through sinusoidal tubes: American Institute of Chemical Engineers Journal, v. 25, p. 725–730.

Payatakes, A. C., 1982, Dynamics of oil ganglia during immiscible displacement in water-wet porous media: Annual Review of Fluid Mechanics, v. 14, p. 365–393.

Rillaerts, E., and Joos, P., 1980, The dynamic contact angle: Chemical Engineering Science, v. 35, p. 883–887.

Ryer, T. A., 1981, Deltaic coals of Ferron Sandstone Member of Mancos Shale: predictive model for Cretaceous coal-bearing strata of Western Interior: American Association of Petroleum Geologists Bulletin, v. 65, no. 11, p. 2323–2340.

Simon, R., and Kelsey, F. J., 1971, The use of capillary tube networks in reservoir performance studies: 1. equal-viscosity miscible displacements: Society of Petroleum Engineers Journal, p. 99–112.

Simon R., and Kelsey, F. J., 1972, The use of capillary tube networks in reservoir performance studies: 2. effect of heterogeneity and mobility on miscible displacement efficiency: Society of Petroleum Engineers Journal, p. 345–361.

Stalkup, F. I., and Ebanks, W. J., Jr., 1986, Permeability variation in a sandstone barrier island-tidal delta complex, Ferron Sandstone (Lower Cretaceous), Central Utah: Society of Petroleum Engineers Paper 15532, p. 1–8.

Swanson, B. F., 1981, A simple correlation between permeabilities and mercury capillary pressures: Journal of Petroleum Technology, p. 2498–2504.

Tendo, F. C., 1984, A three-dimensional computer model of capillary pressure behavior in porous media based on the theory of a network of capillary tubes: The University of Texas at Austin, Master's thesis. 171 p.

Thompson, A. H., Katz, A. J., and Raschke, R. A., 1987, Mercury injection in porous media: a resistance devil's staircase with percolation geometry: Physical Review Letters, v. 58, no. 1, p. 29–32.

Touboul, E., Lenormand, R., and Zarcone, C., 1987, Immiscible displacements in porous media: testing network simulators by micromodel experiments: Society of Petroleum Engineers Paper 16954.

Wardlaw, N. C., and Taylor, R. P., 1976, Mercury capillary pressure curves and the interpretation of pore structure and capillary behavior in reservoir rocks: Bulletin of Canadian Petroleum Geology, v. 24, p. 225–262.

Weber, K. J., 1982, Influence of common sedimentary structures on fluid flow in reservoir models: Journal of Petroleum Technology, March, p. 665–672.

Wong, P. Z., 1988, The statistical physics of sedimentary rocks: Physics Today, p. 24–32.